INVESTIGATION OF HYDRODYNAMIC DEMANDS OF TSUNAMIS IN INUNDATION ZONE

A THESIS SUBMITTED TO
THE GRADUATE SCHOOL OF NATURAL AND APPLIED SCIENCES
OF
MIDDLE EAST TECHNICAL UNIVERSITY

BY

CEREN ÖZER

IN PARTIAL FULFILLMENT OF THE REQUIREMENTS
FOR
THE DEGREE OF MASTER OF SCIENCE
IN
CIVIL ENGINEERING

FEBRUARY 2007

I hereby declare that all information in this document has been obtained and presented in accordance with academic rules and ethical conduct. I also declare that, as required by these rules and conduct, I have fully cited and referenced all material and results that are not original to this work.

Name, Last name : CEREN ÖZER

Signature :

ABSTRACT

INVESTIGATION OF HYDRODYNAMIC DEMANDS OF TSUNAMIS IN INUNDATION ZONE

Özer, Ceren
M.Sc., Department of Civil Engineering
Supervisor : Assoc. Prof. Dr. Ahmet Cevdet Yalçıner

February 2007, 124 pages

This thesis analyzed the new parameter “hydrodynamic demand” representing the damage of tsunami waves on structures and coastlines, maximum positive amplitudes and current velocities occurred during tsunami inundation by using the numerical model TUNAMI-N2. Regular shaped basins were used with two different bottom slopes in analyses in order to understand the behaviour of tsunami wave and investigate the change of important tsunami parameters along different slopes during tsunami inundation. In application, different initial conditions were used for wave profiles such as solitary wave, leading elevation single sinusoidal wave and leading depression sinusoidal wave. Three different initial wave amplitudes were used in order to test the change of distribution of the hydrodynamic demand. The numerical results were compared and discussed with each other and with the results of existing analytical and experimental studies.

Keywords: Tsunami, hydrodynamic demand, inundation, wave front velocity, current velocity, water surface elevation, solitary wave, leading elevation wave, leading depression wave

ÖZ

DEPREŞİM DALGALARININ BASKIN BÖLGESİNDE OLUŞTURDUĞU HİDRODİNAMİK ETKİ DÜZEYLERİNİN ARAŞTIRILMASI

Özer, Ceren
Yüksek Lisans, İnşaat Mühendisliği Bölümü
Tez Danışmanı : Doç. Dr. Ahmet Cevdet Yalçıner

Şubat 2007, 124 sayfa

Bu tez çalışmasında, tsunami dalgalarının kıyı ve kara yapılarına verdiği hasarı ifade eden ve yeni bir parametre olan “hidrodinamik etki düzeyi”nin dağılımları, depreşim dalgası esnasında oluşan maksimum pozitif genlikler ve akıntı hızları, numerik model TUNAMI-N2 kullanılarak analiz edilmektedir. Analizlerde, baskın esnasında oluşan önemli depreşim dalgası parametrelerinin değişimlerini araştırmak amacıyla iki farklı taban eğimine sahip düzgün şekilli basenler kullanılmıştır. Uygulamada tek dalga, öncü yükselen tek sinusoidal dalga ve öncü çöken tek sinusoidal dalga gibi dalga profilleri için farklı başlangıç durumları seçilmiştir. Hidrodinamik etki düzeyi dağılımlarındaki değişimi analiz etmek amacıyla farklı başlangıç dalga genliği ve periyotları kullanılmıştır. Elde edilen numerik sonuçlar birbirleri ve mevcut analitik ve deneysel sonuçlarla karşılaştırılmıştır.

Anahtar Kelimeler: Depreşim dalgası, hidrodinamik etki düzeyi , baskın, dalga önyüzü hızı, akıntı hızı, su yüzeyi yüksekliği, tek dalga, öncü yükselen dalga, öncü çöken dalga

ACKNOWLEDGMENTS

I would like to express my sincere appreciation to Assoc. Prof. Dr. Ahmet Cevdet Yalçıner for his endless and very valuable supports, academic supervision, and for his heartfelt efforts to join me in such newly developed phenomenon and to provide opportunities to open up new frontiers in my researches. I would like to thank Prof. Dr. Ayşen Ergin and Dr. Işıkhan Güler for their hearty supports and great sympathy throughout my thesis, and also for their contributions to my coastal engineering education with their valuable knowledge and experiences.

I dedicate my thanks to the guidance of all referred studies, which throw fresh light on my newly developed research subject.

I would like to acknowledge Prof. Dr. Costas Synolakis for his valuable discussions and recommendations about my research, and for encouraging me about searching this topic not only with official correspondences but also with face-to-face conversations full of sincerety and charity.

The presence of *Alper Tatlı* makes everything less burdensome, more amusing and bearable together with his endless motivation, patience and *love* not only throughout this study but also in all of my life.

Words are inadequate to express my thanksgiving to my precious family, especially to my mother *Nüvit Özer,* for their everlasting supports, endless love and encouragement.

My most willingly thanks are to my dear friend *Ms. Hülya Karakuş* for her very valuable supports, endless patience and encouragement. I want to thank my sincere friend *Mr. Seçkin Çaban* for his great efforts to amuse and encourage me even at hard times. I also want to thank Mr. Mustafa Esen and Mr. Cüneyt Baykal for their friendly and kind aids; and also to Mr. Ilgar Şafak for his very valuable advises, supports and friendship even from far beyond the oceans.

TABLE OF CONTENTS

LIST OF FIGURES

FIGURES

LIST OF TABLES

TABLES

LIST OF SYMBOLS

A	cross-sectional area exposed to drag force
b	width of vertical wall
C_D	drag coefficient for non-breaking waves
C_{D_b}	drag coefficient breaking waves
C_F	coefficient of the force on the wall with time
C_M	mass coefficient
C_p	dynamic pressure coefficient
d	water depth at the toe of the sloping beach
d_{dyn}	equivalent dynamic flow depth
d_s	design flood depth
d_w	water depth at the wall
$d(x, y)$	undisturbed water depth
E_{sw}	100-year still-water elevation above the datum
F_R	Froude number
g	gravitational acceleration
GS	lowest eroded ground elevation above the datum
h	total flow depth
h_p	undisturbed water depth at the face of pile
$h(x, y, t)$	disturbed water depth
H	amplitude of solitary wave
H_1	surge height
H_i	initial wave height
HD	hydrodynamic demand
H_{toe}	wave height at the toe of slope
LDW	Leading Depression Wave

LEW	Leading Elevation Wave
η	surge profile
$\eta(x, y, t)$	elevation with respect to the undisturbed water surface
η_p	local amplitude at the face of pile
η_w	water surface elevation on the wall located at some $x = X_w$
$p(R, \theta, z, t)$	pressure exerted on cylindrical pile
r	radius of cylindrical pile
R	runup of solitary waves
t	duration of impact of debris
t_1 , t_2 , t_3	times when the estimated flow velocity is just captured or is just exceeded
$\tan\theta$	slope of the front face of the bore.
u , v	depth-averaged water particle velocities in the cross-shore x and long-shore *y* directions, respectively
u_c	current velocity
V	instantaneous horizontal velocity in the direction of wave motion
V_f	equivalent wave front velocity at the grid node
V_s	design flood velocity
V_x , V_y	wave front velocities in x and y direction at grid nodes
$Velx$, $Vely$	current velocities at grid nodes in x and y dir respectively
w	weight of the debris impacting the structure
β	angle of sloping beach with horizontal
ρ	fluid density
$\tau_{r\theta}(R, \theta, z, t)$	tangential shear stress on a cylindrical pile
θ_c	angle of current velocity
θ_f	angle of wave front velocity

Dedicated to my precious family and *Eyes-Deep Ocean*

CHAPTER 1

INTRODUCTION

Tsunamis are water waves which transfer short-duration energy to the entire water column in large scales as a result of earthquakes, coastal and submarine landslides, volcanic eruptions, or meteor impacts. The number of waves and polarity of the initial wave depend on the seabed motion, and the following development over the sea bed ground is explained by long wave theory (Sümer et al., 2007).

Tsunamis generated by landslides may access huge amplitudes in closed basins or shallow regions. These waves are generally classified as long period waves and now all adopted as “tsunamis”. In history, the description of tsunamis has first been done 2500 years ago by Thucydides, Herodotus, Aristotle and later on by Strabo. Thucydides in his work *History of the Peloponnesian War* had come to the conclusion that there is a relation between earthquakes, great waves and topography by observing the frequent earthquakes and a tsunami in 426 B.C. He had defined his observations about the changes in the sea as it "subsided from what was then the shore and afterwards swept up again in a huge wave" (Thucydides 247; 3.89) (Sümer et al., 2007).

After the terrible disaster 1896 Great Meiji tsunami in Japan, caused the death of more than 22000 people, the word “tsunami” had begun to have been declared outside Japan. It was used in the meaning of *harbor wave*, since tsunamis had commonly occurred as unusual waves in ports and small bays. Furthermore, *tidal wave* is the English translation of a Greek term which is used for defining tsunamis since tsunamis mostly indicate themselves along the coastlines as surges or rapid changes in water level.

Tsunamis are divided into two categories due to the location of their occurrence. The first category is named as near-field, near-shore or local if the tsunami sources are within 100*km* off the shoreline. The second category, referred to as transoceanic or far-field, is occurred if tsunamis propagate across the open ocean. Nonetheless, this kind of denomination of tsunamis depends on the reference shoreline means that some tsunamis can be called as near-field with respect to the closest shore and as far field with respect to the further locations. For instance, in the December 26, 2004 Great Sumatra Tsunami, since they are very close to the source, tsunami was a near-field tsunami for Aceh, Thailand and the Andaman/ Nicobar. However, tsunami was referred to as far-field for India, Sri Lanka, Maldives and East Africa. In the case of far-field propagation, the wave energy is mostly dispersed along the direction perpendicular to the fault strike.

Tsunamis generated by fault break (tectonic tsunamis) and by landslides have comparatively different characteristics. Waves caused by landslides generally have only near field impact. Their wave lengths are shorter than that of waves triggered by tectonic motions. All the same; the depth, thickness and initial acceleration of the landslide significantly affect the initial amplitude of wave. For tectonic tsunamis, the length of fault rupture and the slip are the determining factors of the wave amplitude. In general tectonic tsunamis radiate energy in a direction perpendicular to the axis of the triggering fault (Ben-Menahem and Rosenman, 1972, in Sümer et al. (2007)), and propagate long distances.

Structural damages by tsunami waves can be estimated by calculating the impact forces on these structures. The impact forces concerned in this study are drag force and hydrodynamic force. A certain number of important studies had been carried out to find the drag force exerted to the coastal structures. The detailed information about this subject is given in Chapter 2.

There are different approaches about the selection of the velocity component normal to the object over the flow depth. Namely, the variation is using either flow (current) velocity or wave front velocity in the computation of drag force. Yeh (2006) studied on the tsunami forces in the runup zone evaluated by using the algorithm recently developed by Carrier et al. (2003). He estimated the horizontal fluid force resulting from tsunami run up/ drawdown processes onto a uniformly sloping beach. Yeh (2006) uses current velocity in the calculation of maximum impact forces.

Ramsden and Raichlen (1990) made a laboratory experiment for calculating the forces on a vertical wall due to the impact of a bore. They use front velocity in their approach. However, their studies and results can not be directly a reference for this thesis study since they investigated a bore generated by a broken wave to produce impact forces. It means that their approach is only valid if the tsunami triggering wave breaks. The detailed information about this study is given in Chapter 2.

Furthermore, Yalçıner and Synolakis in Sümer et al. (2007) computed the hydrostatic force and drag force by using the current velocity. Differently from other approaches, they normalize the drag force by using the hydrostatic force and introduce a new term called damage metrics, recently called *Hydrodynamic Demand*. This term can be referred as an identifier in the determination of structural damage.

This study is focused on investigating the behaviour of current velocity, wave front velocity and distribution of hydrodynamic demand in shallow region and in the inundation zone by using numerical model TUNAMI-N2. In chapter 1, an introduction is given to the study including a brief information about the types and causes of the tsunamis and their different characteristics. Also, it covers an overall view to the different approaches for calculating the impact forces occured during the tsunami inundation. Chapter 2 describes literature survey carried out for this study. It gives the

details of different approaches about calculating the impact forces with the related equations. In Chapter 3, the theoretical and numerical background are given. Theoretical background deals with the direct effect of tsunamis on different coastal structures and numerical background includes equations and details of the new module inserted in numerical model TUNAMI-N2. The application of the numerical model on a regular shaped basin is given in Chapter 4, where different scenarios are used and all parameters in the model are explained in detail. In Chapter 5, general evaluation, comparison and discussion of the results are presented with conclusions. In Chapter 6, suggestions for further studies are given in the light of comparisons and discussions.

CHAPTER 2

LITERATURE SURVEY

The amplification of tsunami amplitudes at coasts and resulting strong flow velocities are main cause of impact by tsunami waves. There are two types of tsunami effects, named as indirect and direct effects. Indirect effects occur due to the resonance of the enclosed basins by tsunami waves. On the other hand, the direct effects, which are very extensive and disastrous, cause the dragging of the whole structures, damages in the buildings with accumulated shoreline debris, undercutting of the foundations and pilings with erosion, and overturning of huge structures.

The two main parameters causing damage during tsunami inundation are water surface elevations and velocity. The approaches for determining the impact forces caused by tsunami inundation need clarification on the selection of type of velocity to be used. There are two different types of velocities to be considered for the computation of hydrodynamic demands during tsunami inundation. These velocities are current velocity and wave front velocity which may show different behaviors. Therefore, it is essential to determine the effects of these velocities when the tsunami waves come to the shoreline and begin to threat the coastal structures and human lives.

Structural damages by tsunami waves can be estimated by calculating the impact forces on structures. The impact forces concerned are in general drag force. Force in the direction of flow exerted by the fluid on the solid is called drag. The *drag* force F_D is generated by the square of velocity component normal to the element and normal to the lift force. The magnitude is adjusted by a drag coefficient C_D, depending on the shape of

structure and Reynolds number. The drag force occurred during tsunami inundation should be estimated in order to determine the structural damage.

A certain number of important studies had been carried out to find the drag force exerted to the coastal structures. There are different approaches about the selection of the velocity component normal to the structure surface over the flow depth. Namely, the variation is using either flow velocity or wave front velocity in the computation of drag force. These approaches are described in the following.

Yalçıner and Synolakis in Sümer et al. (2007) give a brief review of generation, propagation and coastal amplification of tsunamis. A different approach is provided for calculating impact of tsunamis on marine structures directly and indirectly. They introduced a new term called *Hydrodynamic Demand* which is the normalized form of drag force by hydrostatic force. This new term enables the researchers to evaluate the level of damages on structures. The details about this approach are also given in Chapter 3. In this study drag force is calculated from

$$F_D = \frac{1}{2} C_D \, \rho \, A \, u^2 \tag{2.3}$$

where A is the cross-sectional area exposed to drag force, C_D is the drag coefficient which is the shape parameter and should be less than 2, u is the current velocity and ρ is the fluid density. Yalçıner and Synolakis in Sümer et al. (2007) stated that evacuation of coastal areas that are under the risk of tsunami inundation is very essential in order to prevent loss of life. They emphasized that this is only feasible with rationalistic planning by determining the coastal areas under the risk of submarine hazards. They also offered some specific tasks for preparedness and mitigation studies.

Yeh (2006) studied on the tsunami forces in the runup zone evaluated by using the algorithm recently developed by Carrier et al. (2003). In this study, he estimated the horizontal fluid force resulting from tsunami runup/ drawdown processes onto a uniformly sloping beach. The maximum force per unit width is determined by

$$F = \frac{1}{2} C_D \rho \, h \, u^2 \tag{2.1}$$

where C_D is the drag coefficient suggested as 1.0-2.0 by Arnason (2004), ρ is the fluid density, h is the total flow depth and u is the velocity of flow.

He offered some figures showing the spatial distribution of the maximum momentum flux between initial shoreline and the maximum runup locations for various tsunami conditions. In addition, he concluded that since his estimation is theoretically based on clear assumptions, results in one of these figures can be a basis of a design guideline for building tsunami resisting structures in runup zone. He also stated that it is very essential to estimate the drag coefficient C_D accurately for calculating the fluid force on an object.

A further approach was offered by Ramsden and Raichlen (1990) as a Ph.D. study in California Institute of Technology. They performed laboratory experiments and measured the forces on a vertical wall due to the impact of a bore being triggered by a broken solitary wave. The details about their experiment are given in Chapter 3. The measured force was compared with the force calculated from

$$\frac{F_T}{\frac{1}{2}\gamma b (H_1 + d_w)^2} = \left(\frac{\eta + d_w}{H_1 + d_w} \right)^2 + 2 C_F \, {N_F}^2 \frac{\eta H_1}{(H_1 + d_w)^2} \tag{2.2}$$

where F_T is the total force on the vertical wall, η is surge profile, H_1 is the surge height, b is width of vertical wall, d_w is water depth at the wall, C_F

is the force coefficient calculated as $C_F = 1 + (\tan\theta)^{1.2}$ and generally suggested between *1.4* and *2.1*, and $N_F = \frac{c}{\sqrt{gH_1}}$ where c is the measured incident bore velocity.

The velocity used in Ramsden and Raichlen's (1990) approach is the wave front velocity. However, their approach is valid if the solitary waves triggering the tsunami break. Since the existing numerical models do not simulate breaking well, the relations and results in Ramsden and Raichlen (1990) can not be compared with numerical studies.

One of the important studies on the runup of long waves is Synolakis,1987. In this study, runup of solitary waves on plane beaches are investigated by analytical and experimental comparisons. Synolakis (1987) proposed a runup law as the relation for the runup of non-breaking solitary waves as a function of incoming solitary wave height and beach slope. By solving the linearized long wave equations for the canonical problem, Synolakis (1987) derived the runup law for the non-breaking solitary waves as

$$\frac{R}{d} = 2.831(\cot\beta)^{\frac{1}{2}}\left(\frac{H}{d}\right)^{\frac{5}{4}} \tag{2.4}$$

where R is the runup of solitary waves, H is the amplitude of solitary wave, d is the water depth at the toe of the sloping beach, and β is the angle of sloping beach with horizontal.

In addition, the breaking condition of solitary waves on a sloping beach is presented by Gjevik & Pedersen (1981) in Synolakis (1987) as:

$$\frac{H}{d} > 0.479(\cot\beta)^{-\frac{10}{9}} \tag{2.5}$$

The relations (2.4) and (2.5) were obtained from analytical derivations. They are also verified in excellent agreement with numerous laboratory experiments for solitary waves by Synolakis (1987).

He also concluded that the runup variation is different for breaking and non-breaking solitary waves. Furthermore, different criteria had been applied for determining if a solitary wave of given H/d ratio will break as it climbs up a sloping beach and for determining if it will break during the rundown.

Kanoğlu (2004) solved the initial value problem of the nonlinear evolution, shoreline motion and flow velocities of long waves climbing sloping beaches analytically for different initial wave forms. He proposed that, any initial wave form can first be represented in the transformation space using the linearized form of the Carrier-Greeenspan transformation for the spatial variable, and then the nonlinear evolutions of these initial waveforms can be directly evaluated. After necessary transformations, he introduced a simplified equation for the calculation of runup/rundown motion of the shoreline. This approach is applied to Gaussian and leading-depression N-wave initial forms presented by Carrier et al. (2003) and results are compared. The method is also applied to the different N-wave initial forms, such as leading-depression isosceles N-wave and generalized N-wave initial forms, presented by Tadepalli and Synolakis (1994), and some similar trends are observed in the maximum runup results.

Kanoğlu (2004) concluded that his study appears simpler than in Carrier at al. (2003) and produces identical results since his analysis does not need to solve singular elliptic integrals. He also suggested that, based on the convenience of nonlinear shallow-water wave equations for the quantitative and qualitative predictions, the method outlined in his study may be

useful to assess the impact of long waves generated by seafloor displacements and to validate numerical codes.

Long wave runup on piecewise linear topographies is investigated in Kanoğlu and Synolakis (1998). In their study, they develop a general solution method for determining the amplification factor of different ocean topographies consisting of linearly varying and constant-depth segments to study how spectral distributions evolve over bathymetry, and apply their results to study the evolution of solitary waves.

Liu et al. (1995) investigated runup of solitary waves on a circular island. They studied the interactions of solitary waves climbing up a circular island and described a series of large-scale laboratory experiments with waves of different incident height-to-depth ratios and different crest lengths. They also developed a numerical model based on the two-dimensional shallow-water wave equations including runup calculations. Under certain conditions, they observed runup and wave trapping on the back side of the island by using this numerical model.

OCDI in “Technical Standards and Commentaries for Port and Harbor Facilities in Japan” (2002) explains the transformation of tsunami in a bay with related commentaries and technical notes. They stated that during tsunami inundation in a bay, the most important types of transformations of tsunami are the increase in wave height and flow velocity caused by the decrease in the cross-sectional area toward the end of bay, and the increase in wave height induced by seiche in a bay. Under the assumption of small amplitude waves, they suggested to use Green’s equation in order to calculate the influence of the change in cross-sectional area as given below.

$$\frac{H_0}{H} = \left(\frac{B_0}{B}\right)^{1/2} \left(\frac{h_0}{h}\right)^{1/4} \tag{2.6}$$

Here, H is height of long waves for a cross section with the width B and the water depth h (m), and H_0 is height of long waves for a cross section with the width B_0 and the water depth h_0 (m). They also specified that this equation is applicable in case of having gentle variations in both the width and the water depth, and having no reflected waves moving offshore. They added that this equation does not consider the energy loss due to friction and also can not be applied to the area of shallow water when there are reflection effects at the end of the bay.

In the light of these studies in literature, the distribution of a new parameter, suggested by Prof. Dr. Mustafa Erdik and approved by Synolakis and Yalçıner (2005), and named as hydrodynamic demand, is investigated during tsunami inundation together with the distributions of major tsunami parameters as maximum positive amplitudes and maximum currents using numerical model TUNAMI-N2. The details of this study are given in the following sections.

CHAPTER 3

THEORETICAL & NUMERICAL BACKGROUND

3.1 Theoretical Background

When tsunamis begin to approach to the shoreline or propagate into bays, they initially show a classic attribute that is described by linear long wave theory in deep sea (Sümer et al., 2007). Since the wave height increases and wave length decreases while coming close to the shore, nonlinear effects of tsunamis often become significant. In case of wave breaking, the behavior of bores can be clearly observed. There are several examples of this phenomenon in the amateur video clips taken from several locations in Indian Ocean during December 26, 2004 tsunami event. In addition, documents from the 1960 Chilean tsunami impact in Hilo, Hawaii are also very useful sources for understanding this behavior.

The major effect of tsunami is the direct effect on coastal and marine structures which can be very extensive and often disastrous. Tsunami waves can (1) drag the whole structures or their units at land or vessels in the sea, (2) damage the buildings with accumulated shoreline debris carried on the advancing wave fronts, (3) undercut foundations and pilings with erosion caused by the receding waves, (4) overturn structures by suction of receding or thrust of advancing waves, (5) cause damage of large ships with docks during oil or cargo transfer procedures having the risk of destructive fires (see examples in Figure 3.1). The fire damage can be quite unexpected as observed during the 1998 Hokkaido-Nansei-Oki tsunami that Aonae in Okushiri had exhausted by fires triggered after the waves had calm down. Tsunami hazards are also a very great financial

burden to the national economy since tsunami damages are enormously hard to repair.

(a) dragging the whole structures or their units at land or vessels in the sea

(b) damaging the buildings with accumulated shoreline debris carried on the advancing wave fronts

(c) undercutting of foundations and pilings with erosion caused by the receding waves

(d) overturning of structures by suction of receding or thrust of advancing waves

Figure 3.1: Direct Effects of Tsunamis on Coastal and Marine Structures

Borrero et al. (2005) stated that after the landslide scenario in the San Pedro Escarpment in California, a tsunami can be triggered and give damage to the ports of Los Angeles and Long Beach and the losses will range from US$7 to US$42 billion, in addition to the losses due to structural damage.

Tsunami waves cause very strong currents when coming to the shallow waters and as a result of these forceful currents, they can draw very huge and heavy objects far inland. There are many reports and observations about the large objects that were dragged by tsunamis and transported inland. Figure 3.2(a) shows a beach rock drawn by the 1993 Okushiri Tsunami. This rock has been transported nearly 30*m* inshore at 5*m* inundation height from the shoreline (Yeh, 2006). Another mind-bending event as an evident of this phenomenon is the 1868 Arica, Chile Tsunami which had moved a huge ship about 3.2 kilometers (2 miles) inland. The more interesting thing is that the same ship has been moved back to shore during the 1877 Arica Tsunami and had been able to sail. Nonetheless, it is not necessary to have mega tsunamis for object-drawing inshore. 1994 Mindoro, Philippines Tsunami is a very good example during which tsunami waves could have floated a 6000-ton power generating barge, broken its mooring lines, and transported it about 1.6 kilometers (1 mile) inland up to the Baryan River (Synolakis,2003). Figure 3.2(b) shows the barge at its final place after the drawing of tsunamis (Synolakis, 2003). Furthermore, during the December 26, 2004 event a smaller barge and the tug boat were carried about 100m inland at Lhongka as seen in the photograph taken by Prof. Synolakis (Figure 3.2(c)).

It is very essential to estimate the impact forces during tsunami inundation on account of causing collapse of high-cost coastal structures. These catastrophic results of a tsunami event has been explicitly observed in the December 26, 2004 Indian Ocean mega tsunami. The cost of losses estimated as more than 270,000 fatalities, 500,000 injured, and damages well in excess of $10 billion (NIST-NEHRP, 2005).

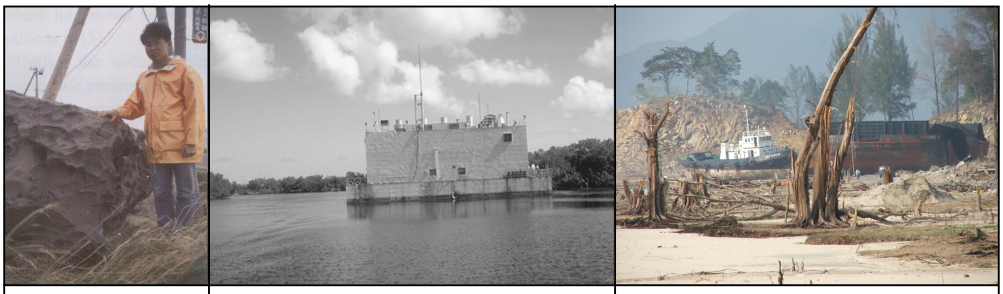

(a) (b) (c)

Figure 3.2: (a) A beach rock drawn by the 1993 Okushiri Tsunami and located about 30*m* inland at 5*m* height from the shoreline (Yeh, 2006). (b) The 6000-ton power generating barge that was carried about 1.6*km* inland by the 1994 Mindoro Tsunami (Synolakis, 2003). (c) A Barge and Tug Boat 100*m* inland (Lhongka).

The estimation of impact forces and currents is a recently-developed topic and not enough study exists as much as those about hydrodynamic evolution and inundation computations (Synolakis, 2003). However, none of them has been compared with laboratory or field data for accuracy.

Different methods and formulas in the literature for calculating forces on piles, on seawalls and structures, and debris impact forces on structures are described in the following section. Detailed information and discussion of results are also given in Synolakis (2003).

First of all, describing the Shallow Water (SW) Equations is a priority to explicitly comprehend the calculation of impact forces given in the following. As defined in Synolakis (2003), the SW equations describe the evolution of the water surface elevation and of the depth-averaged water particle velocity of waves with wavelengths large compared with the depth of propagation. The equations assume that the pressure distribution is hydrostatic every-where, i.e., there is no variation with depth of any of the flow variables other than the hydrostatic pressure. One general form of the SW equations is:

$$
\begin{aligned}
&h_t + (uh)_x + (vh)_y = 0 \\
&u_t + uu_x + vu_y + gh_x = gd_x \\
&v_t + uv_x + vv_y + gh_y = gd_y
\end{aligned}
\qquad (3.1)
$$

where $h(x, y, t)$ is the disturbed water depth which is expressed by the equation $h(x, y, t) = d(x, y) + \eta(x, y, t)$, $d(x, y)$ is the undisturbed water depth, $\eta(x, y, t)$ is the wave elevation measured with respect to the undisturbed water surface, u and v are the depth-averaged water particle velocities in the cross-shore *x* and long-shore *y* directions, respectively, and g is the acceleration of gravity.

3.1.1 Forces due to Structure Conditions

3.1.1.1 Forces on Piles

For calculating the impact forces on coastal structures, it is firstly necessary to determine the integration of pressure and the shear force over the area that is exposed to wave motion (Synolakis, 2003). The instantaneous wave force at time t, in the direction of wave propagation, should be computed to find the total wave force over a cylinder with radius of r. Assuming that a pressure is exerted on cylinder as $p(R, \theta, z, t)$, and a tangential shear stress exists as $\tau_{r\theta}(R, \theta, z, t)$, then the total force is given by:

$$
\begin{aligned}
F_T(t) = &\int_0^{\eta_p(t)+h_p} \left[\int_0^{2\pi} p(\theta, z, t) r \cos\theta \, d\theta \right] dz + \\
&\int_0^{\eta_p(t)+h_p} \left[\int_0^{2\pi} \tau_{r\theta}(\theta, z, t) r \sin\theta \, d\theta \right] dz
\end{aligned}
\qquad (3.2)
$$

where η_p and h_p are the local amplitude and undisturbed water depth at the face of pile, respectively. Here, it is assumed that these two parameters do not depend on the pile diameter changes. Since Navier-Stokes equations are not solved at this level of the calculations, it is impossible to

determine both the pressure and tangential shear stresses through the calculation of velocity gradients for steady flows. Therefore, a classic simplification is carried out in Equation 3.2 and a mass coefficient C_M including some of the dynamic pressure effects and a drag coefficient C_D including all the effects of the viscous forces on the cylinder are considered in the equation. After involving these coefficients, the force on a cylinder is expressed by:

$$F_T(t) = \int_0^{\eta_p(t)+h_p} \pi C_M \rho r^2 \frac{dV}{dt} dz + \int_0^{\eta_p(t)+h_p} C_D \rho r V |V| dz \qquad (3.3)$$

where V is the instantaneous horizontal velocity in the direction of wave motion, and dV/dt is the instantaneous water particle acceleration. Since $\vec{F}$ is a vector in the same direction with the velocity vector $\vec{V}$, then it is obvious that force in Equation (3.3) is in the direction of the wave propagation (Synolakis, 2003). Actually, Equation (3.3) is the sum of added mass and drag force terms. The absolute value of velocity V emphasizes the change of force direction as the changes of the direction of water particle velocity. The details are given in Synolakis (2003).

Dean and Harleman (1966) in Synolakis (2003) stated that the drag force term, that is the second term in Equation (3.3), was defined for steady flows. However, this derivation is used for strongly unsteady flows, such as impact of bores, in which a careful estimation of the coefficients C_D and C_M is essential. Details about the determination of the coefficient C_D are given in *Numerical Background* section above.

Equation (3.3) can also be used to calculate tsunami forces on piles for some cases. For instance, considering small amplitude wave theory, it is only valid for irrotational flow, and therefore is not used in case of wave breaking. Shallow-water wave theory (SW), given in Equation (3.1), is also for irrotational flow. However, it is valid for large amplitudes, for $L/d >> 1$,

while small amplitude wave theory is set up on the condition of $a/h << 1$. If small amplitude approximations are made for the shallow water limits, the horizontal velocity and acceleration are expressed respectively by:

$$u(x,t) = (a\sigma / kh)\cos(kx - \sigma t) \tag{3.4}$$

$$\frac{du}{dt} = -(a\sigma^2 / kh)\sin(kx - \sigma t) \tag{3.5}$$

Substituting Equations (3.4) and (3.5) into the Equation (3.3), assuming that the pile is located at $x = 0$, and using $k = 2\pi / L$ and $\sigma / k = \sqrt{gh}$, the total tsunami force on a pile is expressed by:

$$F_T(t) = -\rho p(\pi r^2 akh)C_M a\sin(\sigma t) + \rho g C_D a^2 r\cos(\sigma t)\left|\cos(\sigma t)\right| \tag{3.6}$$

It should be noted that Equation (3.6) is only valid for small-amplitude long waves (Synolakis, 2003). Equation (3.6) also represents the forces occurred as a result of earthquake-triggered tsunamis generated far field and for landslide tsunamis which are formed as one or two waves generating successively. For near-field tsunamis, where tsunami evolution distance is not sufficient to develop large waves, these equations should be used with all diligence.

Integrating the force over the height of the pile from the seabed to the free water surface, and using the same approximations as Equation (3.3), the total moment is calculated from:

$$M_T(t) = \frac{1}{2}\rho g C_D r a^2 h\cos(\sigma t)\left|\cos(\sigma t)\right| - \frac{1}{2}\rho g C_M \pi r^2 akh^2\sin(\sigma t) \tag{3.7}$$

3.1.1.2 Forces on Seawalls

The impact forces on vertical front faces of the structures had been calculated by Cross (1967) in Ramsden and Raichlen (1990) for which the

properties of incident surges propagating over smooth and roughened bottoms were investigated. The following equation is suggested to calculate the variation of the force on the wall with time as:

$$\frac{F_T}{\gamma \mathrm{b} (H_1)^2} = \frac{1}{2}\left(\frac{\eta_w}{H_1}\right)^2 + C_F \, {N_F}^2 \left(\frac{\eta_w}{H_1}\right) \tag{3.8}$$

where F_T is the total force on the vertical wall, $\eta_w = \eta(x = X_w, t)$ is the water surface elevation on the wall located at $x = X_w$, H_1 is the surge height, b is width of vertical wall, C_F is the force coefficient calculated as $C_F = 1 + (\tan\theta)^{1.2}$, and $N_F = \frac{c}{\sqrt{gH_1}}$ where c is the measured incident bore velocity.

For convenience in practical applications, Cross proposed using the force due to the hydrostatic pressure from the surge depth at the wall as if the wall were not there. It means that he calculated the surge profile η_w as if there were no wall along the inundation zone and the bore would pass through the inundation zone without being reflected from the wall and without having an increase in its wave height.

On the basis of Cross (1967), Ramsden and Raichlen (1990) made laboratory experiments and measured the forces on a vertical wall due to the impact of a bore being triggered by a broken solitary wave. In these experiments, the height of incident bores has shown a variation from 2.4*cm* to 4.9*cm* and their celerity was between 75*cm/s* and 126*cm/s*. The maximum measured forces were about five to seven times the hydrostatic force, depending on the height of the incident bore and the local still water depth. Considering this experiment in detail, the measurements include bore profiles at times before impact and during the reflection process, and bore profiles of the horizontal water particle velocity along the surface of the bore prior to impact, the celerity of the incoming bore, the time history

of the force on the wall, and the variation of the runup height on the wall as a function of time. Ramsden and Raichlen (1990) used the water depth at the wall d_w and rewrote Equation (3.8) as

$$\frac{F_T}{\frac{1}{2}\gamma \mathrm{b}\,(\mathrm{H}_1 + d_w)^2} = \left(\frac{\eta_w + d_w}{H_1 + d_w}\right)^2 + 2\,C_F\,{N_F}^2\,\frac{\eta_w\,H_1}{(H_1 + d_w)^2} \qquad (3.9)$$

The measured force in the experiment was compared with the force calculated from Equation (3.9). According to these relations, it is proved that the impact force depends on the local water depth at the sea wall d_w, the bore height H_1, and the slope of the front face of the bore $\tan\theta$.

Ramsden and Raichlen (1990) approach is valid for the conditions after the wave breaking. Since the numerical model TUNAMI-N2 used in this study does not simulate breaking well, the relations and results in Ramsden and Raichlen (1990) can not be used for the comparison with the numerical results of this study.

3.1.1 Forces due to Flow Conditions

Forces occurred during tsunami inundation should be investigated in order to determine the practical design conditions of the coastal structures. The Coastal Construction Manual (CCM), released by the Federal Emergency Management Agency (FEMA) in USA, states that loads to be formed during flood are (Synolakis, 2003):

- Hydrostatic forces, such as loads from standing or slowly moving water, denoted by F_{sta}, and buoyancy forces, denoted by $F_{bouyancy}$
- Hydrodynamic forces from rapidly moving water, broken and breaking waves, tsunami runup, denoted by F_D, and from structure effects, denoted by F_{dyn}

- Forces from breaking waves, denoted by F_{brkw}
- Forces from debris impact, denoted by F_i

There are no published results in literature about the determination of tsunami loads on rectangular structures. All the existing instructions make the load calculations based on the Design Flow Elevation (DFE), which is defined as the difference between the 100-year still-water elevation above datum and the lowest eroded ground elevation (Sümer et al., 2007). The worst case scenario for the tsunami disaster is the tsunami flooding together with the flooding from very strong rains (Synolakis, 2003). Hence, it should be over-viewed whether DFE is different than base flood elevation (BFE), represented the elevation associated with the "100-year flood", or a flood with a 1% chance of occurrence in any given year. Furthermore, DFE have to include the effects of tsunamis. By the consideration of all these points, CCM suggests that the design flood depth is expressed by:

$$d_s = E_{sw} - GS \tag{3.10}$$

where E_{sw} is the 100-year still-water elevation above the datum, and GS is the lowest eroded ground elevation, above the datum, adjacent to the structure, excluding the effects of local scour. In respect of CCM, if the flood velocities are accelerated due to some conditions, such as existence of a flood zone near the building site, steep slopes at the site, or some other buildings or obstructions adjacent to the structure, then the upper bound of the design flood velocity is calculated from:

$$V_s = 2\sqrt{gd_s} \tag{3.11}$$

which is twice the long wave celerity or called SW velocity at a depth of d_s.

The lateral hydrostatic load per unit width is estimated from:

$$F_{sta} = \left(\frac{1}{2}\right)\rho g d_s^{\,2} \tag{3.12}$$

The hydrostatic buoyancy force is calculated directly by the Archimedes' principle of buoyancy, which says that buoyancy force equals to the weight of the displaced fluid. If the structure is a floating body, buoyancy force is directly equal to the weight of the body. However, in case of having tied the structure foundation to the sea bottom, the buoyancy force should be determined by using the submerged volume of the body. Then, the buoyancy force is calculated from:

$$F_{bouyancy} = \rho\, g\, V_{submerged} = \gamma\, V_{submerged} \tag{3.13}$$

The drag force F_D is calculated from the following formula as:

$$F_D = \left(\frac{1}{2}\right) C_D \rho V^2 A \tag{3.14}$$

where A is the submerged frontal area of the pile that is exposed to wave motion and $A = 2rd_s$. For the calculation of impact loads on piles, CCM suggests $C_D = 1.2$ for non-breaking waves, and $C_{D_b} = 1.75$ for breaking waves that is used with $H_b = 0.78 d_s$. If CCM statements about the design flood velocity given in Equation (3.11) is used in drag force calculation and A is substituted into Equation (3.14), then drag force is expressed by:

$$F_D = 4 C_D \rho g d_s r \tag{3.15}$$

For the impact forces on vertical walls from breaking waves, CCM recommends the following formula for calculating the wave force F_{brkw} per unit width as:

$$F_{brkw} = 1.1 C_p \rho g d_s^{\,2} + 2.41 \rho g d_s^{\,2} \tag{3.16}$$

where C_p is the dynamic pressure coefficient ranged from 1.6 for an "accessory structure with low hazard to human life" to 2.8 for a coastal building to 3.6 for a high occupancy building or critical facility (Synolakis, 2003).

In the calculation of hydrodynamic force on a rectangular structure, CCM recommends two different approaches. The determining factor of these approaches is flood velocity V and CCM suggests using two different formulas for calculation of hydrodynamic force depending on whether the flood velocity V is larger or smaller than 3.03*m/sec*. CCM also recommends using an equivalent dynamic flow depth calculated from:

$$d_{dyn} = \left(\frac{1}{2}\right)\frac{C_D V^2}{g} \tag{3.17}$$

Since CCM recommends using Equation 3.11 in tsunami force calculations, then substituting Equation 3.11 into Equation 3.17, dynamic flow depth is:

$$d_{dyn} = 2C_D d_s \tag{3.18}$$

When the flood velocity *V*<3.03*m/sec*, which is the same condition as flow depth during tsunami flooding is smaller than to a limiting depth $d_s = 1.74\,m$, as shown in Synolakis (2003), the hydrodynamic force is given by:

$$F_{dyn} = \left(\frac{1}{2}\right)\rho g d_{dyn}^2 = 2C_D \rho g d_s^2 \tag{3.19}$$

Here, C_D is the drag coefficient and depends on the relative ratio of width of the structure b to the design flood depth d_s at the front of the structure. CCM recommends using $C_D = 1.25$ for $b/d_s < 12$, and $C_D = 2.0$ for $b/d_s > 12$. The reason is that when the width of the structure increases,

the drag force is also increases, because the frontal area of the structure increases and the suction pressures become smaller than hydrostatic pressure on the back face.

When the flood velocity *V*>3.03*m/sec*, CCM recommends calculating the hydrodynamic force from:

$$F_{dyn} = \left(\frac{1}{2}\right) C_D \rho V^2 d_s b \tag{3.20}$$

Debris loads cause serious damages during tsunami inundation. For instance, during the 1946 Alaska tsunami, in the area mostly exposed to significant tsunami hazard on Unimak and Senak Island, lots of logs had been dragged by tsunami waves from a nearby lumber plant and carried to elevations up to 42 m (Synolakis, 2003). The tsunami-borne logs are still present along the southern coastlines of Unimak and Senak.

The size of the object being carried by the flow should be predicted for calculating the debris impact loads. It is also necessary to estimate whether the objects are dragging along the beach face or the ocean floor. CCM describes a methodology for calculating forces from debris impact forces F_i , given by:

$$F_i = wV/(gt) \tag{3.21}$$

where w is the weight of the object impacting the structure, V is its velocity, g is the acceleration of gravity and t is the duration of impact. CCM recommends that if there is not enough criteria about the size of the debris, weight of the object can be considered as $w \cong 454\,kg$, with $V = \sqrt{gd_s}$. Obviously, large objects like vehicles can not be carried with the same speed as the tsunami current velocity. Therefore, Equation (3.21) has to be estimated with caution (Synolakis, 2003).

In addition, the calculation of the local DFE differs while the tsunami waves are thrust in land. As the wave evolves up on dry land, its velocity is not simply related to the square root of the gravitational acceleration times the flow depth, which is simply the long wave velocity. During tsunami inundation, the velocity in the runup zone can be as high as 3*m/sec*, yet the local depth might be smaller than 30*cm* (Sümer et al., 2007). If numerical results seem to be not significantly reasonable, then Sümer et al. (2007) recommends predicting the tsunami depth at the initial shoreline.

For the duration of debris impact t, CCM recommends certain ranges according to the types of structure materials (see Table 3.1). Heavier structures on short piles have higher stiffness, therefore low values would be used for heavier structures in the ranges, and the upper values are preferred for lighter structures on longer piles (Synolakis, 2003).

Table 3.1: Ranges for the Duration of Debris Impact t according to the Types of Structure Materials (CCM)

Ranges for t (sec)	Type of structure material
0.7-1.1	wooden walls
0.5-1.0	wooden piles
0.2-0.4	reinforced concrete walls
0.3-0.6	concrete piles
0.3-0.6	reinforced concrete piles, concrete masonry walls and pipes

No guidelines exist in literature for erosion due to the tsunami flooding. However, quite a few data has been collected about erosion and deposition during tsunami inundation, which have yet to be translated and put into standards and guidelines referred for the construction of engineered structures (Sümer et al., 2007). In literature, there are a large number of studies about scour around cylindrical piers, valid for steady flows and for steady flows together with the wave motion. Nevertheless,

the only study about erosion due to tsunami flooding was performed by Tonkin et al. (2003) in Sümer et al. (2007), which was a laboratory experiment, investigated the erosion caused by solitary waves attacking towards a circular cylinder.

3.2 Numerical Background

The current paradigm is to model tsunamis with the nonlinear shallow-water (NSW) equations. They can be derived directly from the Navier-Stokes equations, if one neglects viscous effects and depth-averages the resulting Euler equations. Their standard form is directly same with Equation (3.1). Another representation of this relation is given by:

$$\begin{aligned} &\frac{\partial \eta}{\partial t} + \frac{\partial [u(d+\eta)]}{\partial x} + \frac{\partial [v(d+\eta)]}{\partial y} = 0 \\ &\frac{\partial u}{\partial t} + u\frac{\partial u}{\partial x} + v\frac{\partial u}{\partial y} + g\frac{\partial \eta}{\partial x} = 0 \\ &\frac{\partial v}{\partial t} + u\frac{\partial v}{\partial x} + v\frac{\partial v}{\partial y} + g\frac{\partial \eta}{\partial y} = 0 \end{aligned} \tag{3.22}$$

where $\eta(x, y)$ is the water elevation, u and v are the depth-averaged horizontal velocities in x and y directions, respectively, $d(x, y)$ is the undisturbed basin depth, and g is the gravitational acceleration.

Different methods for the numerical solution of these equations exist in literature (Yeh et al., 1996). The current state of art for some models such as MOST (Titov and Synolakis, 1998) allows for real time tsunami inundation forecasting by incorporating real-time data from tsunameters (Titov et al., 2005). MOST, TUNAMI-N2 and COMCOT calculate tsunami inundation by computing the wave evolution on dry land and have been validated by comparing their results with exact analytical solutions and laboratory measurements, and results from field surveys. The model

MOST is used most often in United States for developing inundation maps (Borrero et al, 2003). TUNAMI-N2 was originally authored by Imamura (1993) for the Tsunami Inundation Modeling Exchange (TIME) program (Goto et al., 1997, Shuto et al., 1990). It is a registered copyright of Professors Imamura, Yalçıner and Synolakis and has been applied to several tsunami events (Yalçıner et al., 2001, 2002, 2003, 2004; Kurkin et al., 2003; Zahibo et al., 2003; Zaitsev et al., 2002) and also computation of resonant oscillations of basins for understanding indirect tsunami effects (Yalçıner and Pelinovsky, 2005).

In this thesis study, TUNAMI-N2 is applied by inserting new modules which calculate and compare wave front and current velocities, maximum positive amplitudes and hydrodynamic demand.

3.2.1 Parameters for the Computation of Hydrodynamic Demand

The main parameters used in the calculation of hydrodynamic demand are flow velocity and flow depth. First of all, it is necessary to identify the difference between water elevation, flow depth and runup. Figure 3.3 clearly illustrates these parameters.

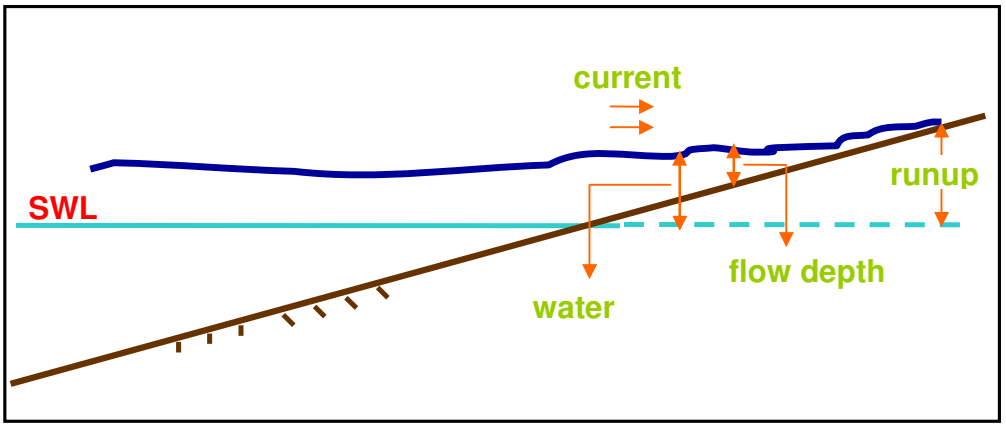

Figure 3.3: Sectional View of Water Elevation, Flow Depth and Runup

3.2.1.1 Calculation of Wave Front Velocity and Current Velocity

Wave front velocity is the velocity value occurred just in front of the wave where flow depth is zero. Figure 3.4 shows the location of wave front and its velocity.

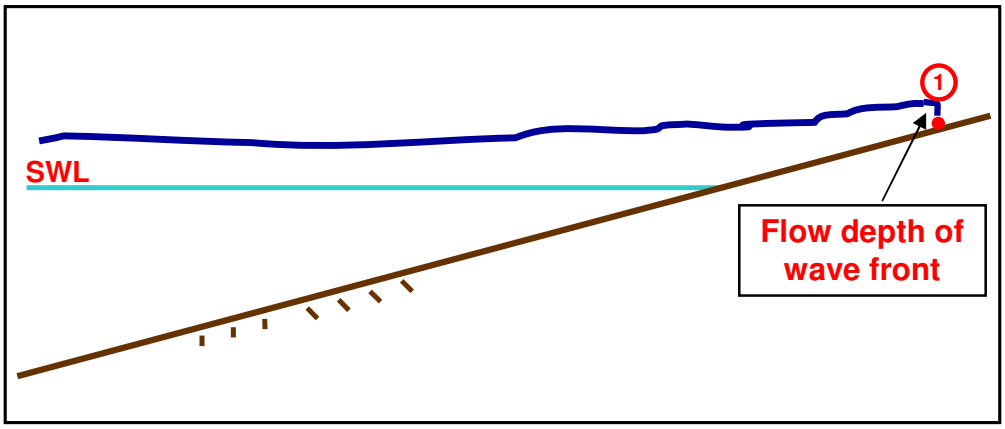

Figure 3.4: Sectional View of Wave Front Location

The numerical model divides the study domain into grid lines, uses finite difference method and calculates tsunami parameters at every grid nodes. Actually, wave front velocity should be calculated at point 1 where flow depth of wave front is zero (see Figure (3.4)). However, this point may not coincide with a grid node and the location of wave front can not be captured absolutely. Therefore, certain front depths (every 10*cm* between 0-100*cm*) are used in calculations.

Figure 3.5 shows the top view of illustration of wave front velocity calculation. As shown in figure, the study domain is divided into grid lines having the spacing of *dx* both in x and y-direction.

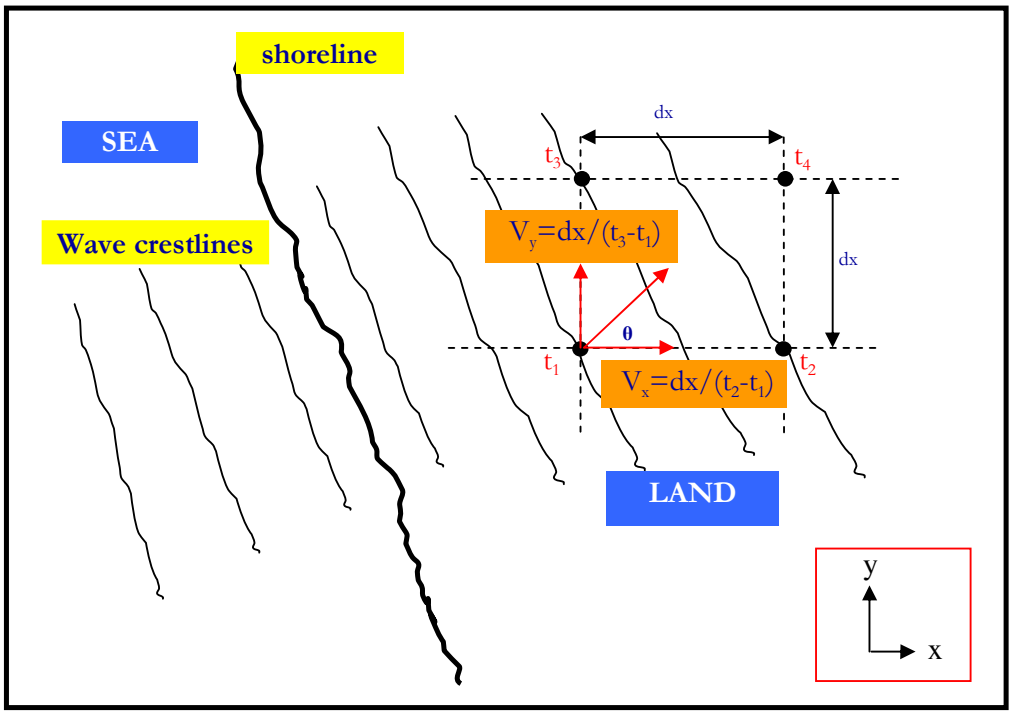

Figure 3.5: Top View of Illustration of Wave Front Velocity Calculation

During tsunami inundation, the model stores the times when the selected flow depth of wave front is just captured or at first time exceeded at each grid nodes. Afterwards, wave front velocity and its angle are calculated using the following relations:

$$V_x = \frac{dx}{t_2 - t_1} \tag{3.23}$$

$$V_y = \frac{dx}{t_3 - t_1} \tag{3.24}$$

$$\left|V_f\right| = V_x^{\,2} + V_y^{\,2} \tag{3.25}$$

$$\theta_f = \tan^{-1}\left(\frac{V_y}{V_x}\right) \tag{3.26}$$

where V_x and V_y are the wave front velocities in x and y direction at the grid nodes, respectively; t_1, t_2, t_3 are the times when the estimated flow

depth is just captured or is just exceeded at corresponding grid node, V_f is the equivalent wave front velocity at the grid node and θ_f is its angle.

The relations for current velocity are given in Equations (3.27) and (3.28) as:

$$u_c = \sqrt{Velx^2 + Vely^2} \tag{3.27}$$

$$\theta_c = \tan^{-1}\left(\frac{Vel_y}{Vel_x}\right) \tag{3.28}$$

where u_c is the current velocity and θ_c is its angle. Actually, $Velx$ and $Vely$ are directly equal to u and v that were calculated from Equation (3.22).

3.2.2 Calculation of Hydrostatic Force and Drag Force

For the computation of forces on the coastal and land structures, drag and hydrostatic forces can be used. The relation for the hydrostatic force is given by

$$F_h = \frac{1}{2}\rho_w g d^2 w = \frac{1}{2}\rho_w \; g \; d \; A \tag{3.29}$$

For the drag force, the relation is given by

$$F_D = \frac{1}{2}C_D \rho_w A u^2 \tag{3.30}$$

These approaches can be applied to calculate forces of flow onto the objects. The hydrostatic force on structures is calculated by obtaining the hydrostatic pressure exerted onto the calculated cross-sectional area of structure. Figure 3.6 illustrates this phenomenon.

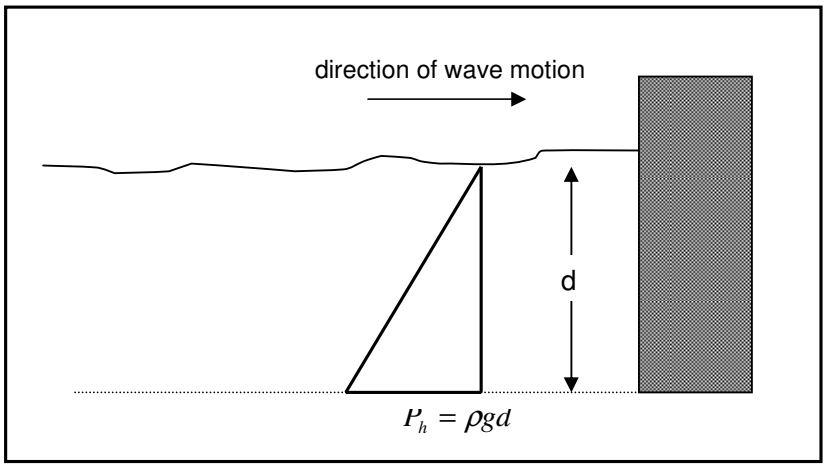

Figure 3.6: Sectional View of Hydrostatic Pressure on a Coastal Structure

3.2.3 Description of Hydrodynamic Demand

Hydrodynamic demand defined in this study is a dimensionless parameter represented as the ratio of drag force (exerted by the flow) to hydrostatic force onto the structure. The reason is that hydrostatic force can be taken as a reference force in order to obtain comparative dimensionless value for drag force.

The normalization of drag force by hydrostatic force gives

$$HD = \frac{F_D}{F_h} = \frac{\frac{1}{2} C_D \rho_w A u^2}{\frac{1}{2} \rho_w g d A} = C_D \frac{u^2}{g d} \tag{3.31}$$

Actually, $u^2/(gd)$ part is the square of Froude Number F_R, which is similarly obtained by flow velocity and flow depth. Therefore, hydrodynamic demand can be represented by:

$$HD = C_D * F_R{}^2 \tag{3.32}$$

The drag coefficient C_D mainly depends on structure shape and secondarily the flow conditions. It describes a characteristic amount of aerodynamic drag caused by water flow. Two objects having the same frontal area and exposed to same flow velocity will experience a drag force proportional to their C_D values. Therefore, drag coefficient for same shaped structures can change with the Reynolds number (a useful dimensionless number that is the ratio of the inertial force of the medium over its viscous force) and also with the roughness of the surfaces.

Table 3.2 summarizes all the suggestions for the value of drag coefficient C_D.

Table 3.2: Suggestions for the Value of Drag Coefficient C_D

Reference	**Structure Type**	C_D **value**
CCM in Synolakis (2003)	Piles	1.2 for non-breaking waves 1.75 for breaking waves
CCM in Synolakis (2003)	All Type of Coastal structures	1.25 for $b/d_s < 12$ 2.0 for $b/d_s > 12$
Arnason (2004) in Yeh (2006)	All Type of Coastal structures	1.0 – 2.0
Yalçıner and Synolakis in Sümer et al. (2007)	All Type of Coastal structures	less than 2

For the definition of hydrodynamic demand, the Froude number part of Equation (3.31) is taken into account. Using current or wave front velocity, the following relations can be developed for the determination of hydrodynamic demand as:

$$HD_1 = \frac{u_c^{\,2}}{gh}$$

$$HD_2 = \frac{V_f^{\,2}}{gh} \tag{3.33}$$

where u_c is current velocity, V_f is wave front velocity, h is the flow depth and g is gravitational acceleration.

In order to identify the distribution of hydrodynamic demands in inundation zone, different wave characteristics as different wave type, initial amplitude, period and directions, sea bottom slope and structural distribution are investigated in the following section.

CHAPTER 4

MODEL APPLICATION

The numerical model TUNAMI-N2 is used to investigate the distribution of hydrodynamic demands in inundation zone. A new module is inserted in the model to calculate the hydrodynamic demands as given in Equation (3.33), wave front and current velocities as described in Figure 3.5 and in Equations (3.23)-(3.25) & (3.27), and their angles as given in Equations (3.26) & (3.28).

4.1 Model Parameters

Figure 4.1 shows a typical cross-section of the study domain. Several wave shape, wave height, wave period and directions are used in two different bottom slopes with and without coastal and land structures.

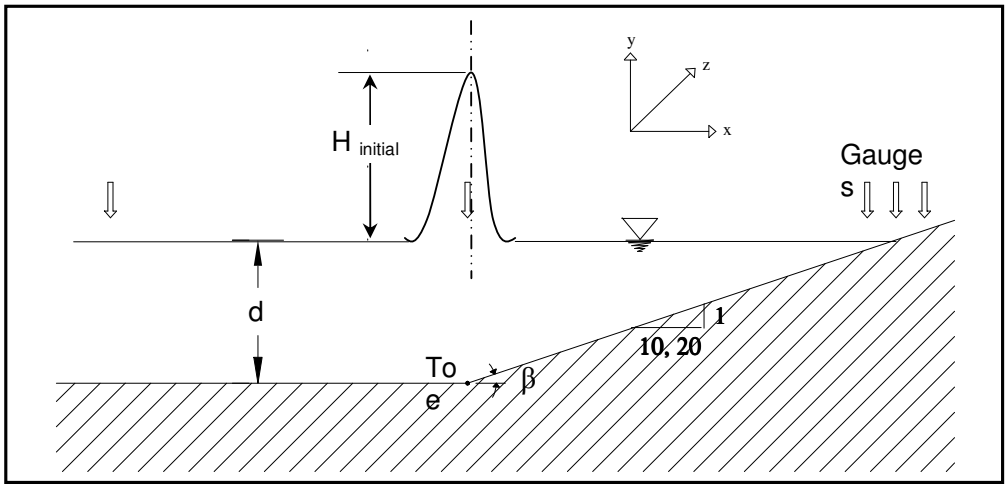

Figure 4.1: Cross Section of the Basin, Location of the Initial Wave and the Gauge Locations where the Water Surface Elevations are computed.

Table 4.1 gives the initial wave heights in the numerical model and their values at the toe of each slope, as *1/10* and *1/20*, accordingly. The simulations were performed for two different wave approaches: perpendicular (90º) and oblique (45º). For each wave approaches, two different wave shapes were selected, as leading elevation wave (LEW), leading depression wave (LDW), both of which are single sinusoidal waves. The first three initial wave heights were applied at a location about 235*m* before the toe of slope. The reason for this is to avoid the effects of flow depth changes to the wave height at the toe. The maximum positive and maximum negative amplitudes are given in the table for each wave angle and bottom slope. The last two rows indicate that these two simulation series start to propagate the first waves from the toe location.

Table 4.1: Parameters used in the Model

		Angle= 90º		Angle= 45º	
		Wave height at the toe(m)		Wave height at the toe(m)	
Initial wave height(m)	wave type / slope	LEW	LDW	LEW	LDW
0.33	1/10	+0.35 -0.43	-0.35 +0.48	+0.30 -0.36	-0.30 +0.39
	1/20	+0.34 -0.33	-0.34 +0.33	+0.29 -0.29	-0.29 +0.30
0.74	1/10	+0.79 -1.00	-0.79 +1.06	+0.68 -0.82	-0.68 +0.83
	1/20	+0.76 -0.74	-0.76 +0.75	+0.65 -0.65	-0.65 +0.66
0.92	1/10	+0.98 -1.24	-0.98 +1.30	+0.84 -1.03	-0.84 +1.04
	1/20	+0.94 -0.92	-0.95 +0.93	+0.81 -0.81	-0.81 +0.83
0.5	1/10,1/20	0.5	0.5	0.5	0.5
1.0	1/10,1/20	1.0	1.0	1.0	1.0

Figure 4.2 and Figure 4.3 show three-dimensional view and top view of the study area, respectively. Two basins having open boundaries and the bottom slopes of *1/10* and *1/20* are shown with their dimensions. As seen from figures, the location of shoreline is same for both of the basins.

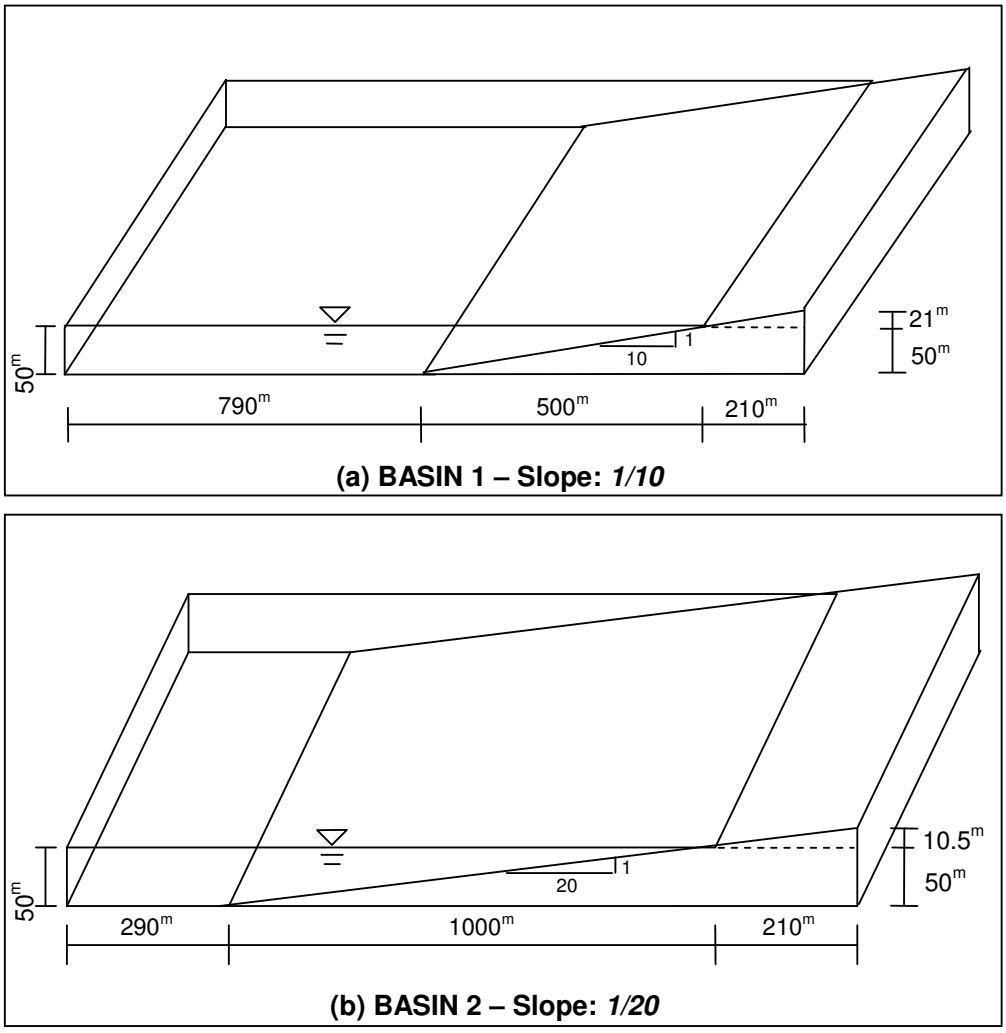

Figure 4.2: Three-Dimensional View of **(a)** Basin 1 with slope of *1/10* and **(b)** Basin 2 with slope of *1/20*.

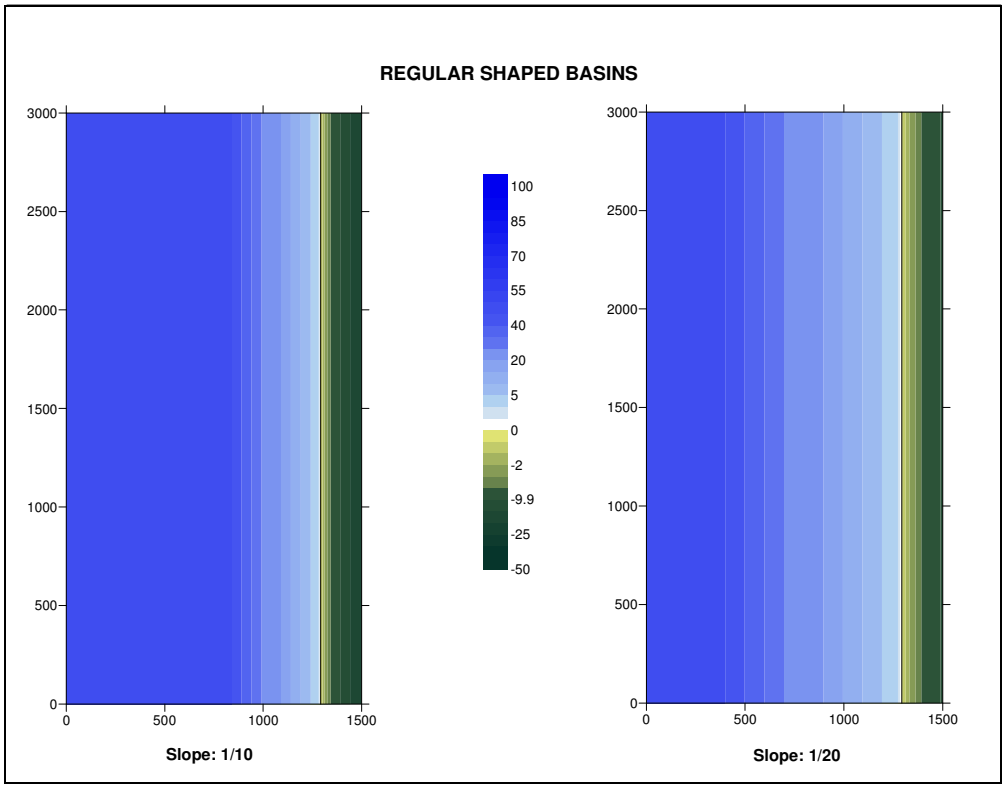

Figure 4.3: Top View of Basin 1 with Bottom Slope of 1/10 and Basin 2 with Bottom Slope of 1/10

Figure 4.4 shows top view of the study domain with its dimensions as $1500m$ in x-direction and $3000m$ in y-direction. Grid spacing is the same in both directions as $5m$. Therefore, study domain has 301 and 601 grid nodes in x and y directions, respectively. After checking the necessary duration for the arrival of wave to the shoreline with trial simulations, the simulation time was estimated as 4 minutes for both of the wave periods.

As described in Chapter 2, there are different approaches for the decision of flow velocity type used in impact force calculations. Therefore, it is necessary to compare the results of wave front velocity calculations with

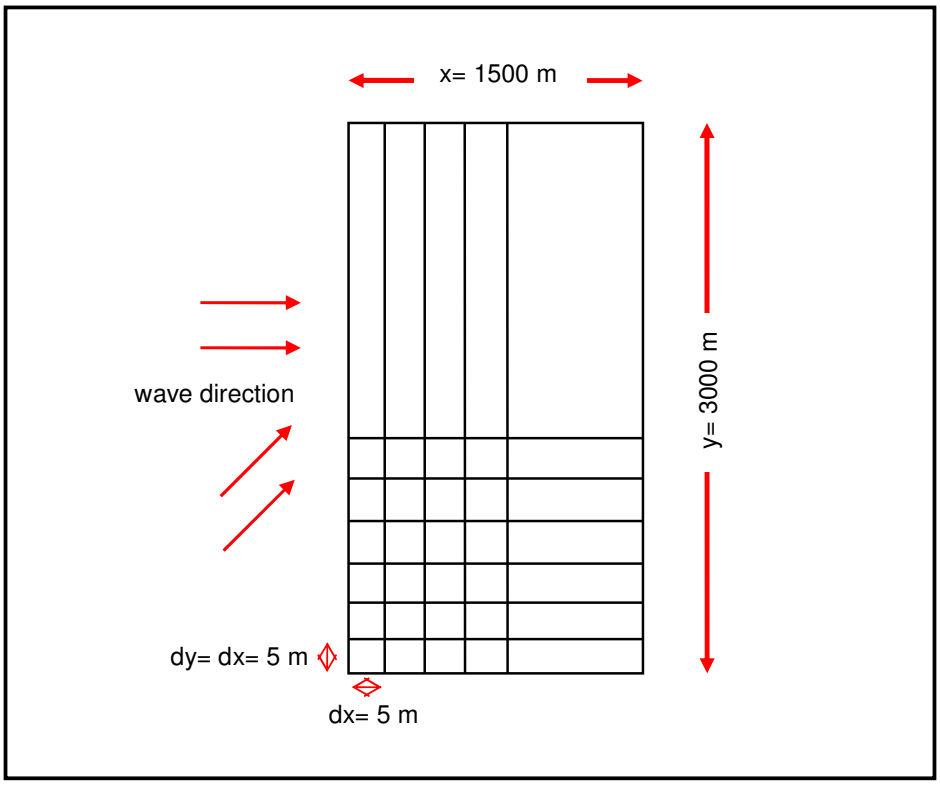

Figure 4.4: Top View of Study Domain with its Dimensions and Grid Lines

previous studies, and decide to use either current or wave front velocity or both of them in further calculations, comparisons and discussions.

4.2 Front Velocity Comparison

In order to compare the wave front velocity computations obtained in numerical study with the experimental ones, the Ph. D. study of Synolakis (1987) was used. His study provides snapshots of solitary wave section climbing up on a 1/19.85 sloping beach (see Figures 4.5(a) and 4.5(b)).

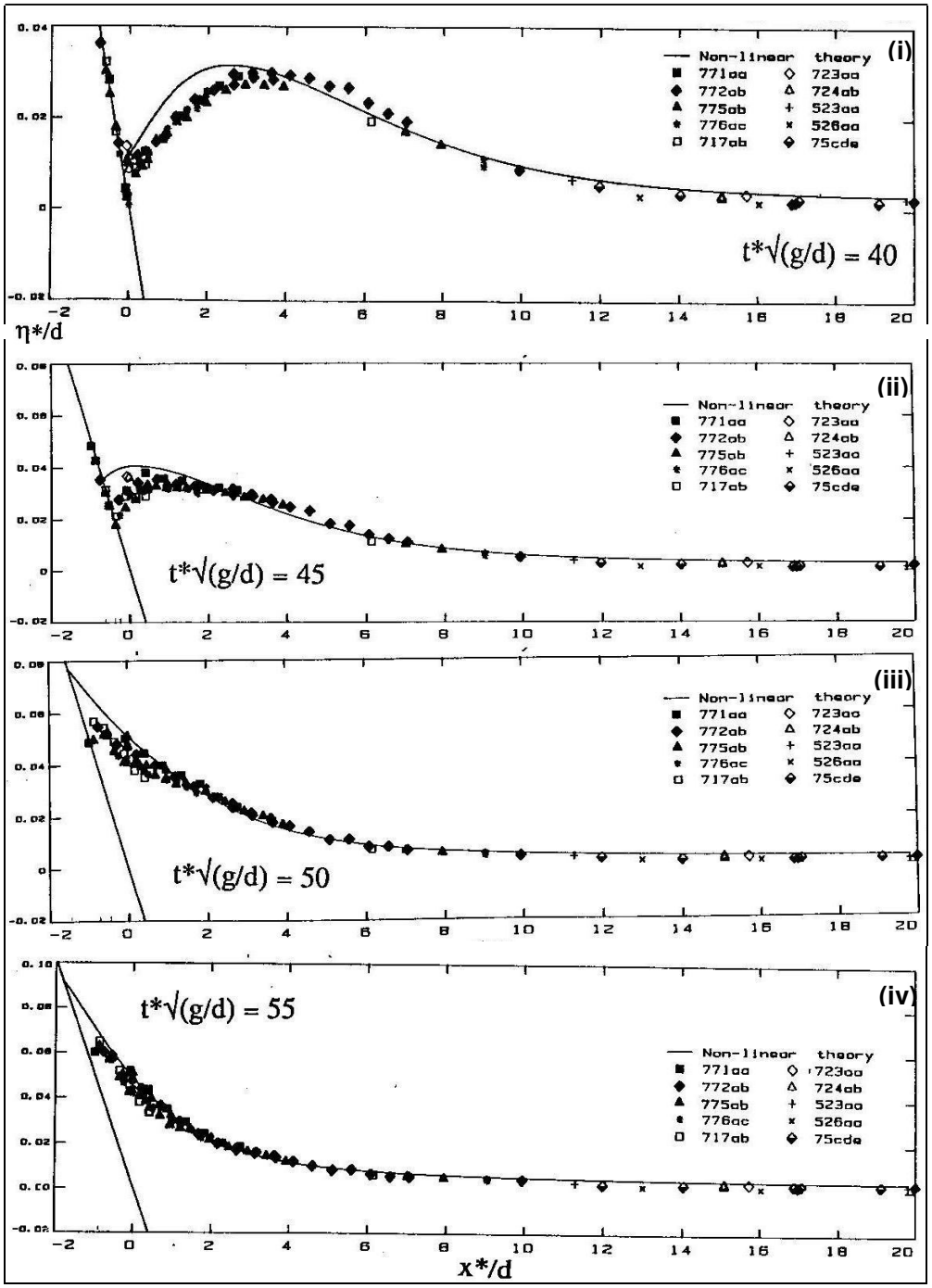

Figure 4.5 (a): Comparison between laboratory data and the nonlinear model for a 0.0185 solitary wave up on a 1/19.85 beach. Profiles are shown as functions of x at t= 40(i), 45(ii), 50(iii) and 55 (iv). Different symbols indicate different realizations of the same experiment (Synolakis, 1987).

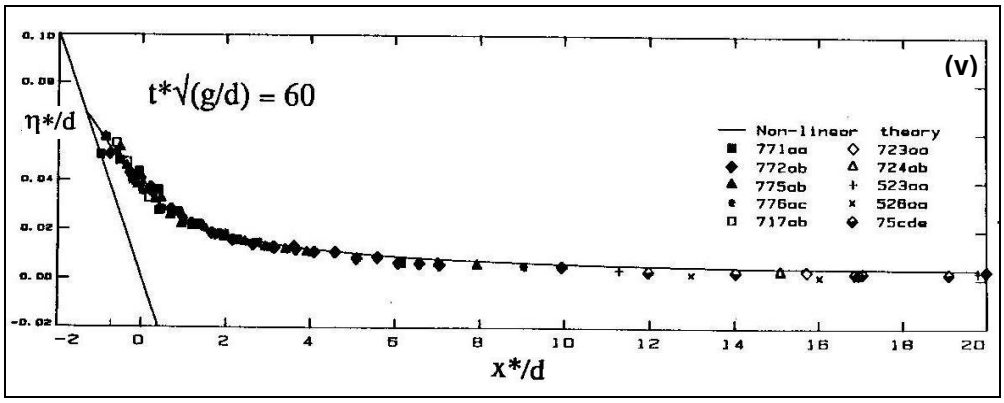

Figure 4.5 (b): Comparison between laboratory data and the nonlinear model for a 0.0185 solitary wave up on a 1/19.85 beach. Profiles are shown as functions of x at t=50 (iv) and 60(v). Different symbols indicate different realizations of the same experiment (Synolakis, 1987).

Same study was performed in numerical model. Wave front velocity of the solitary wave in inundation zone was calculated for the comparison. The bottom slope was used as 1/19.85 in simulations in order to be compatible with the experimental results obtained in Synolakis (1987).

Figure 4.6 shows the values of front velocities obtained by experimental studies in Synolakis (1987) and by numerical model, accordingly. The figure indicates that there is proportionality with experimental and numerical results of wave front velocity. Since only one experiment is not sufficient for a comparison, further analysis using front velocity is not performed anymore. It is necessary to make experiments for further comparison between front and current velocities. Data used in Figure 4.6 are given in Table 4.2 for each flow depths from 0 to 100*cm* used in the calculation of front velocity in numerical model.

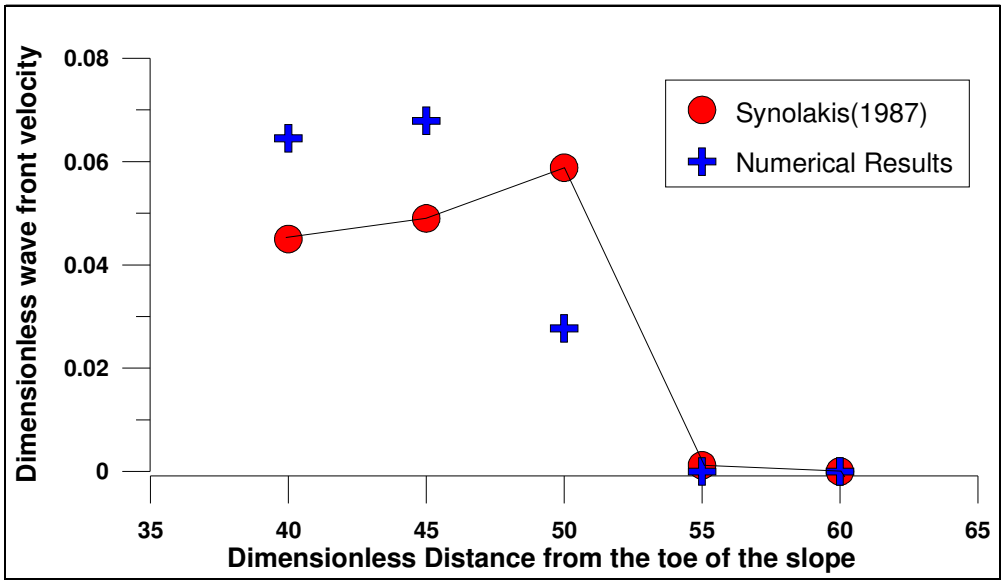

Figure 4.6: Comparison between Numerical Results found from TUNAMI-N2 and Experimental Results from Synolakis (1987)

Table 4.2: Wave Front Velocities for every certain dimensionless water depth from 0 to 0,020 at dimensionless time t=40, 45, 50, 55 and 60. The last row shows the wave front velocities calculated from the graphs of Synolakis (1987) given in Figure 4.5.

depth \ time	40	45	50	55	60
0	0.0625	0.0670	0.0262	0	0
10	0.0645	0.0679	0.0277	0	0
20	0.0623	0.0677	0.0283	0	0
30	0.0640	0.0679	0.0283	0	0
40	0.0618	0.0682	0.0312	0	0
50	0.0610	0.0698	0.0323	0	0
60	0.0612	0.0702	0.0318	0	0
70	0.0646	0.0689	0	0	0
80	0.0709	0.0714	0	0	0
90	0.0805	0.0698	0	0	0
100	0.0827	0.0131	0	0	0
Synolakis (1987)	0.045	0.049	0.059	0.0012	0

4.3 Computation and Comparison of Parameters Effecting Tsunami Impact

Tsunami effect in the inundation zone is directly related to (1) maximum positive amplitude, (2) maximum current velocity, (3) hydrodynamic demand, (4) maximum negative amplitude and (5) flow depth. Maximum positive amplitude is important for several coastal regions. Maximum current velocity is important for erosion/deposition pattern and debris drag. Hydrodynamic demand is an instantaneous value during inundation depending on water velocity and flow depth. Maximum negative amplitude is essential for the ships and boats at shallow region since water depth decreases. Flow depth is another governing parameter for the hydrodynamic demand.

First three parameters, that are maximum positive amplitude, maximum current velocity and hydrodynamic demand, are determining factors for tsunami impact in inundation zone. Besides, flow depth is a secondary parameter but also important for computation of the hydrodynamic demand. The hydrodynamic demand is an instantaneous parameter depending on current velocity and flow depth at the same time. Since current velocity and flow depth are changing independently, then the maximum value of hydrodynamic demand also varies with time. However, this situation is not so significant in steeper slopes (*1/10*).

In Kanoğlu (2004), it is emphasized that the maximum current velocities and accelerations are observed under backward motion (rundown) of the wave. In this study, the simulation duration is 4 minutes which fully covered forward motion of the wave and partly covered backward motion especially for the slope of *1/20*.

The distributions of these three parameters in inundation zone are investigated by numerous simulations using different wave and shore

conditions. The study domains are given in Figure 4.7 in detail. The distributions of maximum coastal amplitudes, maximum current velocities and hydrodynamic demands will be presented using the extracted parts of the whole bathymetry including the shore-parallel and shore-perpendicular structures, respectively.

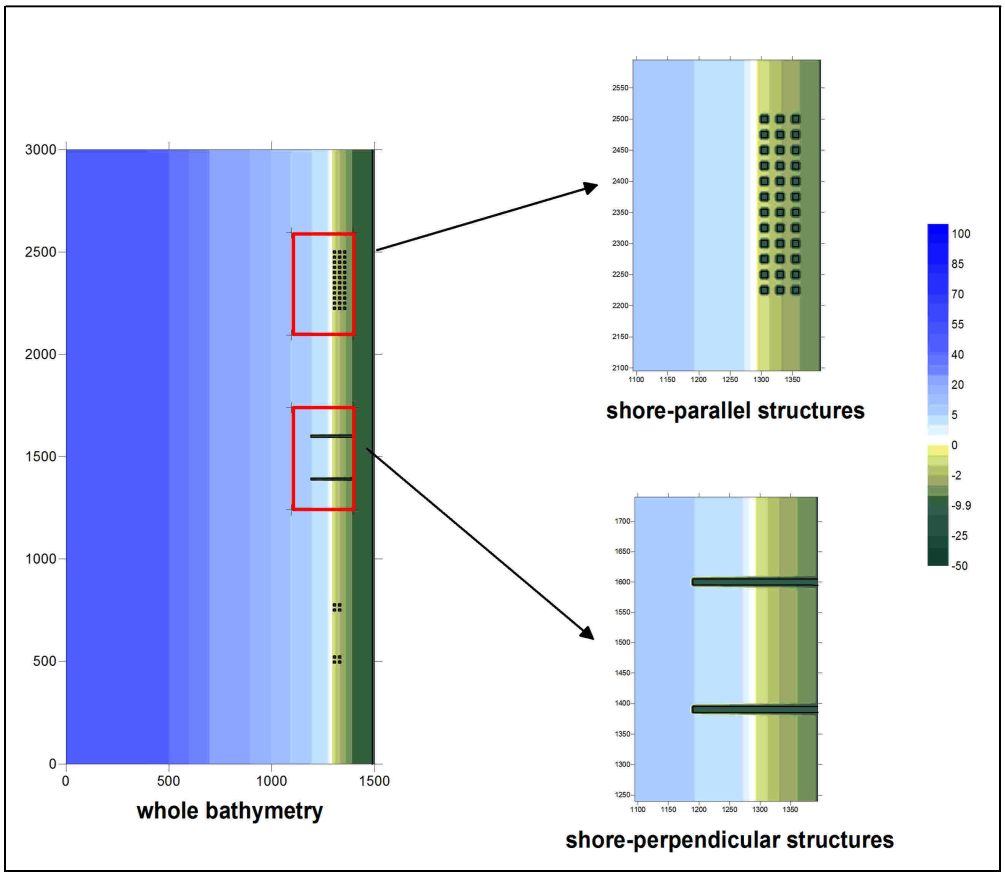

Figure 4.7: Top View of Shore-Parallel Structures and Shore-Perpendicular Structures Extracted from the Whole Bathymetry

4.3.1 Distribution of Maximum Positive Amplitudes for Perpendicular Approach of the Wave (angle=90º)

In this section, the distributions of maximum positive amplitudes (maximum water surface elevations) in basins 1 and 2 are presented which were computed during various simulations. The results are given for each bottom slope.

Figure 4.8 shows distribution of maximum positive amplitudes for LEW type single sinusoidal wave with period of 3 minutes and different initial amplitudes for bottom slope of *1/10*. Figure 4.9 shows distribution of maximum positive amplitudes for LDW type single sinusoidal wave with period of 3 minutes and different initial amplitudes for bottom slope of *1/10*. As seen from these Figures, higher amplitude incoming wave causes higher maximum coastal amplitudes. For the case of leading depression type of incoming wave (LDW), the coastal amplitudes are much higher comparing to the case of leading elevation type of incoming wave (LEW).

Figure 4.10 shows distribution of maximum positive amplitudes for LEW type single sinusoidal wave with period of 3 minutes and different initial amplitudes for bottom slope of *1/20*. Figure 4.11 shows distribution of maximum positive amplitudes for LDW type single sinusoidal wave with period of 3 minutes and different initial amplitudes for bottom slope of *1/20*. As seen from these Figures, similar trend is observed in terms of having higher coastal amplitudes for higher amplitudes of incoming waves as in *1/10* slope case. When slope effect is checked, milder slope (*1/20*) causes higher coastal amplitudes for LDW than the amplitudes for the steeper slope (*1/10*). In contrary, milder slope (*1/20*) causes lower coastal amplitudes for LEW than the amplitudes for the steeper slope *1/10* (see Appendix A, Figures A.1-A4 for the results of same kind of simulations using different incoming wave amplitudes).

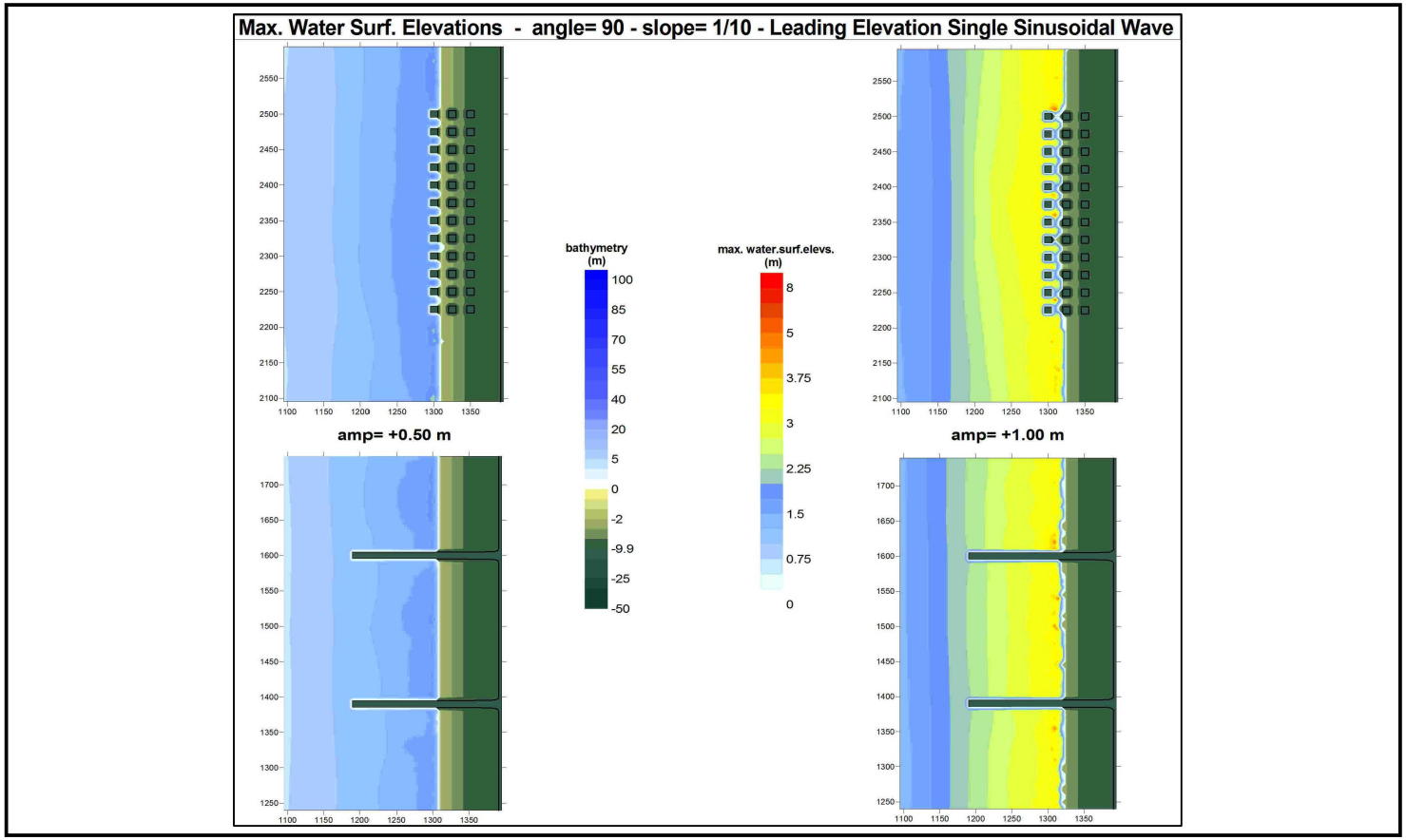

Figure 4.8: Distribution of Maximum Positive Amplitudes for Perpendicular Approach of the Wave (angle=90º) with Period of 3 min. for LEW with the Bottom Slope of 1/10 (Incoming Wave Amplitudes= +0.5m, +1.0m at the toe)

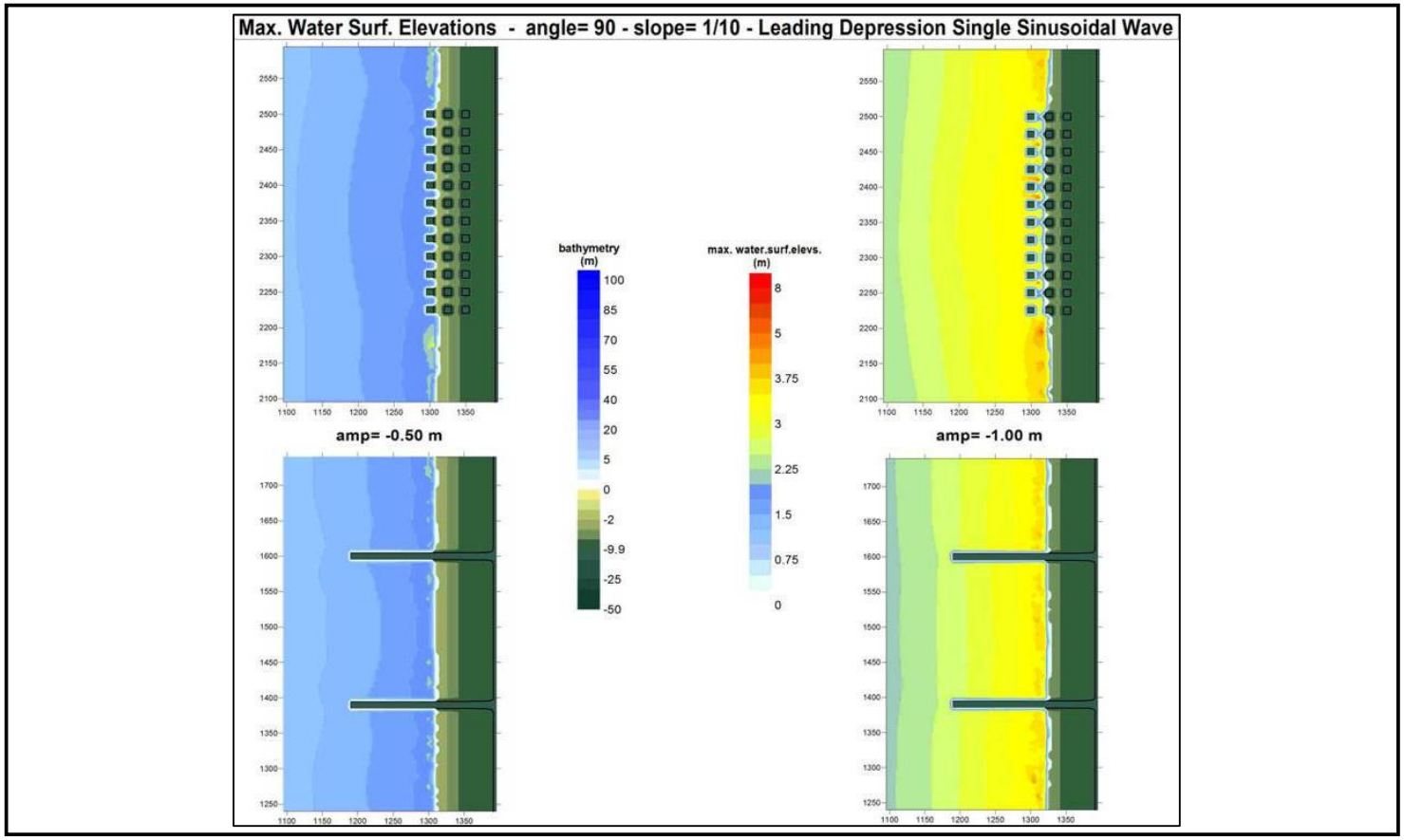

Figure 4.9: Distribution of Maximum Positive Amplitudes for Perpendicular Approach of the Wave (angle=90º) with Period of 3 min. for LDW with the Bottom Slope of 1/10
(Incoming Wave Amplitudes= +0.5m, +1.0m at the toe)

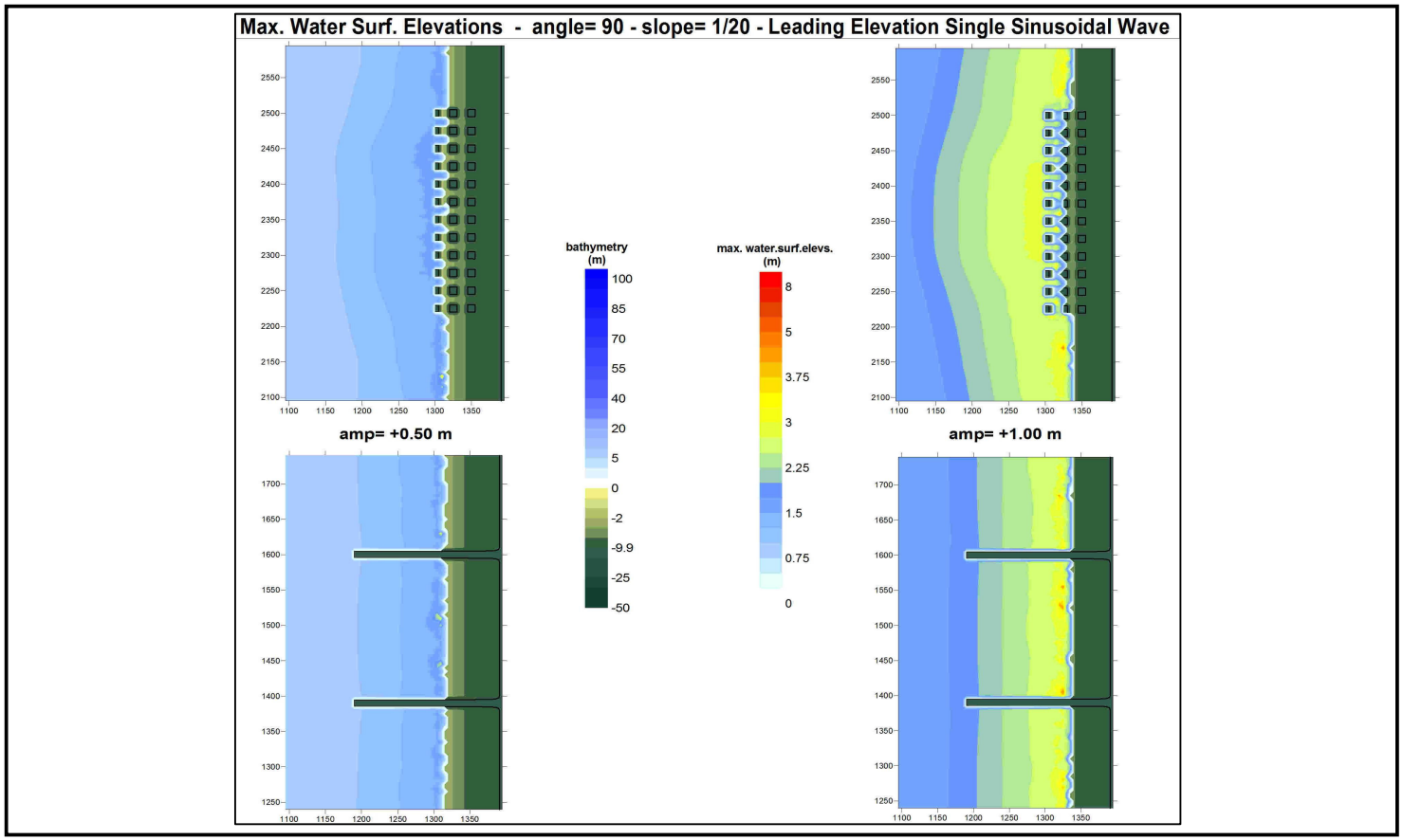

Figure 4.10: Distribution of Maximum Positive Amplitudes for Perpendicular Approach of the Wave (angle=90º) with Period of 3 min. for LEW with the Bottom Slope of 1/20
(Incoming Wave Amplitudes= -0.5m, -1.0m at the toe)

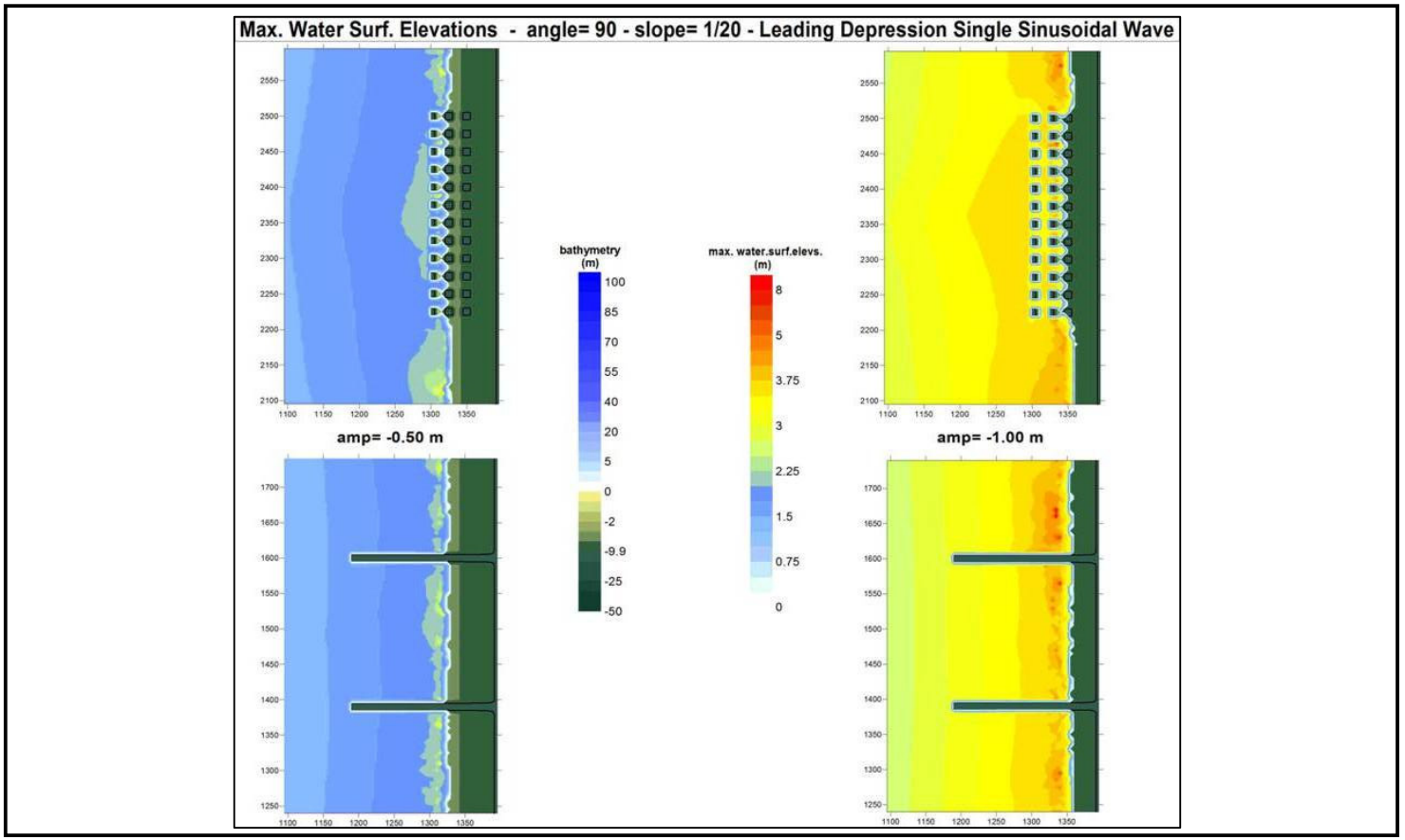

Figure 4.11: Distribution of Maximum Positive Amplitudes for Perpendicular Approach of the Wave (angle=90º) with Period of 3 min. for LDW with the Bottom Slope of 1/20
(Incoming Wave Amplitudes= -0.5m, -1.0m at the toe)

4.3.2 Distribution of Maximum Positive Amplitudes for Oblique Approach of the Wave (angle= 45º)

Figure 4.12 shows distribution of maximum positive amplitudes for LEW type single sinusoidal wave with period of 3 minutes and different initial amplitudes for bottom slope of *1/10*. Figure 4.13 shows distribution of maximum positive amplitudes for LDW type single sinusoidal wave with period of 3 minutes and different initial amplitudes for bottom slope of *1/10*. As seen from these Figures, when waves are approaching obliquely, higher coastal amplitudes are observed at the wave side of the shore-perpendicular structures. But, when single structures are located parallel to the shoreline, then the lower amplitudes are observed at wave side. LDW causes higher coastal amplitudes comparing to the LEW.

Figure 4.14 shows distribution of maximum positive amplitudes for LEW type single sinusoidal wave with period of 3 minutes and different initial amplitudes for bottom slope of *1/20*. Figure 4.15 shows distribution of maximum positive amplitudes for LDW type single sinusoidal wave with period of 3 minutes and different initial amplitudes for bottom slope of *1/20*. As seen from these Figures, similar trend is observed in terms of having higher coastal amplitudes for higher amplitudes of incoming waves as in *1/10* slope case. When the effects of bottom slopes are compared, steeper slope (*1/10*) causes higher coastal amplitudes both for LEW and LDW than the amplitudes for the milder slope (*1/20*) for oblique-approaching incoming waves. It is noted that this trend is in contrary with the case of perpendicular-approaching incoming wave. Looking at the effects of wave direction, it is observed that perpendicularly-approaching waves cause higher coastal amplitudes than obliquely-approaching waves (see Appendix A, Figures A.5-A8 for the results of same kind of simulations using different incoming wave amplitudes).

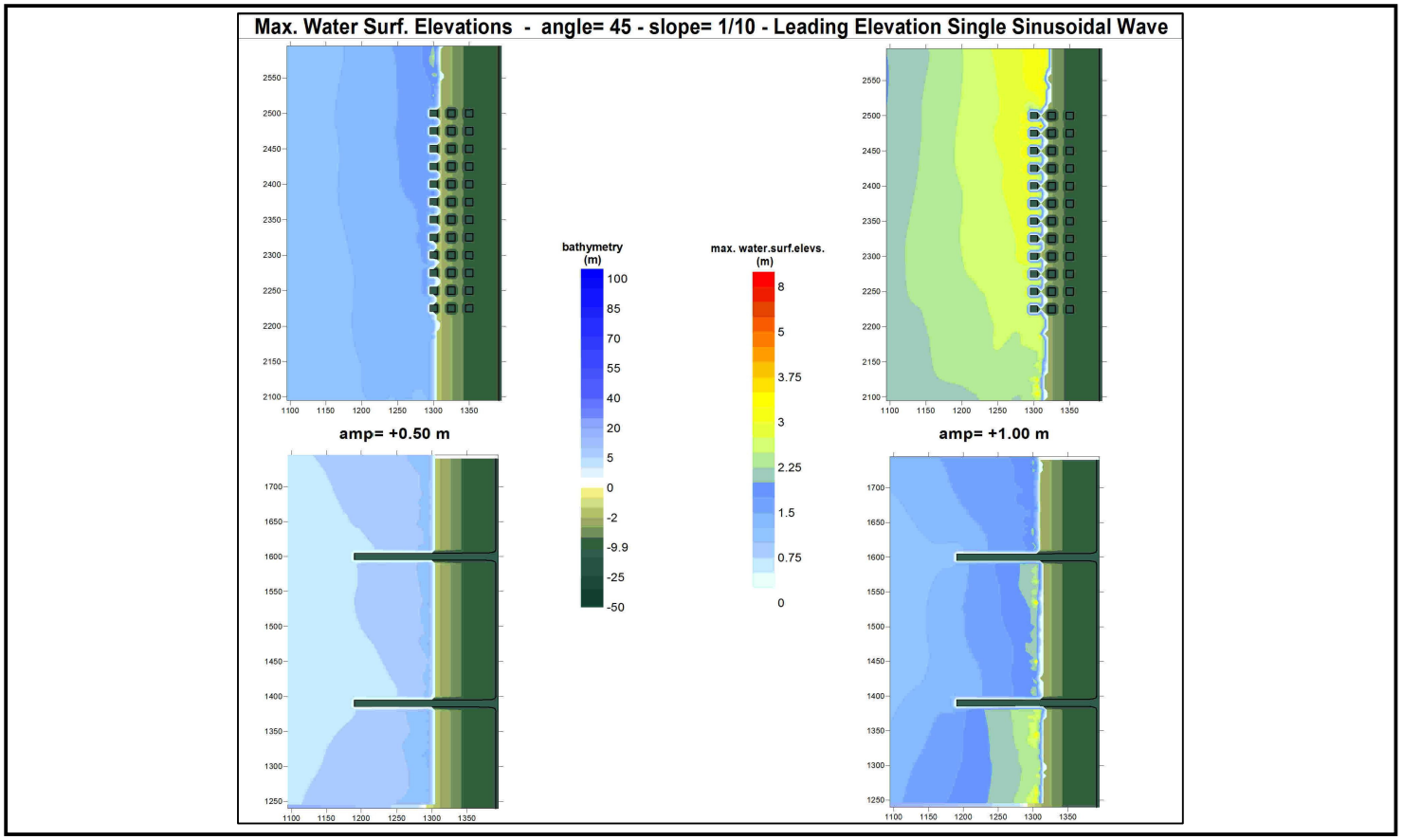

Figure 4.12: Distribution of Maximum Positive Amplitudes for Oblique Approach of the Wave (angle=45º) with Period of 3 min. for LEW with the Bottom Slope of 1/10 (Incoming Wave Amplitudes= +0.5m, +1.0m at the toe)

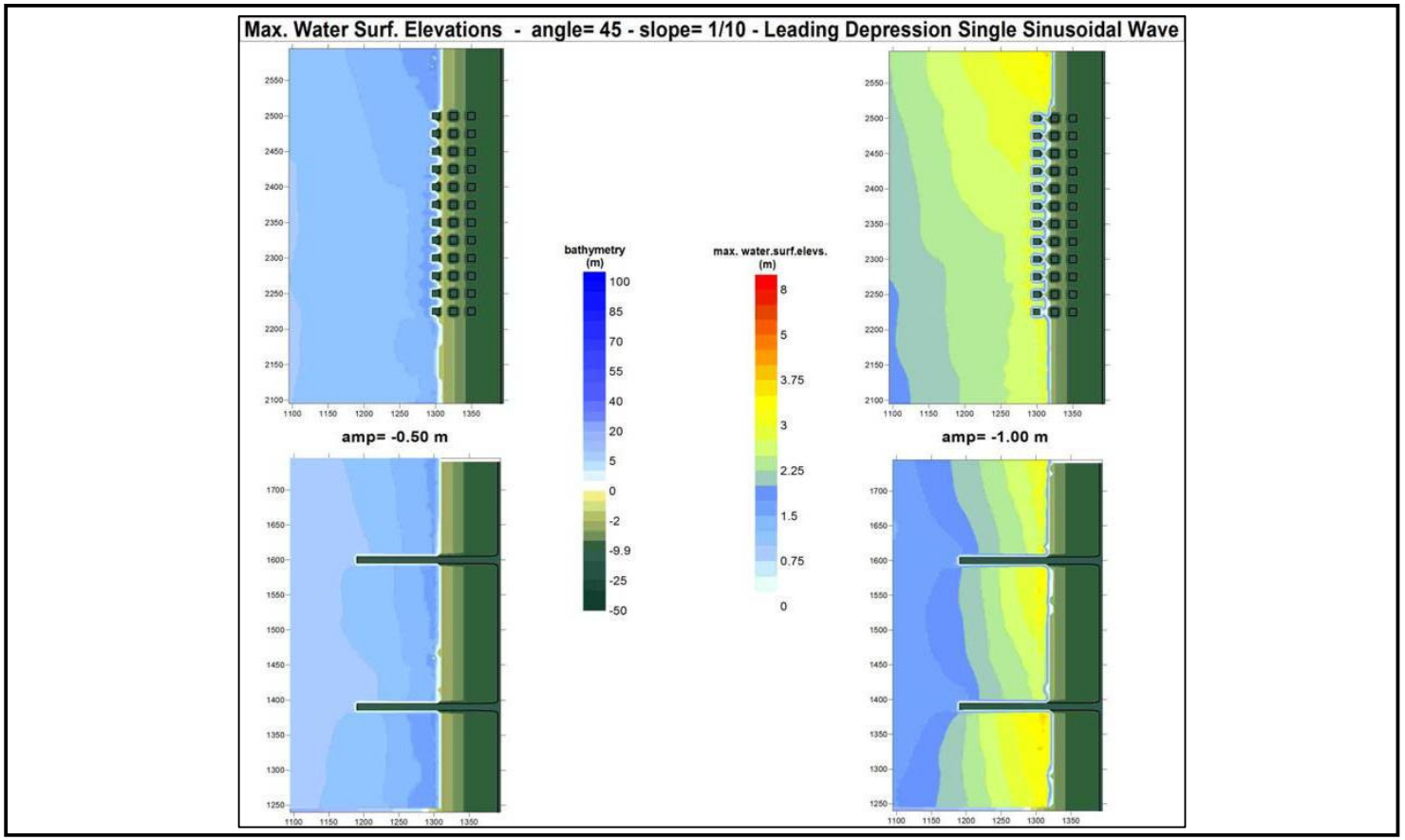

Figure 4.13: Distribution of Maximum Positive Amplitudes for Oblique Approach of the Wave (angle=45º) with Period of 3 min. for LDW with the Bottom Slope of 1/10
(Incoming Wave Amplitudes= +0.5m, +1.0m at the toe)

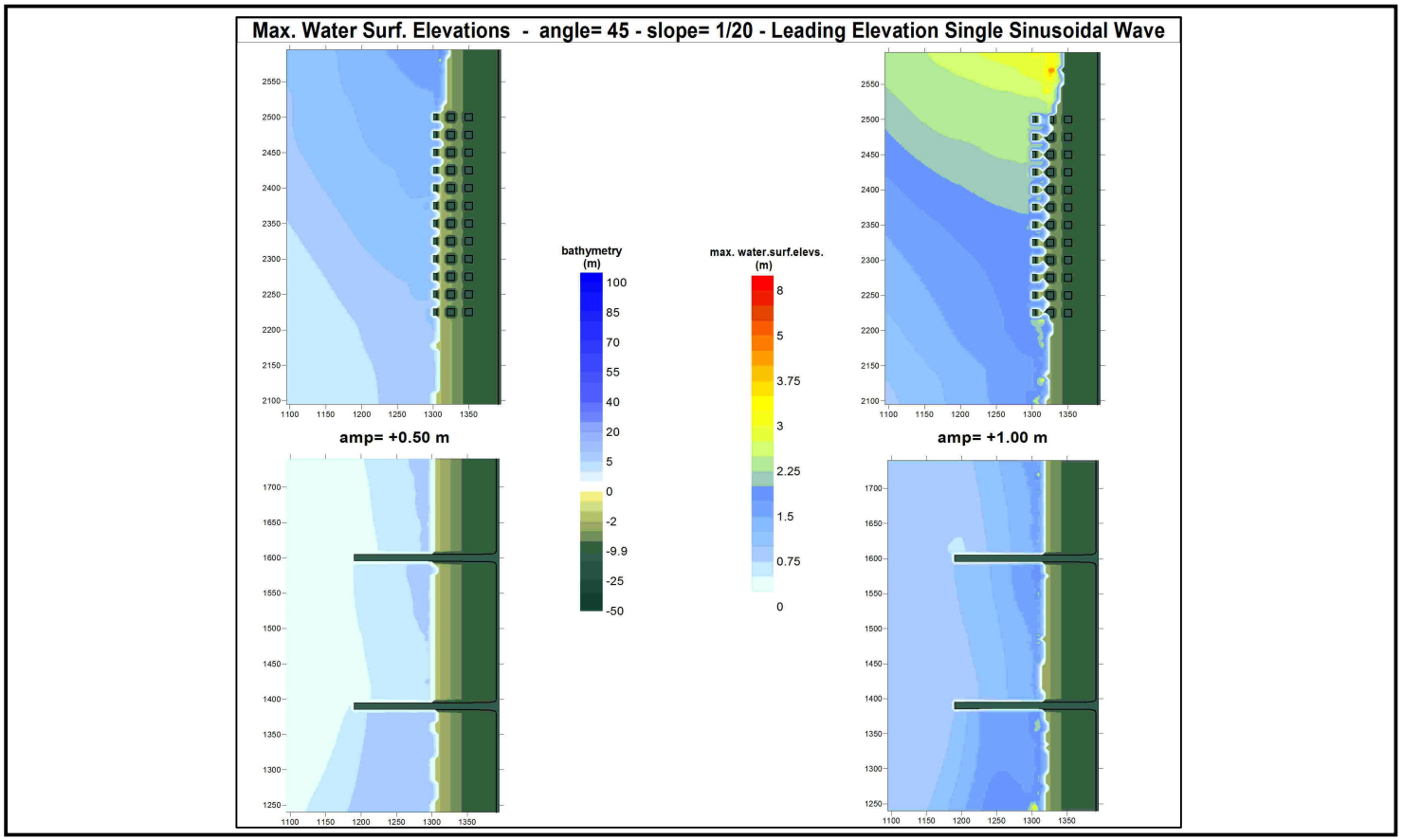

Figure 4.14: Distribution of Maximum Positive Amplitudes for Oblique Approach of the Wave (angle=45º) with Period of 3 min. for LEW with the Bottom Slope of 1/20 (Incoming Wave Amplitudes= -0.5m, -1.0m at the toe)

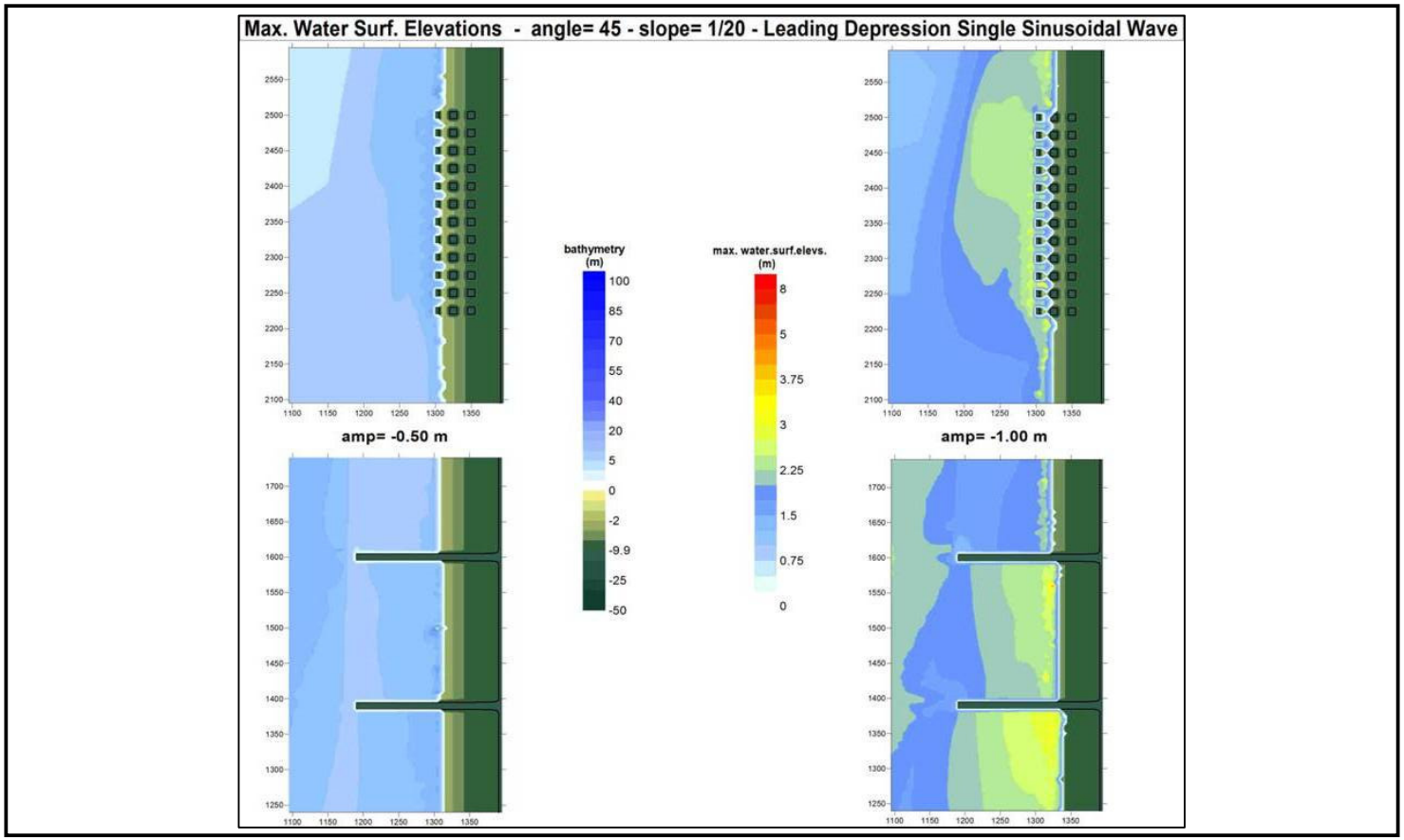

Figure 4.15: Distribution of Maximum Positive Amplitudes for Oblique Approach of the Wave (angle=45º) with Period of 3 min. for LDW with the Bottom Slope of 1/20
(Incoming Wave Amplitudes= -0.5m, -1.0m at the toe)

4.3.3 Distribution of Maximum Current Velocities for Perpendicular Approach of the Wave (angle=90º)

In this section, the distributions of maximum current velocities in basins 1 and 2 are presented which were computed during various simulations. The results are given for each bottom slope.

Figure 4.16 shows distribution of maximum current velocities for LEW type single sinusoidal wave with period of 3 minutes and different initial amplitudes for bottom slope of *1/10*. Figure 4.17 shows distribution of maximum current velocities for LDW type single sinusoidal wave with period of 3 minutes and different initial amplitudes for bottom slope of *1/10*. As seen from these Figures, higher amplitude incoming waves cause higher maximum currents. For the bottom slope of *1/10*, there is not significant difference of current velocities between the cases of LEW and LDW.

Figure 4.18 shows distribution of maximum current velocities for LEW type single sinusoidal wave with period of 3 minutes and different initial amplitudes for bottom slope of *1/20*. Figure 4.19 shows distribution of maximum current velocities for LDW type single sinusoidal wave with period of 3 minutes and different initial amplitudes for bottom slope of *1/20*. As seen from these Figures, similar trend is observed in terms of having higher currents for higher amplitudes of incoming waves as in *1/10* slope case. When the effects of bottom slopes are compared; (1) the inundation distance is longer for milder slope (*1/20*), (2) milder slope (*1/20*) causes higher current velocities at shallow regions in inundation zone. Furthermore, comparing with steeper slope (*1/10*), the difference of current velocities between LEW and LDW are slightly noticeable in milder slope case (see Appendix A, Figures A.9-12 for the results of same kind of simulations using different incoming wave amplitudes).

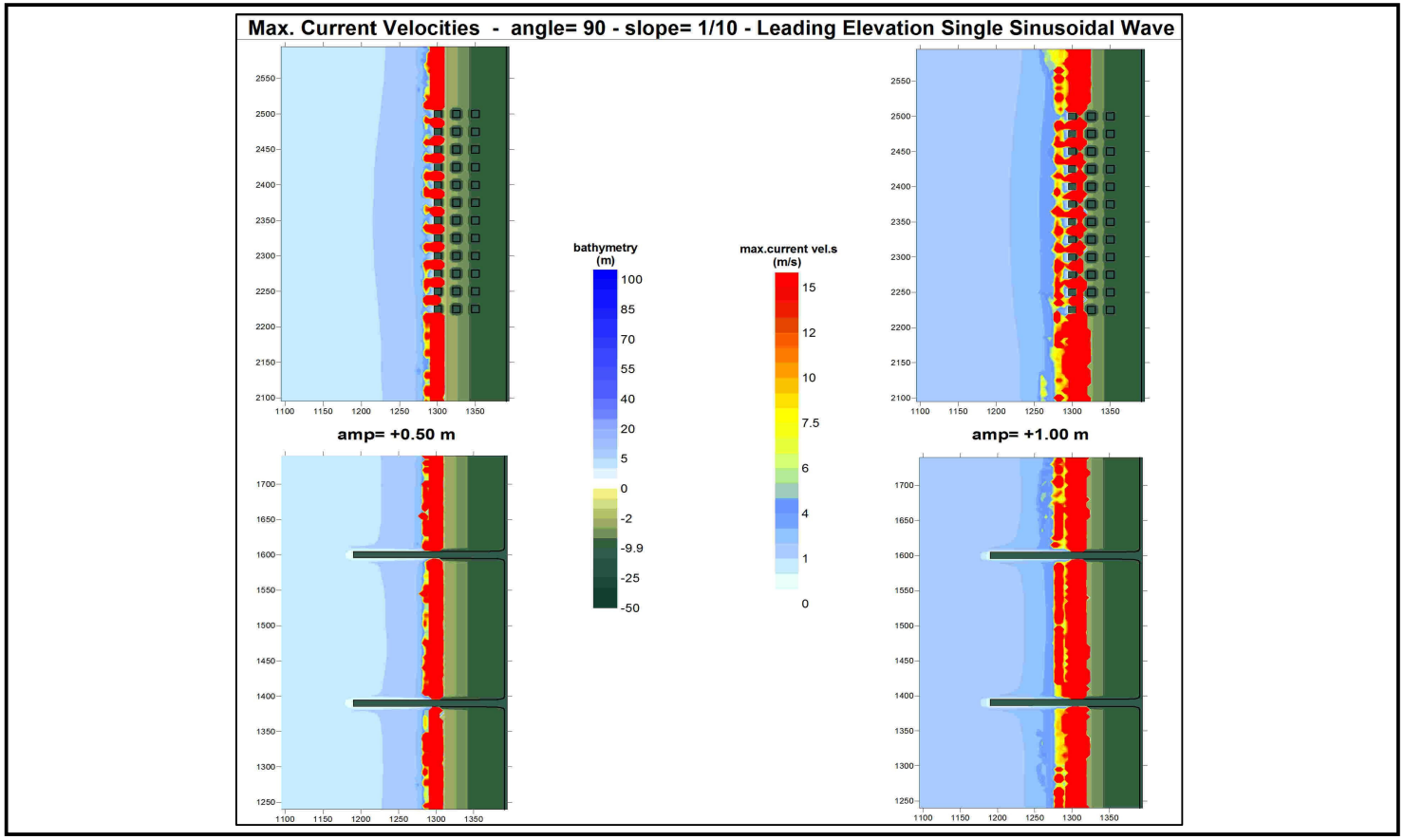

Figure 4.16: Distribution of Maximum Current Velocities for Perpendicular Approach of the Wave (angle=90º) with Period of 3 min. for LEW with the Bottom Slope of 1/10 (Incoming Wave Amplitudes= +0.5m, +1.0m at the toe)

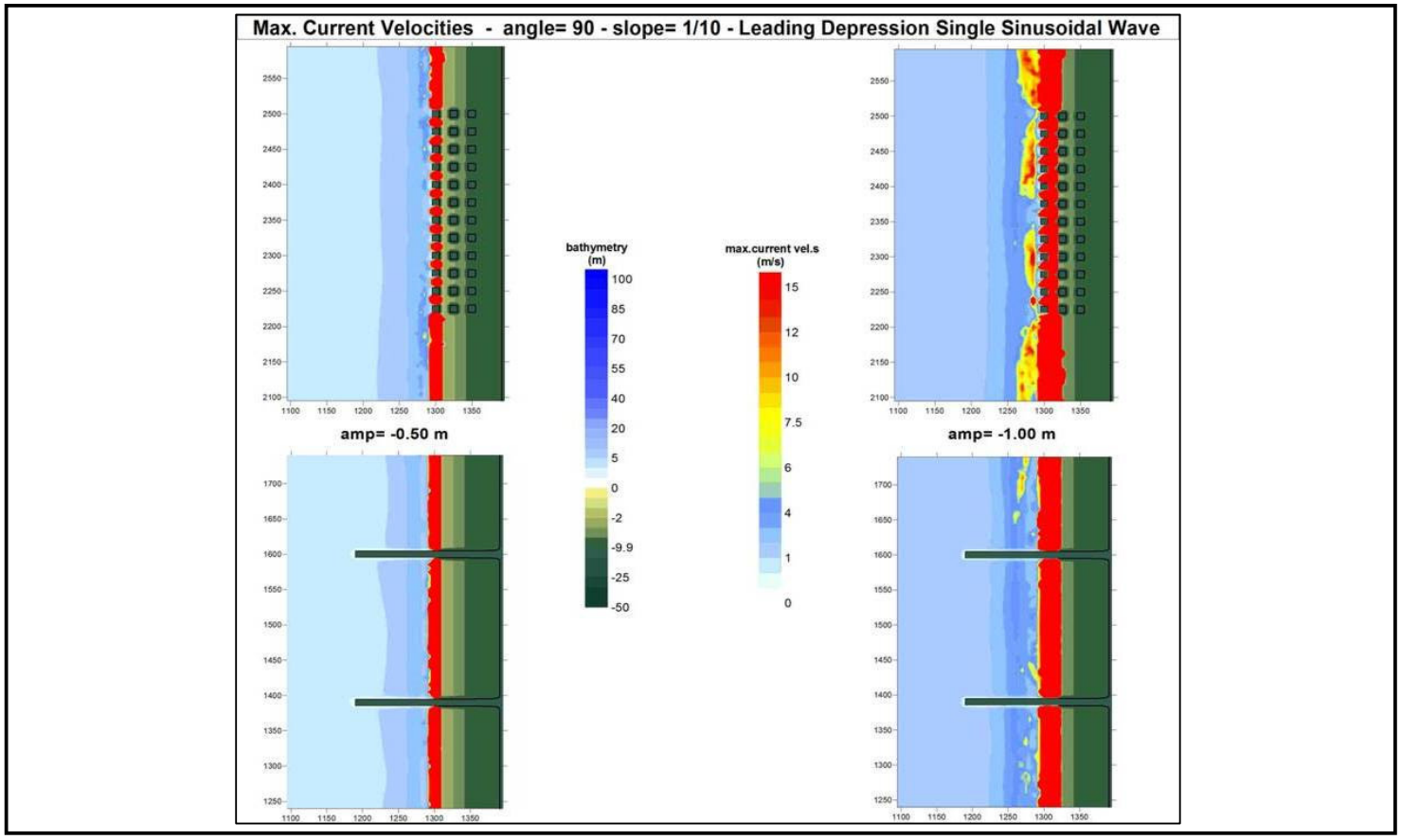

Figure 4.17: Distribution of Maximum Current Velocities for Perpendicular Approach of the Wave (angle=90º) with Period of 3 min. for LDW with the Bottom Slope of 1/10
(Incoming Wave Amplitudes= -0.5m, -1.0m at the toe)

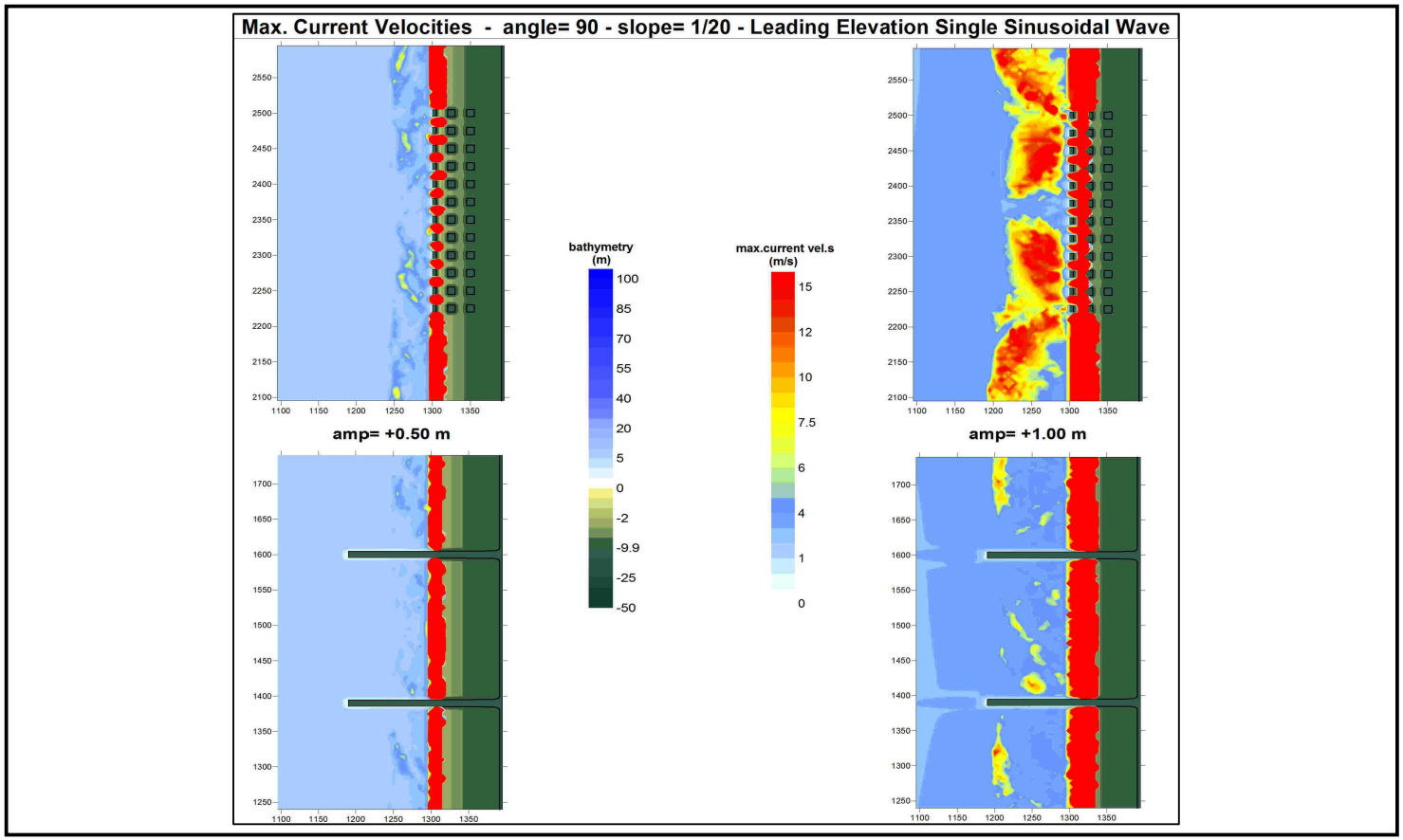

Figure 4.18: Distribution of Maximum Current Velocities for Perpendicular Approach of the Wave (angle=90º) with Period of 3 min. for LEW with the Bottom Slope of 1/20
(Incoming Wave Amplitudes= +0.5m, +1.0m at the toe)

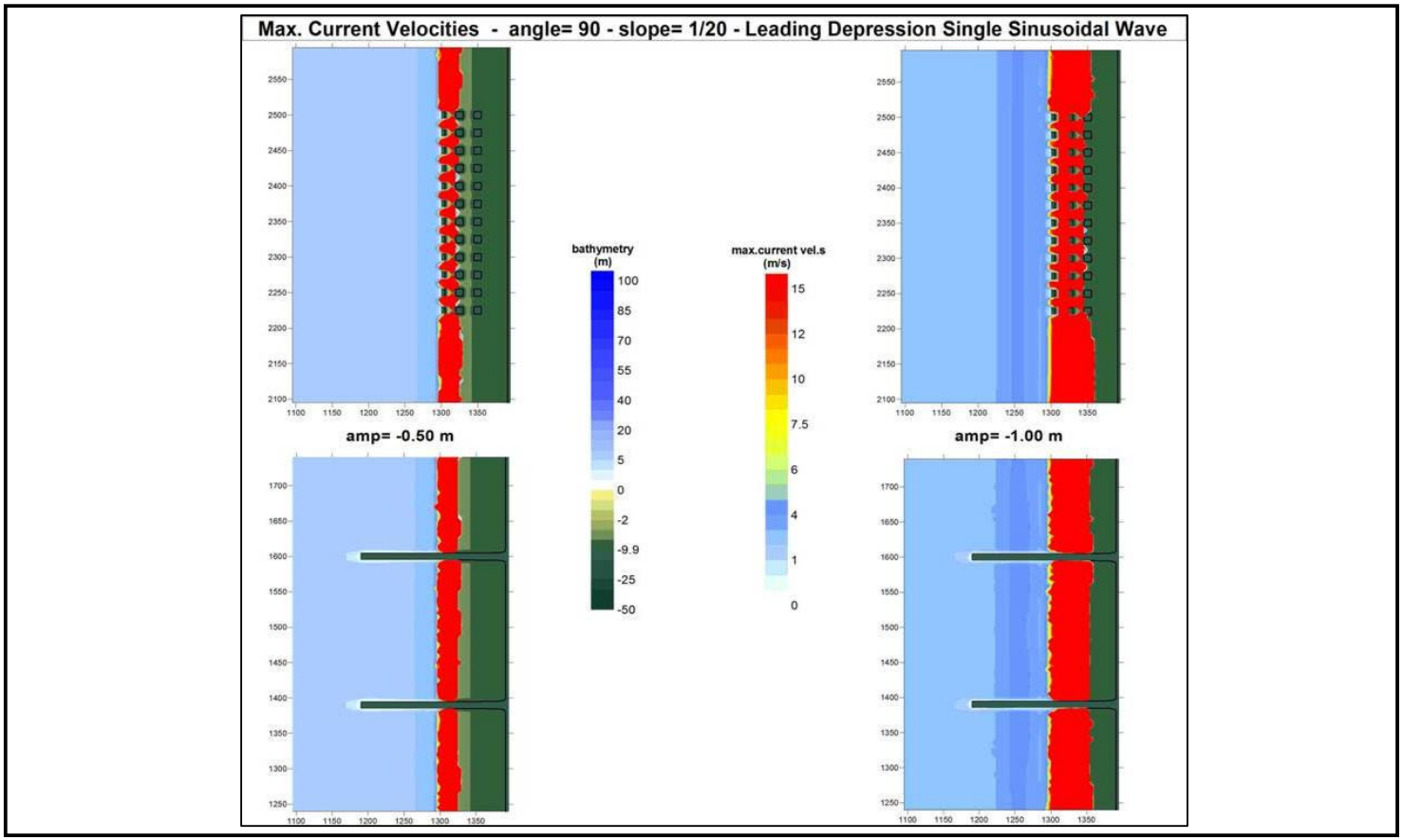

Figure 4.19: Distribution of Maximum Current Velocities for Perpendicular Approach of the Wave (angle=90º) with Period of 3 min. for LDW with the Bottom Slope of 1/20
(Incoming Wave Amplitudes= -0.5m, -1.0m at the toe)

4.3.4 Distribution of Maximum Current Velocities for Oblique Approach of the Wave (angle=45º)

Figure 4.20 shows distribution of maximum current velocities for LEW type single sinusoidal wave with period of 3 minutes and different initial amplitudes for bottom slope of *1/10*. Figure 4.21 shows distribution of maximum current velocities for LDW type single sinusoidal wave with period of 3 minutes and different initial amplitudes for bottom slope of *1/10*. As seen from these Figures, for oblique approach of the incoming wave, LDW causes higher current velocities, but there is nor so significant difference between the current velocities comparing the wave and lee side of the shore-perpendicular and shore-parallel structures.

Figure 4.22 shows distribution of maximum current velocities for LEW type single sinusoidal wave with period of 3 minutes and different initial amplitudes for bottom slope of *1/20*. Figure 4.23 shows distribution of maximum current velocities for LDW type single sinusoidal wave with period of 3 minutes and different initial amplitudes for bottom slope of *1/20*. As seen from these Figures, steeper slope (*1/10*) causes slightly higher current velocities than milder slope (*1/20*). When bottom slopes are compared, the inundation distance is longer for milder slope (*1/20*). Furthermore, comparing with steeper slope (*1/10*), the difference of current velocities between LEW and LDW are slightly noticeable in milder slope case. In milder slope (*1/20*), current velocities are higher for LDW type of incoming wave (see Appendix A, Figures A.13-A16 for the results of same kind of simulations using different incoming wave amplitudes).

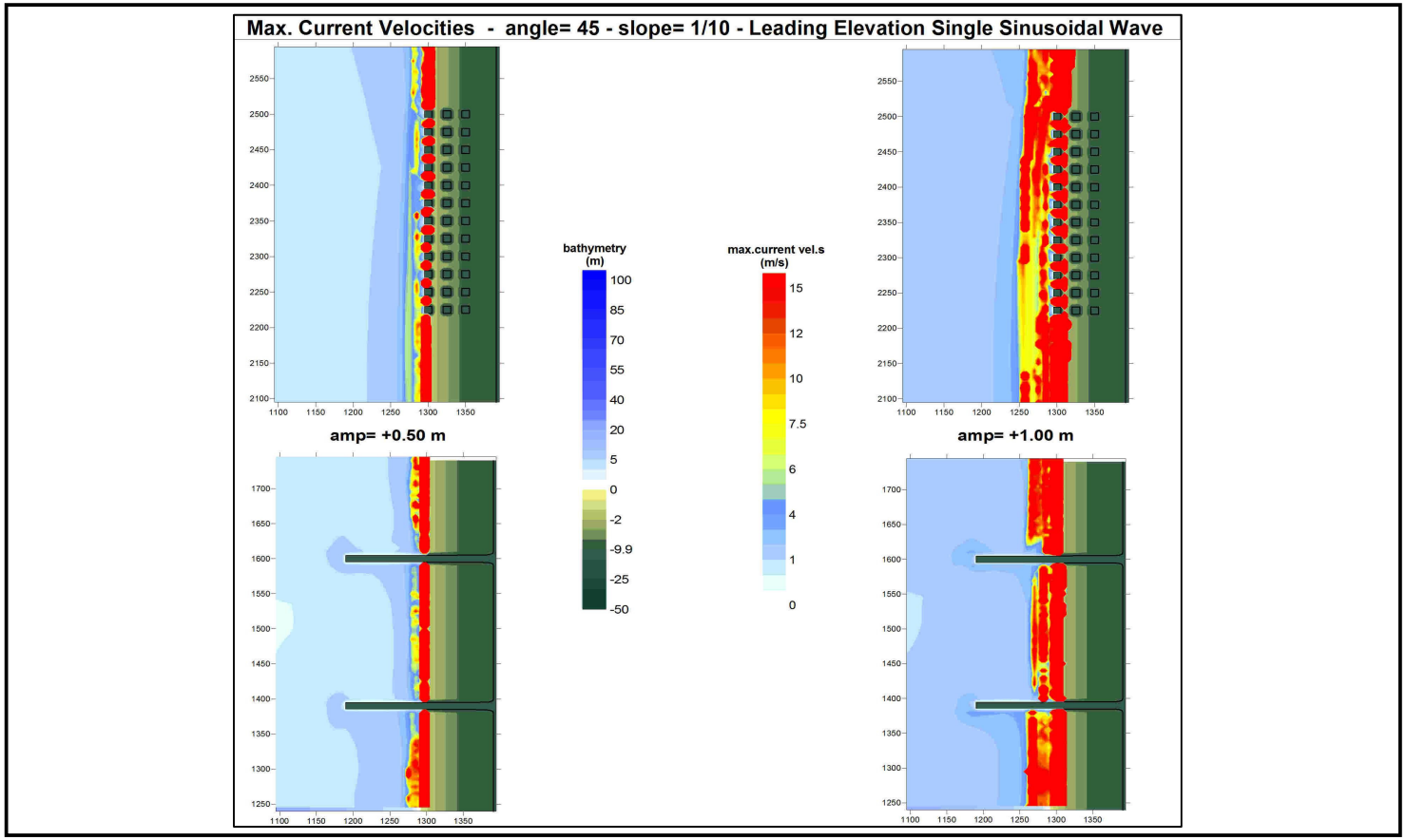

Figure 4.20: Distribution of Maximum Current Velocities for Oblique Approach of the Wave (angle=45º) with Period of 3 min. for LEW with the Bottom Slope of 1/10 (Incoming Wave Amplitudes= +0.5m, +1.0m at the toe)

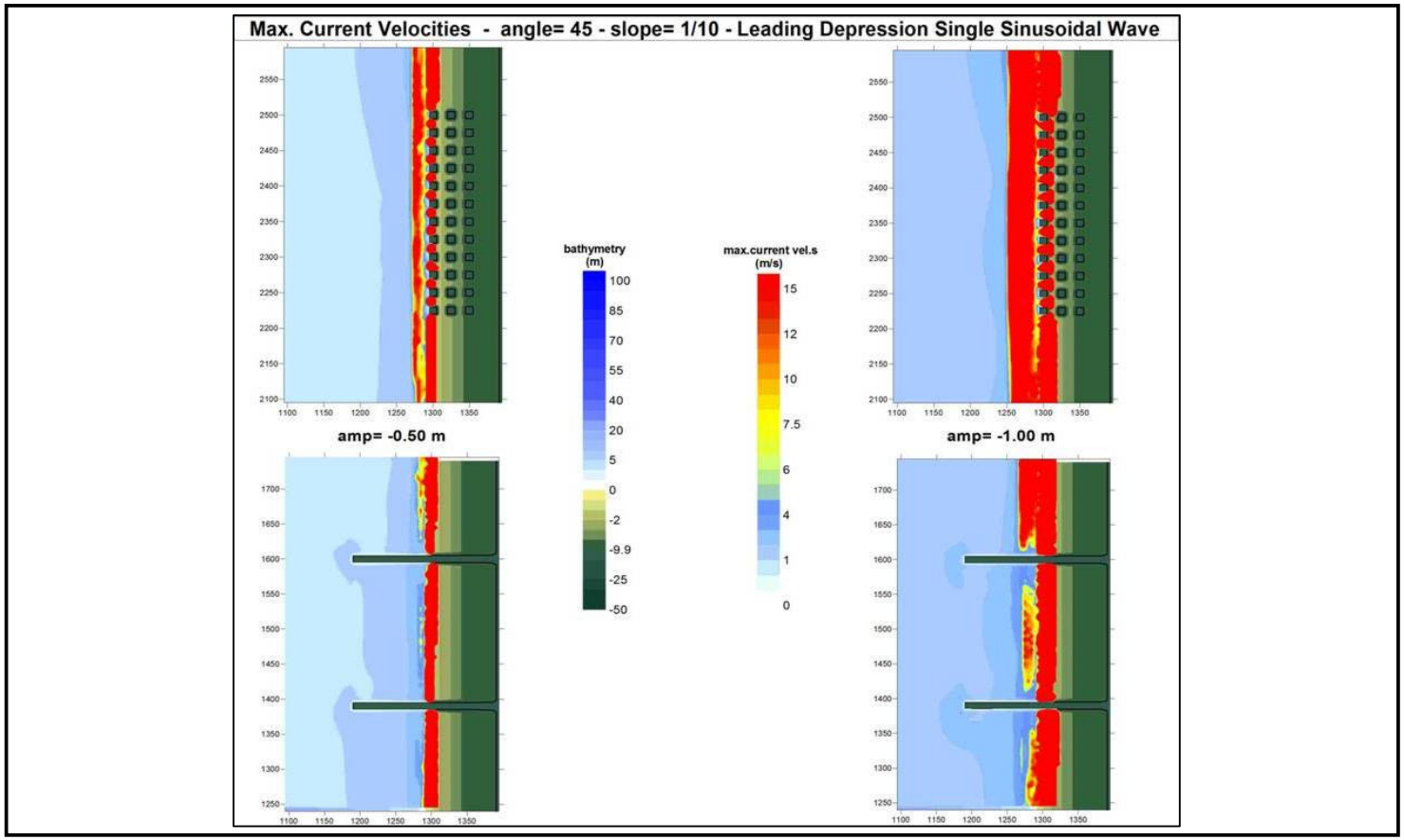

Figure 4.21: Distribution of Maximum Current Velocities for Oblique Approach of the Wave (angle=45º) with Period of 3 min. for LDW with the Bottom Slope of 1/10 (Incoming Wave Amplitudes= -0.5m, -1.0m at the toe)

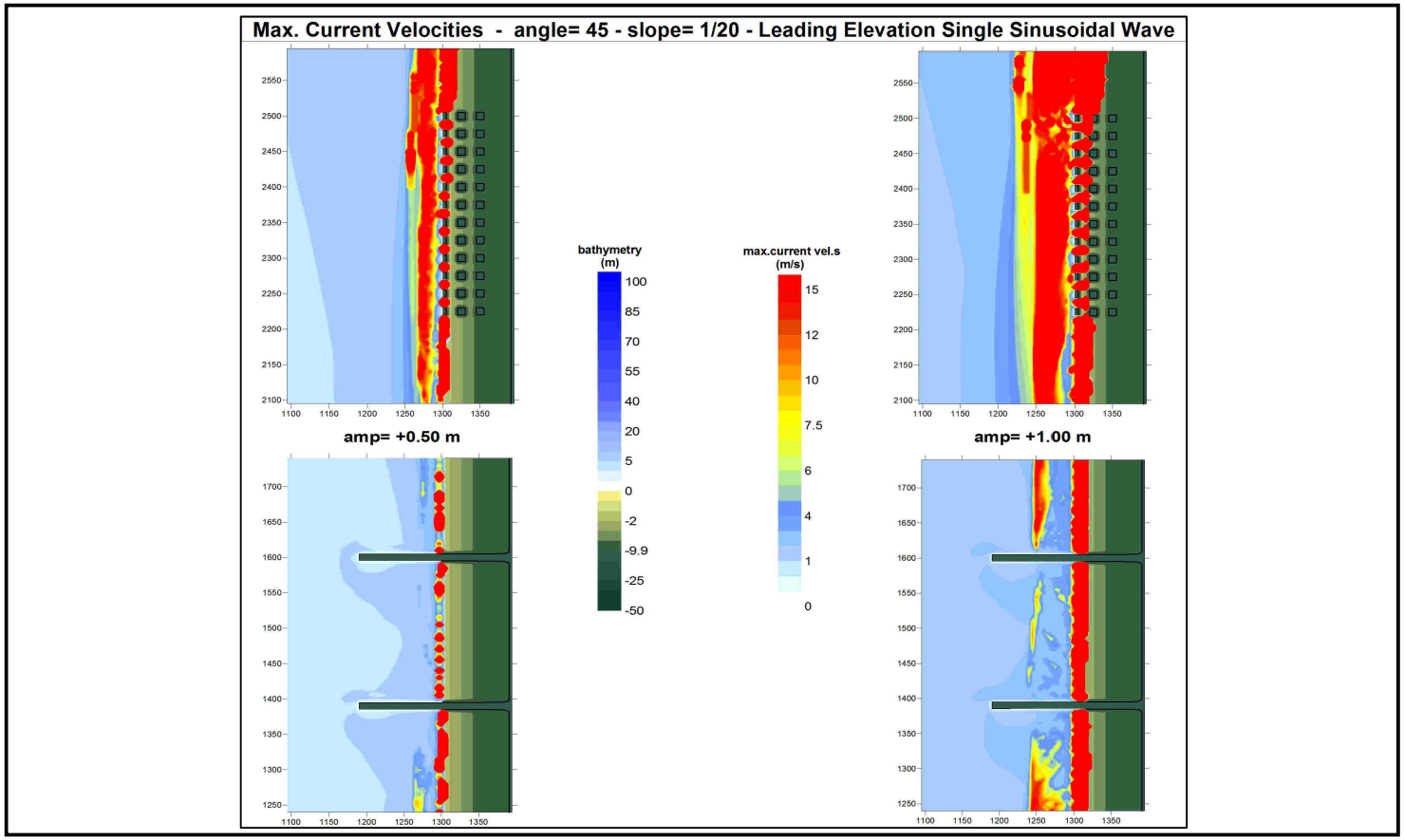

Figure 4.22: Distribution of Maximum Current Velocities for Oblique Approach of the Wave (angle=45º) with Period of 3 min. for LEW with the Bottom Slope of 1/20 (Incoming Wave Amplitudes= +0.5m, +1.0m at the toe)

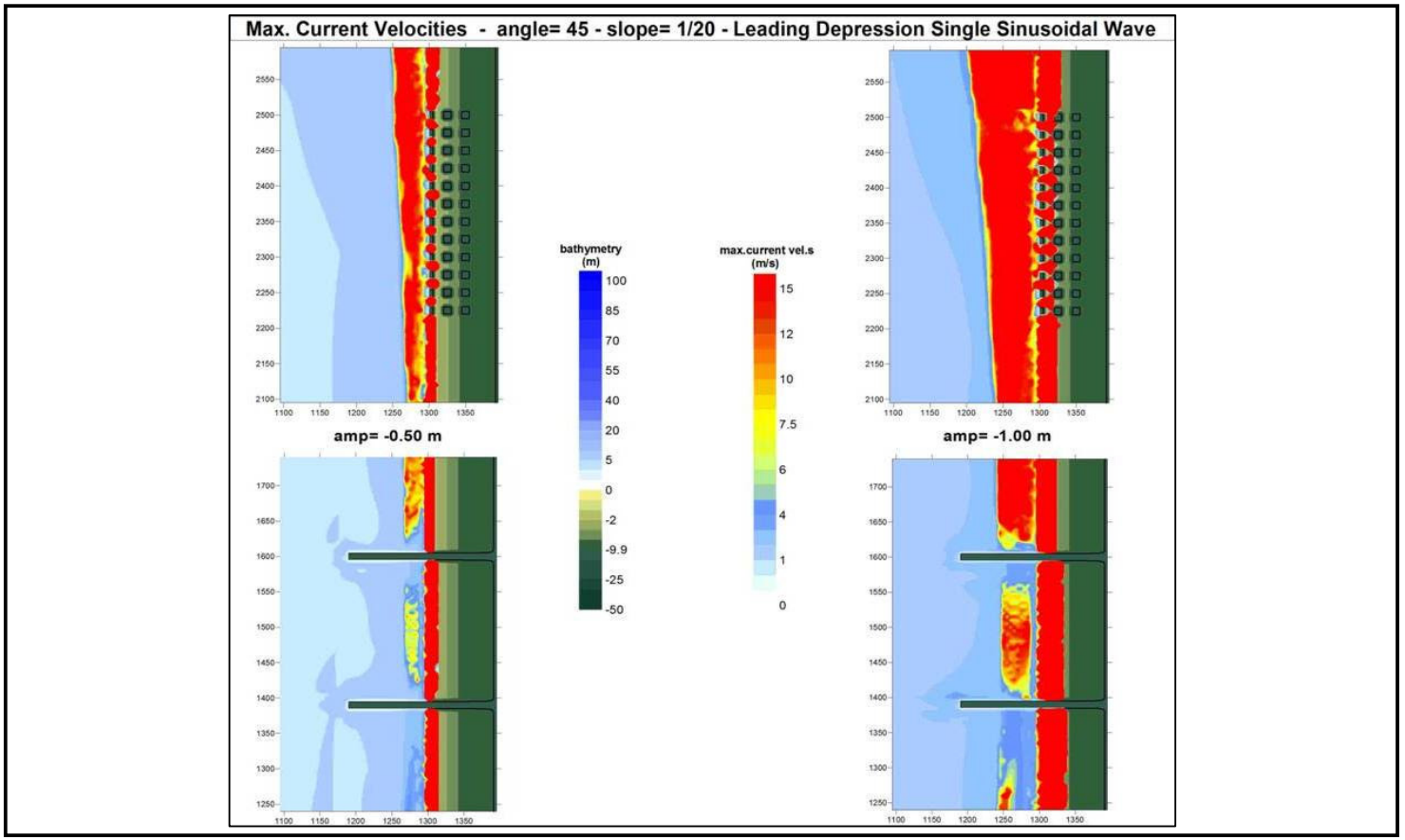

Figure 4.23: Distribution of Maximum Current Velocities for Oblique Approach of the Wave (angle=45º) with Period of 3 min. for LDW with the Bottom Slope of 1/20 (Incoming Wave Amplitudes= -0.5m, -1.0m at the toe)

4.3.5 Distribution of Maximum Hydrodynamic Demands for Perpendicular Approach of the Wave (angle=90º)

In this section, the distributions of maximum hydrodynamic demands in basins 1 and 2 are presented which were computed during various simulations. The results are given for each bottom slope.

Figure 4.24 shows distribution of maximum hydrodynamic demands for LEW type single sinusoidal wave with period of 3 minutes and different initial amplitudes for bottom slope of *1/10*. Figure 4.25 shows distribution of maximum hydrodynamic demands for LDW type single sinusoidal wave with period of 3 minutes and different initial amplitudes for the wave shape for slope *1/10*.

As seen from these Figures, higher-amplitude incoming waves cause higher hydrodynamic demand. Comparing the effect of wave shape, LDW causes higher hydrodynamic demand than LEW.

Figure 4.26 shows distribution of maximum hydrodynamic demands for LEW type single sinusoidal wave with period of 3 minutes and different initial amplitudes for bottom slope of *1/20*. Figure 4.27 shows distribution of maximum hydrodynamic demands for LDW type single sinusoidal wave with period of 3 minutes and different initial amplitudes for bottom slope of *1/20*.

As seen from these Figures, for LEW type of incoming wave, higher hydrodynamic demands are observed in milder slope (*1/20*). In contrary, for LDW type of incoming wave, the difference is not so significant (see Appendix A, Figures A.17-A20 for the results of same kind of simulations using different incoming wave amplitudes).

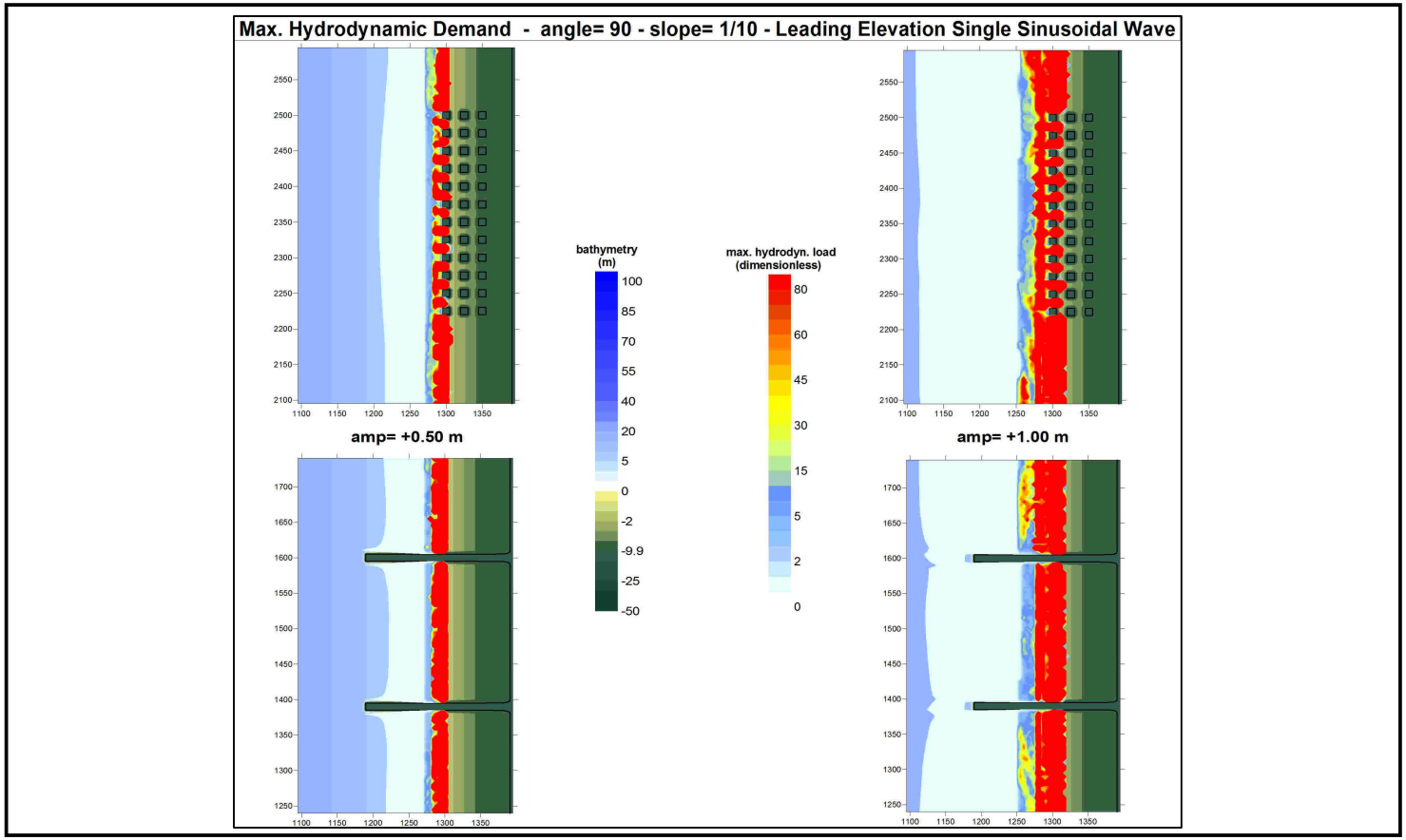

Figure 4.24: Distribution of Maximum Hydrodynamic Demands for Perpendicular Approach of the Wave (angle=90º) with Period of 3 min. for LEW with the Bottom Slope of 1/10
(Incoming Wave Amplitudes= +0.5m, +1.0m at the toe)

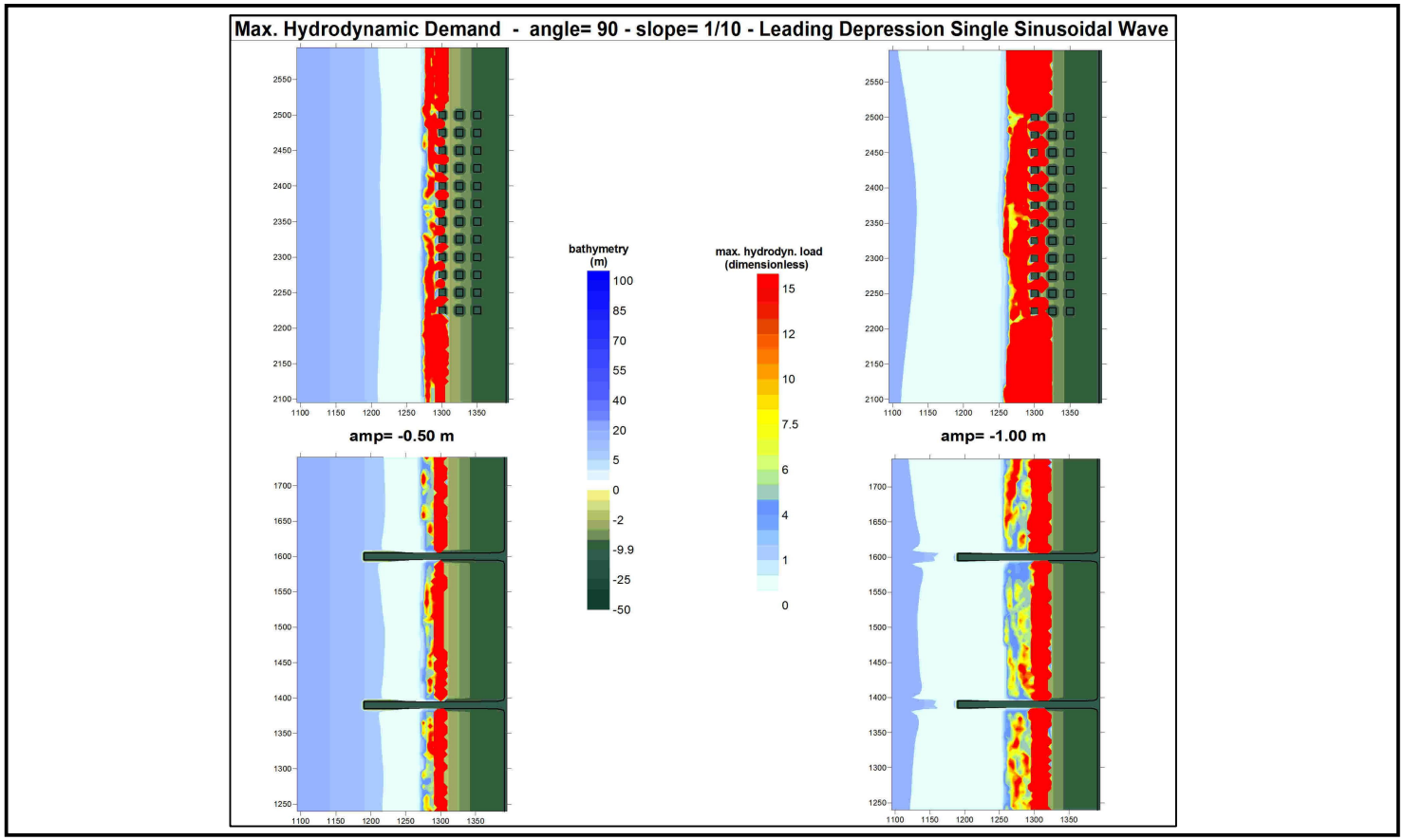

Figure 4.25: Distribution of Maximum Hydrodynamic Demands for Perpendicular Approach of the Wave (angle=90º) with Period of 3 min. for LDW with the Bottom Slope of 1/10
(Incoming Wave Amplitudes= -0.5m, -1.0m at the toe)

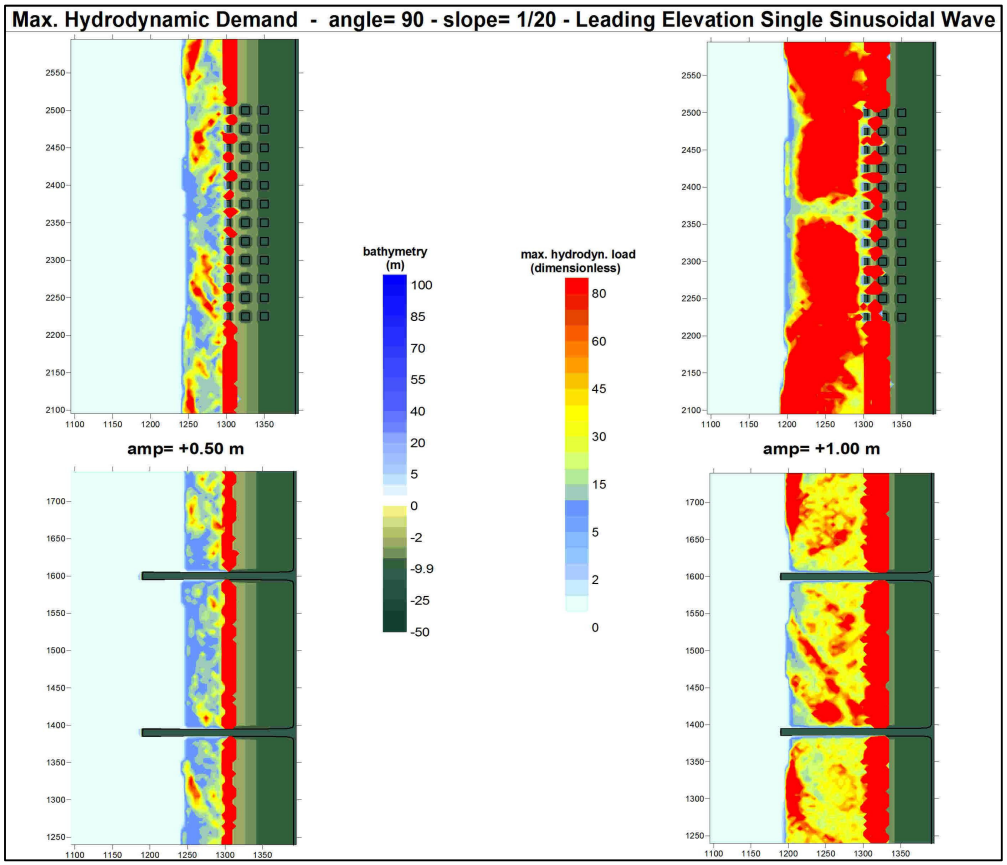

Figure 4.26: Distribution of Maximum Hydrodynamic Demands for Perpendicular Approach of the Wave (angle=90º) with Period of 3 min. for LEW with the Bottom Slope of 1/20
(Incoming Wave Amplitudes= +0.5m, +1.0m at the toe)

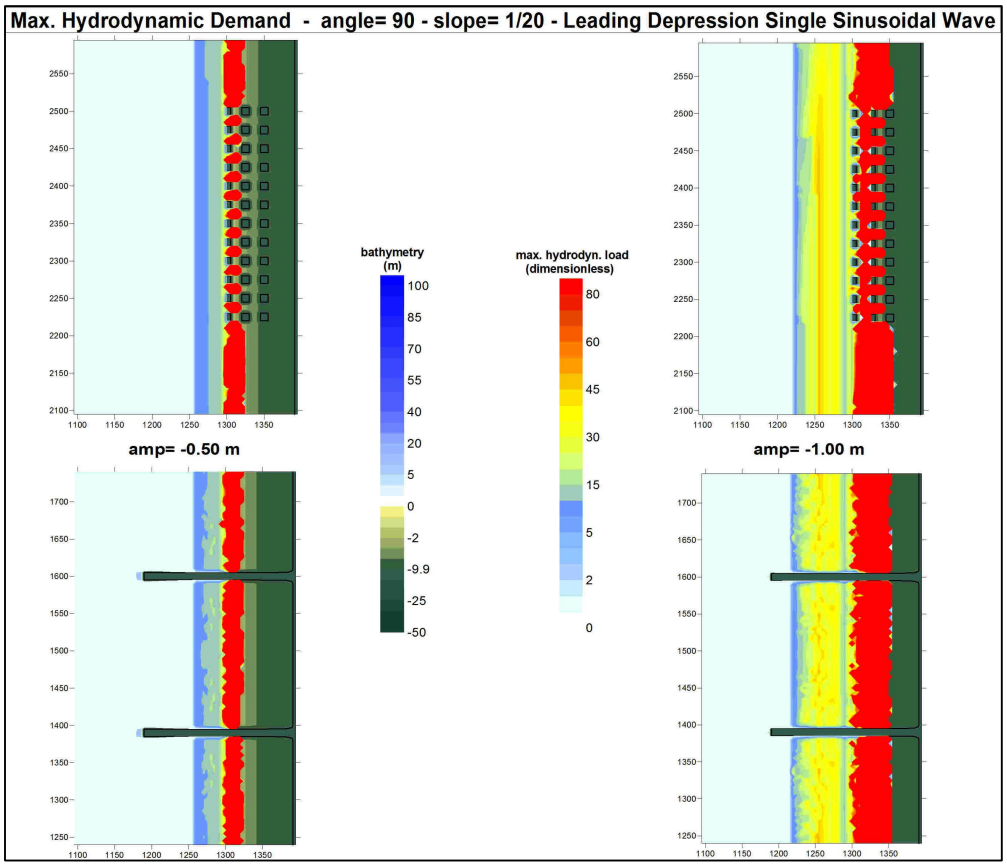

Figure 4.27: Distribution of Maximum Hydrodynamic Demands for Perpendicular Approach of the Wave (angle=90º) with Period of 3 min. for LDW with the Bottom Slope of 1/20
(Incoming Wave Amplitudes= -0.5m, -1.0m at the toe)

4.3.6 Distribution of Maximum Hydrodynamic Demands for Oblique Approach of the Wave (angle=45º)

Figure 4.28 shows distribution of maximum hydrodynamic demands for LEW type single sinusoidal wave with period of 3 minutes and different initial amplitudes for bottom slope of *1/10*.

Figure 4.29 shows distribution of maximum hydrodynamic demands for LDW type single sinusoidal wave with period of 3 minutes and different initial amplitudes for bottom slope of *1/10*.

Figure 4.30 shows distribution of maximum hydrodynamic demands for LEW type single sinusoidal wave with period of 3 minutes and different initial amplitudes for bottom slope of *1/20*.

Figure 4.31 shows distribution of maximum hydrodynamic demands for LDW type single sinusoidal wave with period of 3 minutes and different initial amplitudes for bottom slope of *1/20*.

As seen from these Figures, when waves are approaching obliquely, lower hydrodynamic demands are observed at the wave side of the shore-parallel structures. For shore-perpendicular structures, the difference is not so significant (see Appendix A, Figures A.21-A.24 for the results of same kind of simulations using different incoming wave amplitudes).

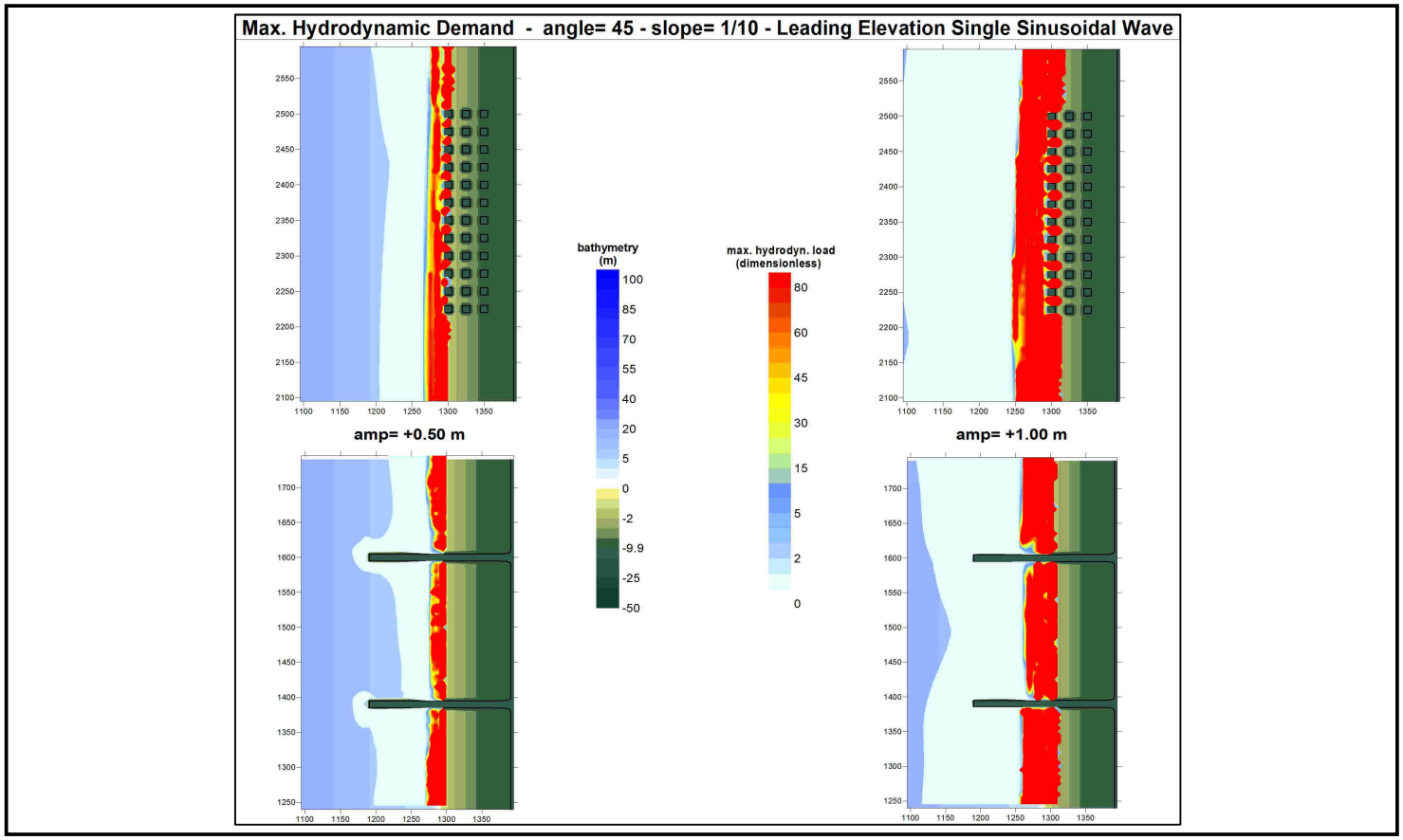

Figure 4.28: Distribution of Maximum Hydrodynamic Demands for Oblique Approach of the Wave (angle=45º) with Period of 3 min. for LEW with the Bottom Slope of 1/10
(Incoming Wave Amplitudes= +0.5m, +1.0m at the toe)

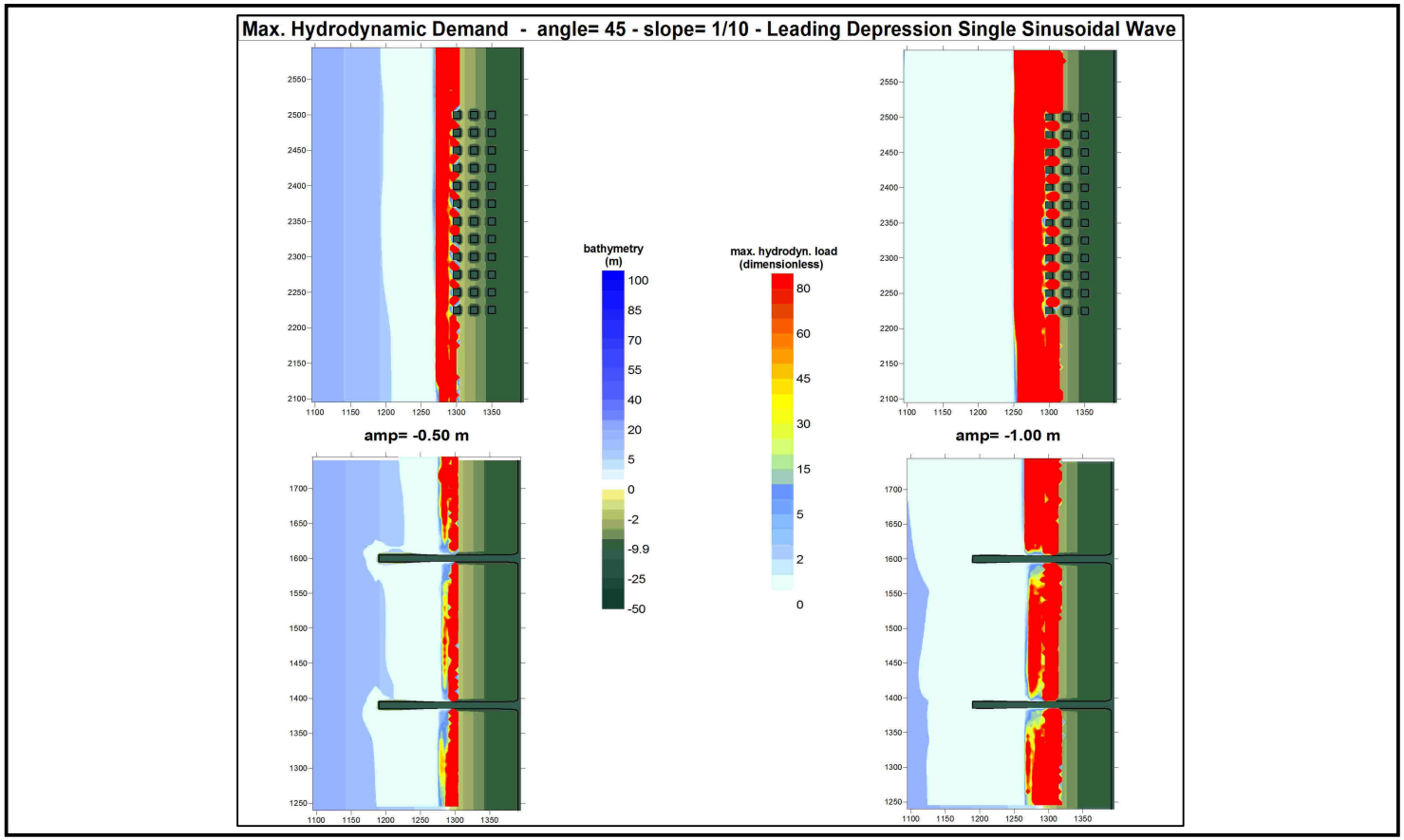

Figure 4.29: Distribution of Maximum Hydrodynamic Demands for Oblique Approach of the Wave (angle=45º) with Period of 3 min. for LDW with the Bottom Slope of 1/10
(Incoming Wave Amplitudes= -0.5m, -1.0m at the toe)

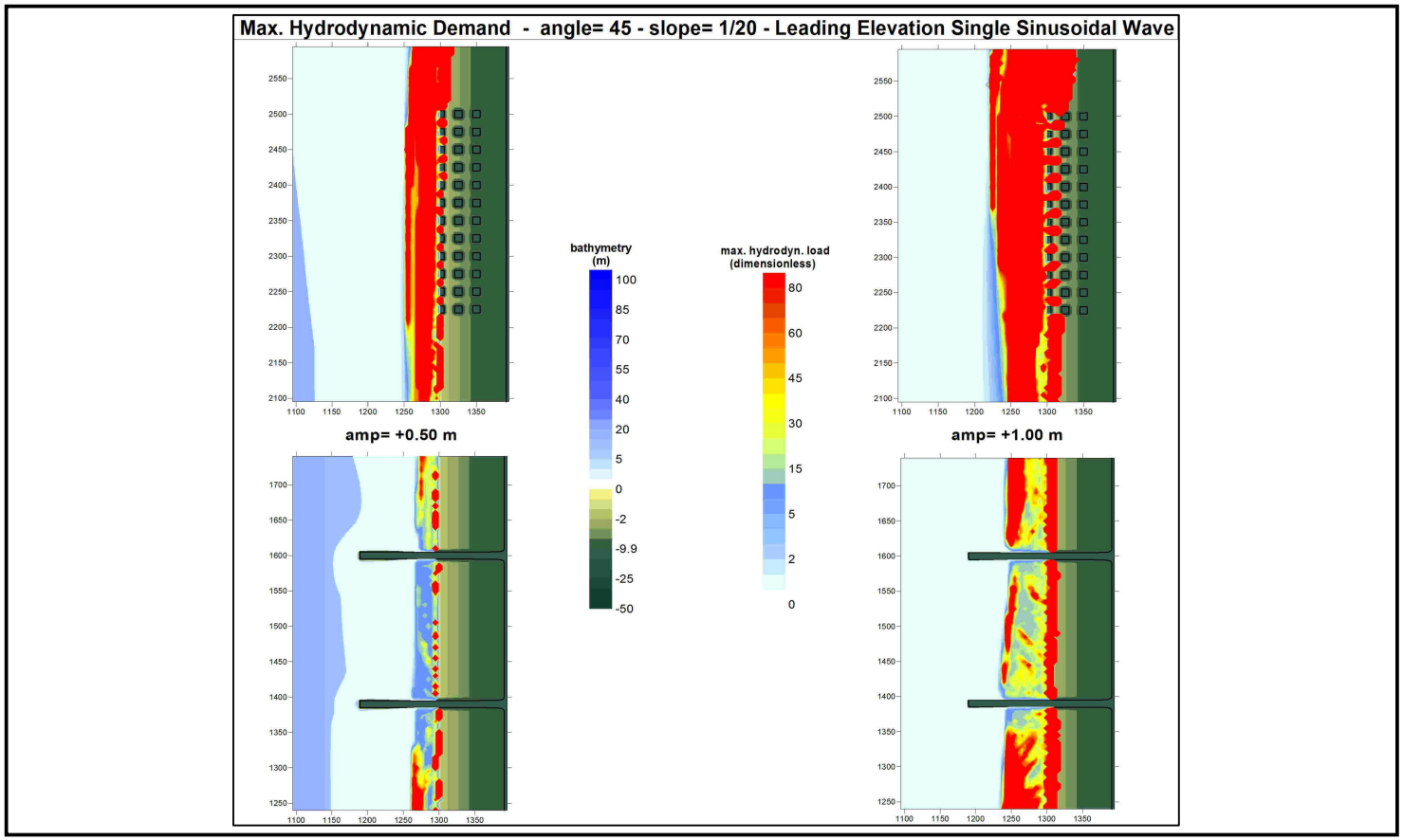

Figure 4.30: Distribution of Maximum Hydrodynamic Demands for Oblique Approach of the Wave (angle=45º) with Period of 3 min. for LEW with the Bottom Slope of 1/20
(Incoming Wave Amplitudes= +0.5m, +1.0m at the toe)

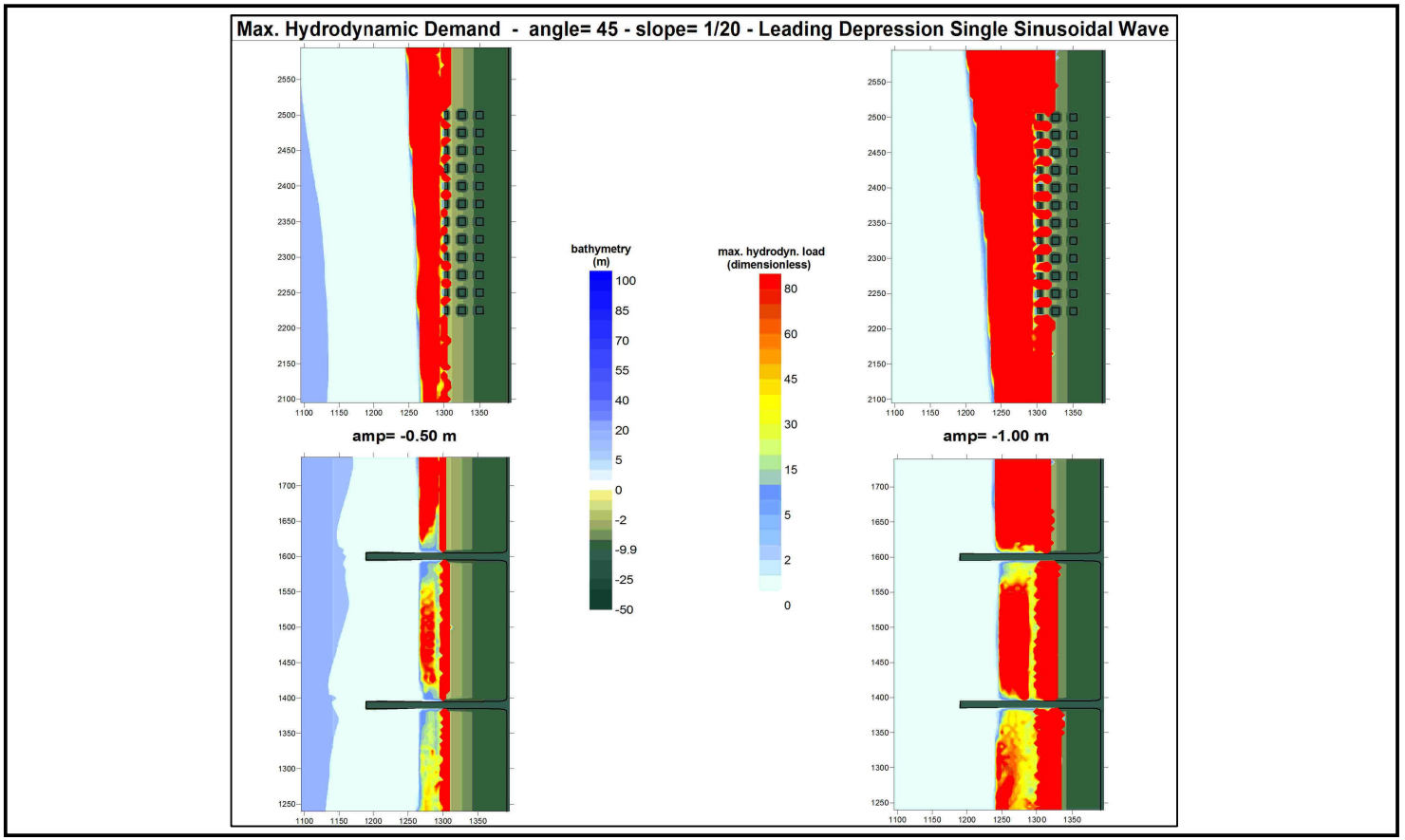

Figure 4.31: Distribution of Maximum Hydrodynamic Demands for Oblique Approach of the Wave (angle=45º) with Period of 3 min. for LDW with the Bottom Slope of 1/20
(Incoming Wave Amplitudes= -0.5m, -1.0m at the toe)

4.3.7 Distribution of Hydrodynamic Parameters for Perpendicular Approach of the Wave with Period of 1 Minute on Bottom Slopes of *1/10* and *1/20*

Figure 4.32 shows distribution of maximum positive amplitudes for LEW type single sinusoidal wave with period of 1 minute and different initial amplitudes for bottom slope of *1/10*.

Figure 4.33 shows distribution of maximum positive amplitudes for LEW type single sinusoidal wave with period of 1 minute and different initial amplitudes for bottom slope of *1/20*.

Figure 4.34 shows distribution of maximum current velocities for LEW type single sinusoidal wave with period of 1 minute and different initial amplitudes for bottom slope of *1/10*.

Figure 4.35 shows distribution of maximum current velocities for LEW type single sinusoidal wave with period of 1 minute and different initial amplitudes for bottom slope of *1/20*.

Figure 4.36 shows distribution of maximum hydrodynamic demands for LEW type single sinusoidal wave with period of 1 minute and different initial amplitudes for bottom slope of *1/10*.

Figure 4.37 shows distribution of maximum hydrodynamic demands for LEW type single sinusoidal wave with period of 1 minute and different initial amplitudes for bottom slope of *1/20*.

As seen from these Figures, the effects of the slopes, incoming wave amplitudes and structural orientation on the maximum positive amplitude, maximum current velocities and maximum hydrodynamic demands for wave period of 1 minute are similar as for wave period of 3 minutes in LEW.

The period effect for LEW is compared in the following by using the respective figures. Figure 4.32 with Figure 4.8 (having wave periods of 1 minute and 3 minutes, respectively) show that there is not significant difference between the inundation distances of waves having different

periods selected in this study. However, it is observed that higher maximum amplitudes occur in the shallower regions in the inundation zone for longer periods. Comparing Figure 4.33 and Figure 4.10 (having wave periods of 1 minute and 3 minutes, respectively), the similar trend exists such as there is not significant difference between the inundation distances of waves having different periods selected in this study. However, it is observed that higher maximum currents occur in the shallower regions in inundation zone for longer periods of LEW. It is also noticed that current velocities of 1 minute period of incoming wave are lower than that of waves having 3 minute period in milder slopes (*1/20*). But this trend is not so significant in steeper slope (*1/10*). Furthermore, comparison of Figure 4.37 and Figure 4.26 gives that maximum hydrodynamic demands increase as wave period decreases in milder slope (*1/20*). The reason of this result may be occurrence of smaller flow depth for shorter wave periods.

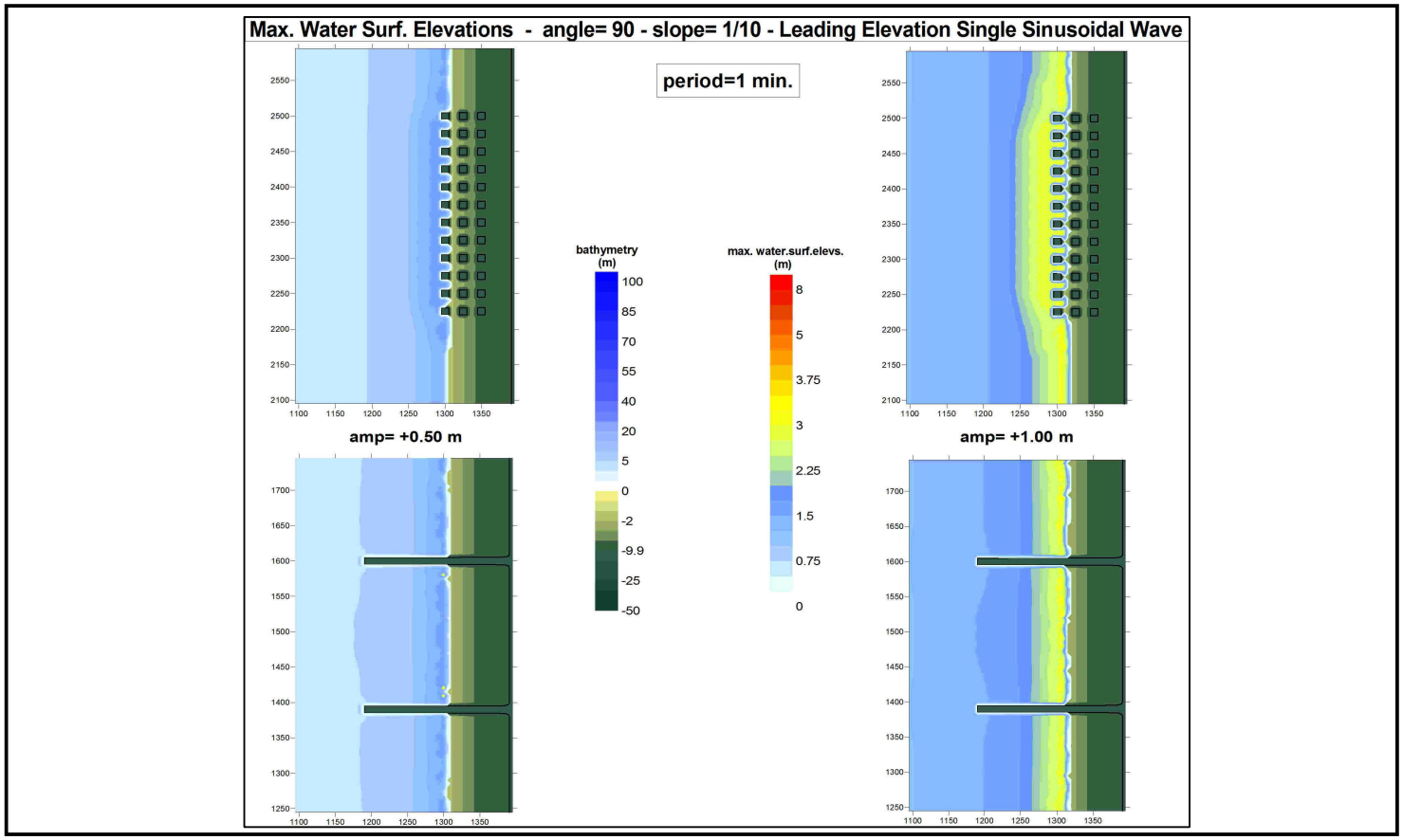

Figure 4.32: Distribution of Maximum Positive Amplitudes for Perpendicular Approach of the Wave (angle=90º) with Period of 1 min. for LEW with the Bottom Slope of 1/10 (Incoming Wave Amplitudes= +0.5m, +1.0m at the toe)

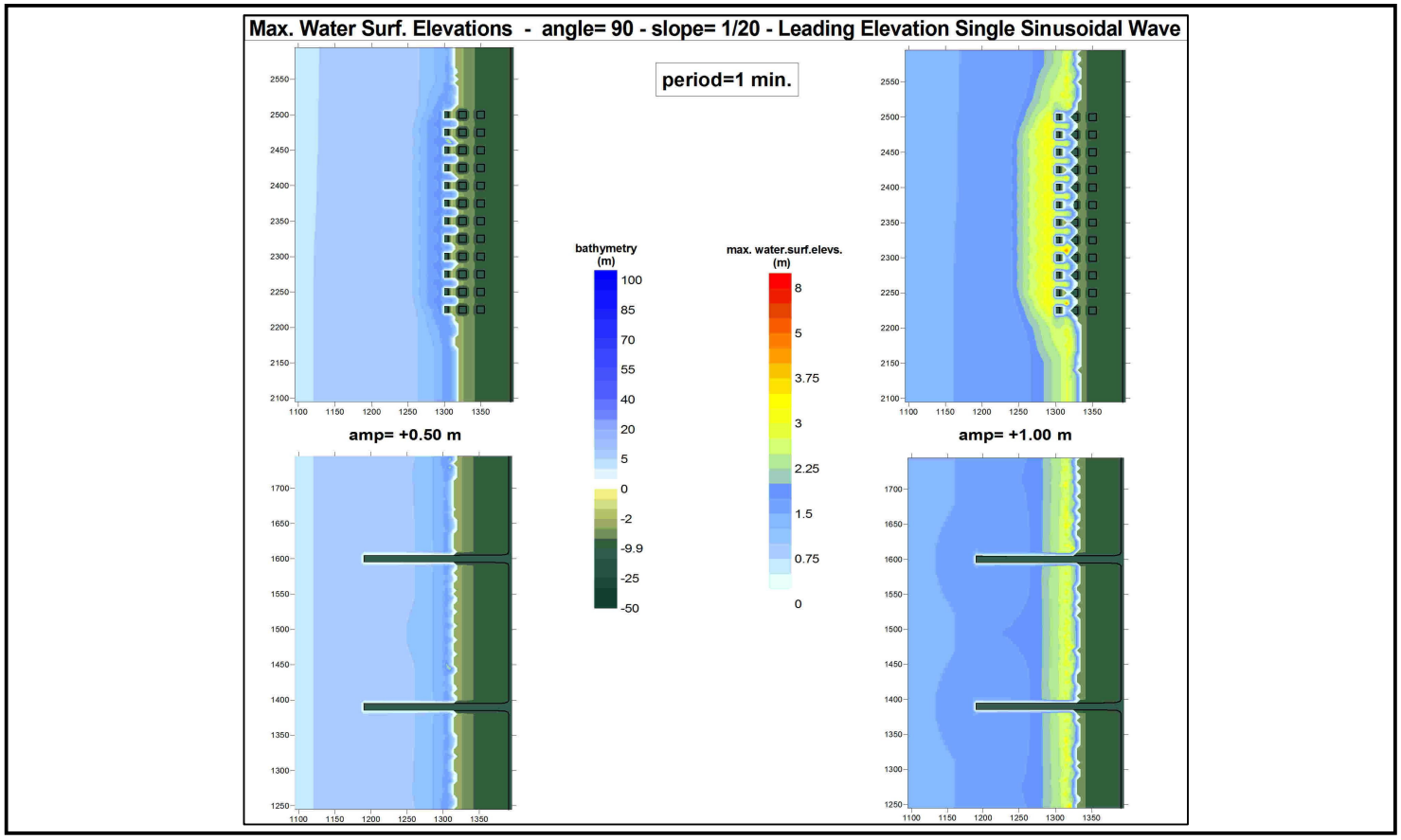

Figure 4.33: Distribution of Maximum Positive Amplitudes for Perpendicular Approach of the Wave (angle=90º) with Period of 1 min. for LEW with the Bottom Slope of 1/20
(Incoming Wave Amplitudes= -0.5m, -1.0m at the toe)

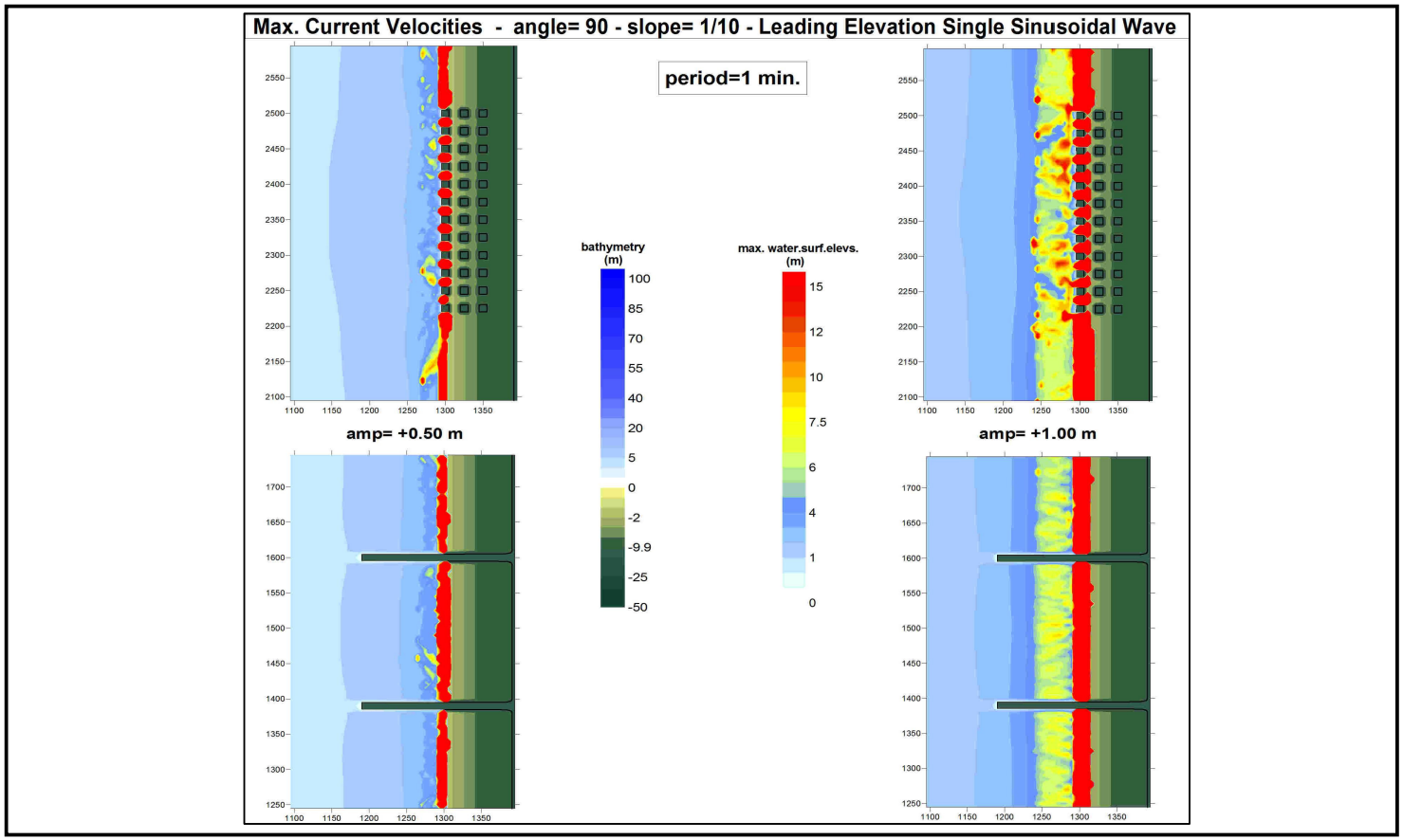

Figure 4.34: Distribution of Maximum Current Velocities for Perpendicular Approach of the Wave (angle=90º) with Period of 1 min. for LEW with the Bottom Slope of 1/10 (Incoming Wave Amplitudes= +0.5m, +1.0m at the toe)

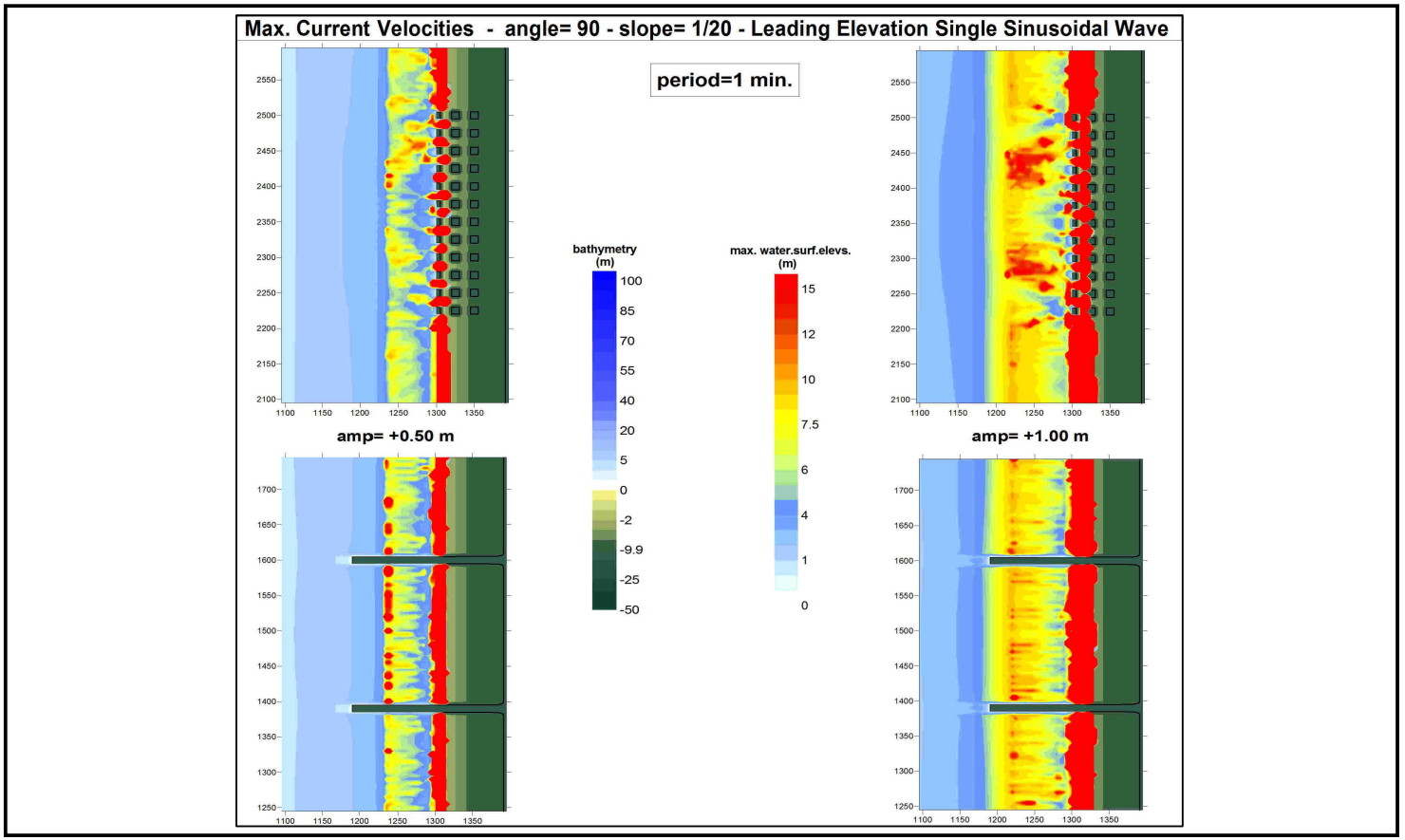

Figure 4.35: Distribution of Maximum Current Velocities for Perpendicular Approach of the Wave (angle=90º) with Period of 1 min. for LEW with the Bottom Slope of 1/20
(Incoming Wave Amplitudes= -0.5m, -1.0m at the toe)

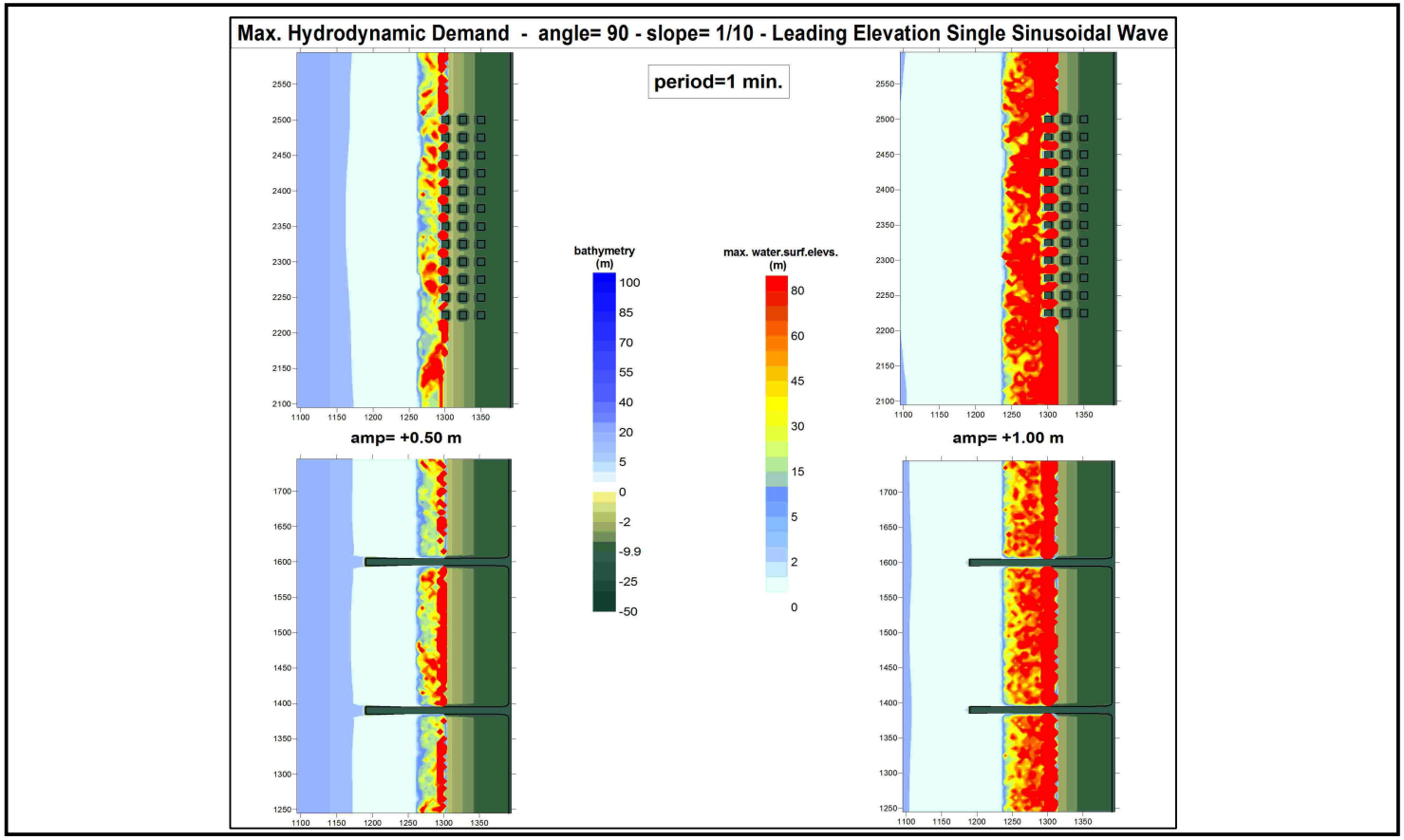

Figure 4.36: Distribution of Maximum Hydrodynamic Demands for Perpendicular Approach of the Wave (angle=90º) with Period of 1 min. for LEW with the Bottom Slope of 1/10
(Incoming Wave Amplitudes= -0.5m, -1.0m at the toe)

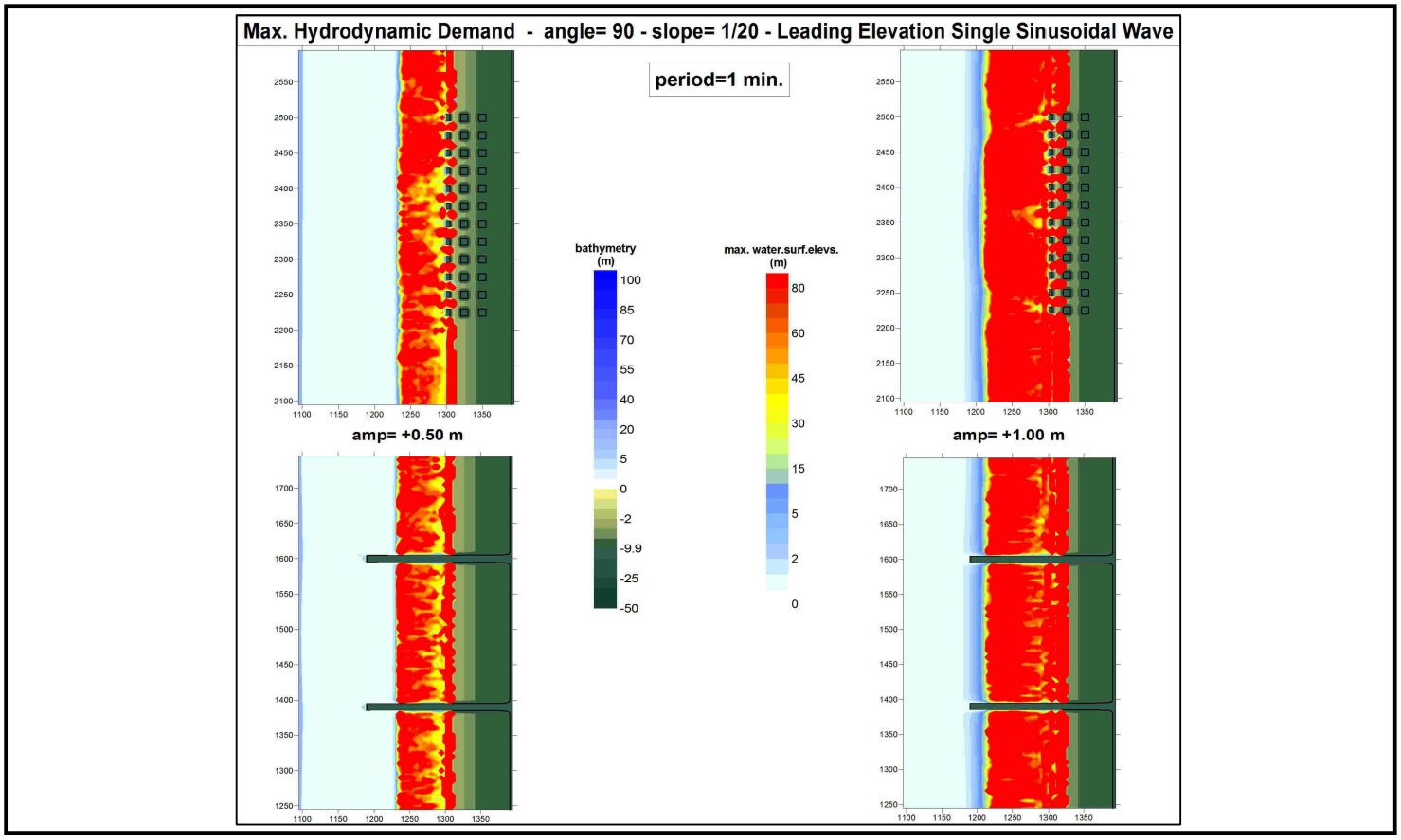

Figure 4.37: Distribution of Maximum Hydrodynamic Demands for Perpendicular Approach of the Wave (angle=90º) with Period of 1 min. for LEW with the Bottom Slope of 1/20
(Incoming Wave Amplitudes= -0.5m, -1.0m at the toe)

CHAPTER 5

GENERAL EVALUATION, DISCUSSION AND CONCLUSIONS

In this chapter, the results obtained in previous part are evaluated separately considering the effects of incoming wave amplitude, period, direction, type and bottom slope on the selected hydrodynamic parameters occurred during tsunami inundation.

5.1 Wave Amplitude Effect

Figure 5.1 shows the two different amplitudes of incoming wave on a same bottom slope.

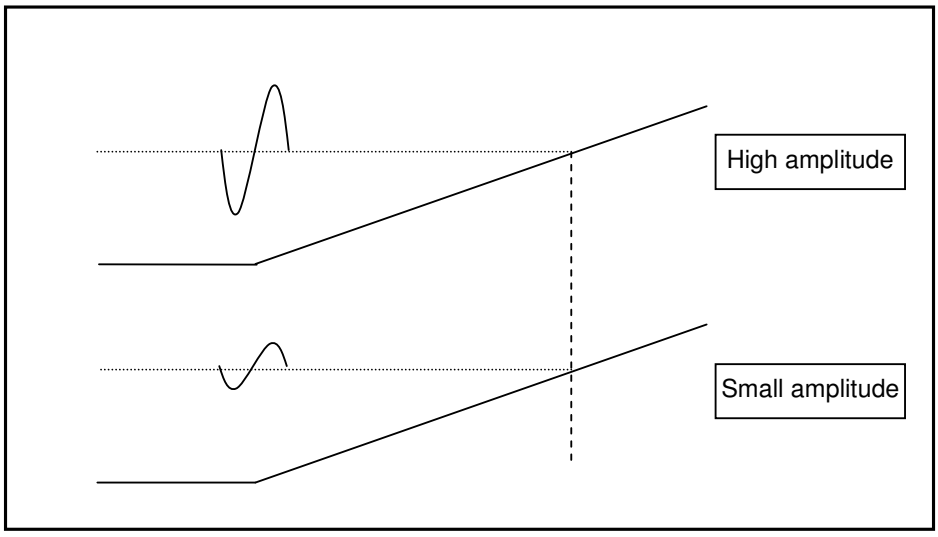

Figure 5.1: View of Two Different Amplitudes of Incoming Wave on Same Bottom Slope

The general condition obtained for hydrodynamic parameters in simulations is that higher-amplitude waves cause higher values of hydrodynamic parameters during tsunami inundation in shallower region and also inland.

5.2 Wave Period Effect

Figure 5.2 shows the two different periods of incoming wave on a same bottom slope.

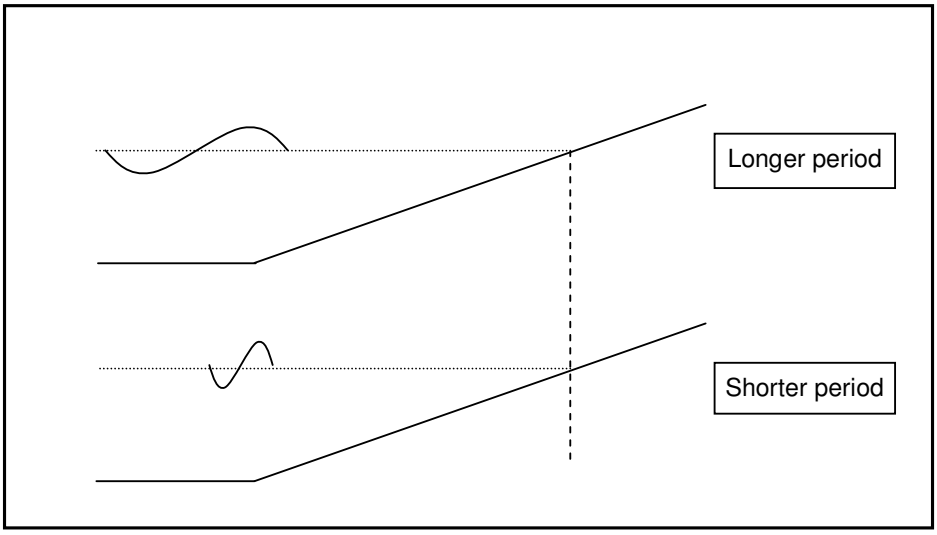

Figure 5.2: View of Two Different Periods of Incoming Wave on Same Bottom Slope

The general condition obtained for hydrodynamic parameters in simulations is that longer-period incoming waves cause higher maximum coastal amplitude and current. But in contrary, higher maximum hydrodynamic demands occur with shorter wave period. The reason for this result may be occurrence of smaller flow depths for smaller wave periods.

5.3 Bottom Slope Effect

Figure 5.3 shows the two different bottom slopes having the same incoming wave amplitude and wave shape. On the milder slope, wave propagates slower on the shallower depth and through longer distances. This situation is the main reason of the slope effect.

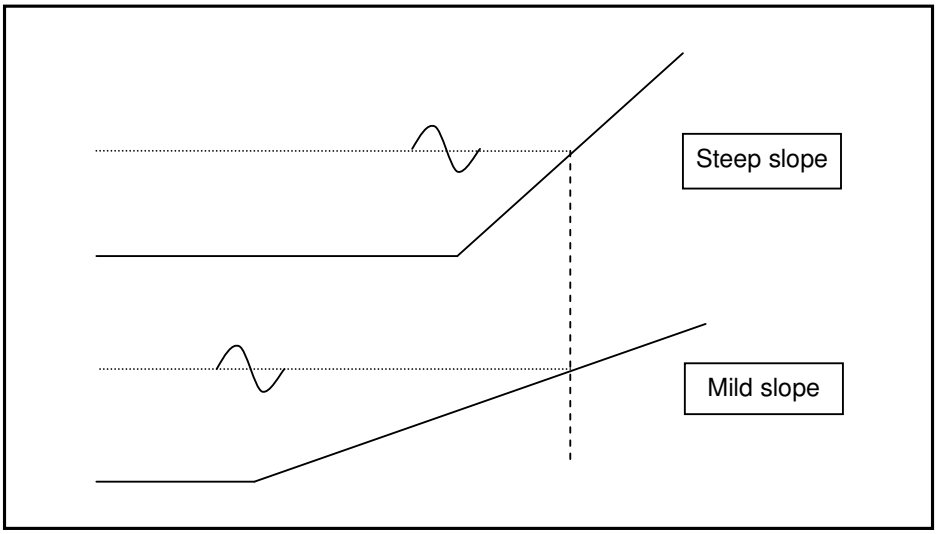

Figure 5.3: View of Two Different Bottom Slopes (1/10, 1/20) with the Same Incoming Wave Amplitude and Wave Shape

Through the simulations, it is observed that stronger currents occur on milder slopes when the same wave is inputted onto two different slopes. For the maximum coastal amplitudes, the slope effect also depends on the shape of incoming wave. Simulations show that milder slope causes higher maximum coastal amplitudes for LDW, and lower amplitudes for LEW cases. The reason for this situation is discussed in respective section.

5.4 Wave Shape Effect

Figure 5.4 shows two different shapes (LEW, LDW) of single sinusoidal incoming wave having the same wave amplitude on same bottom slope.

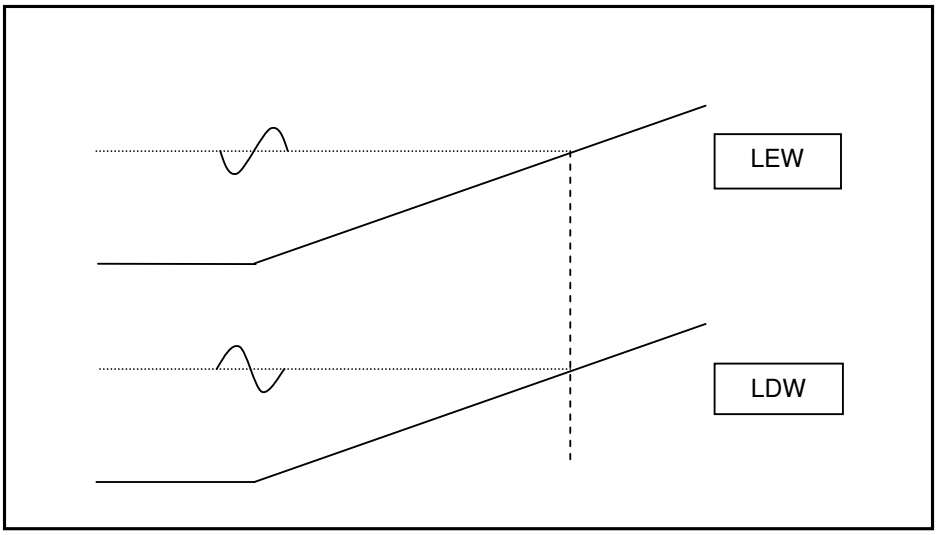

Figure 5.4: View of Two Different Shapes (LEW, LDW) of Single Sinusoidal Incoming Wave with the Same Wave Amplitude on Same Bottom Slope

The main difference in coastal behavior of these two wave shapes is the result of the differences in forward-backward motion, reflection pattern and momentum distribution on the slope and in inundation zone. As mentioned in the part of “bottom slope effect”, this complexity cause contrary in the evaluation of the slope effect on hydrodynamic parameters.

5.5 Wave Direction Effect

Direction and length (period) of any incoming wave are the most important parameters governing their transformation (i.e. change of wave height and direction) on the slopes. When waves approach obliquely, transformation

phenomenon occurs in addition to shoaling and reflection phenomena. Therefore, the effects of wave direction on the hydrodynamic parameters become more complex.

In general, the expected distributions of hydrodynamic parameters (higher values at the wave side for shore-perpendicular and at the lee side of the shore-parallel structures) are obtained for the oblique approach of the wave. However, there are some irregular distributions which are considered as the result of above mentioned complexity of additional long wave transformation phenomenon on the selected slopes.

5.6 Grid Size Effect

In order to check the grid size effect on the results, a smaller grid size with the same wave and bathymetric conditions were simulated. Figures 5.5 - 5.10 show the comparison of the distribution of hydrodynamic parameters for grid sizes of 2.5m and 5m on 1/20 bottom slope for LEW with perpendicular approach. These figures provide that the distributions of all hydrodynamic parameters are similar for both simulations with different grid sizes. Since the distributions are evaluated quantitatively in this study, there are small and acceptable differences between the results of simulations using two different grid sizes. Peak values of hydrodynamic parameters are plotted for the both grid sizes and it is observed that these values are also located in the same zones as shown in the same Figures.

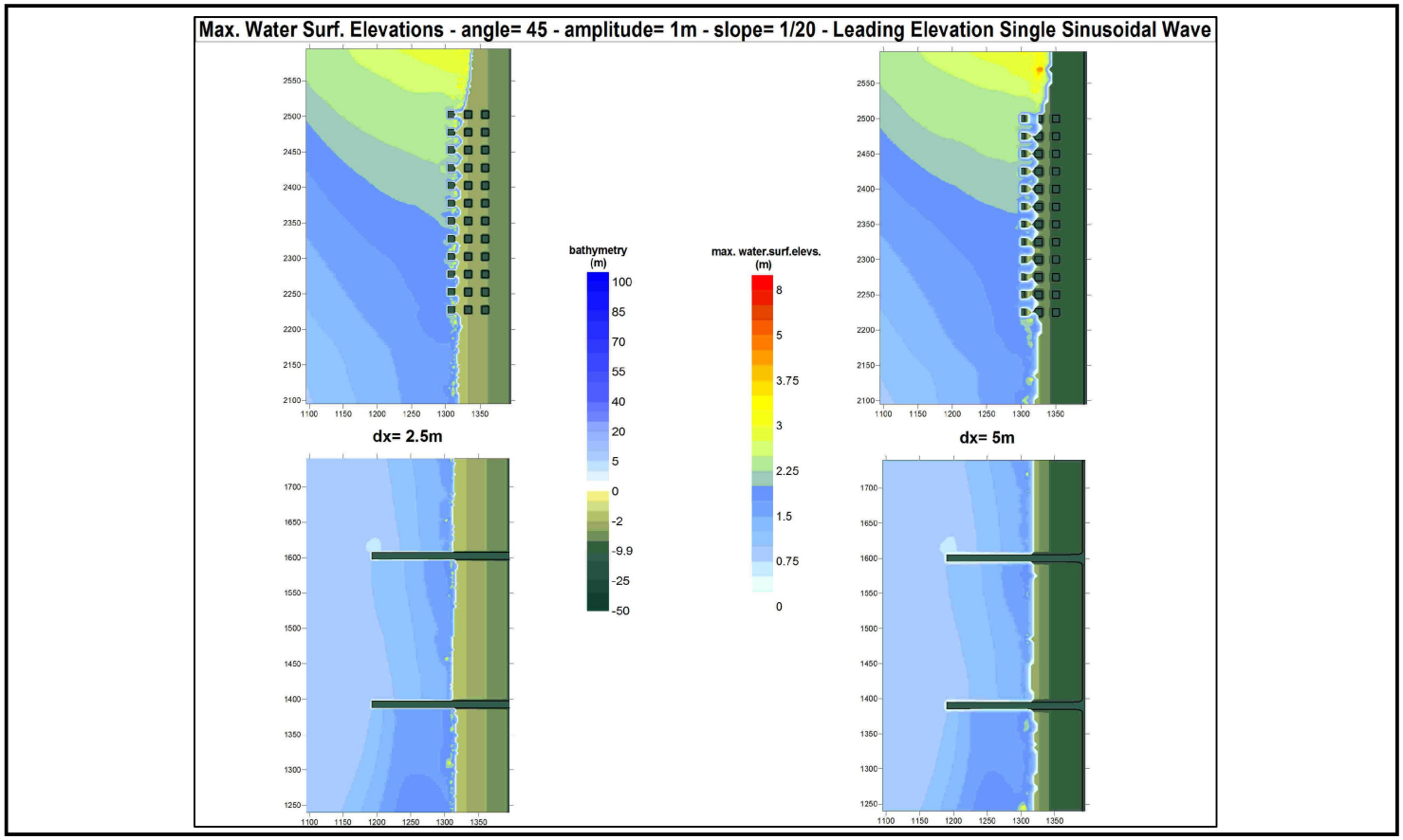

Figure 5.5: Comparison of Distribution of Maximum Positive Amplitudes for the Grid Sizes of 2.5*m* and 5*m*, with Oblique Approach of the Wave (angle=45º), Period of 3*min.* and Bottom Slope of *1/20* for LEW (Incoming Wave Amplitude= +1.0*m* at the toe)

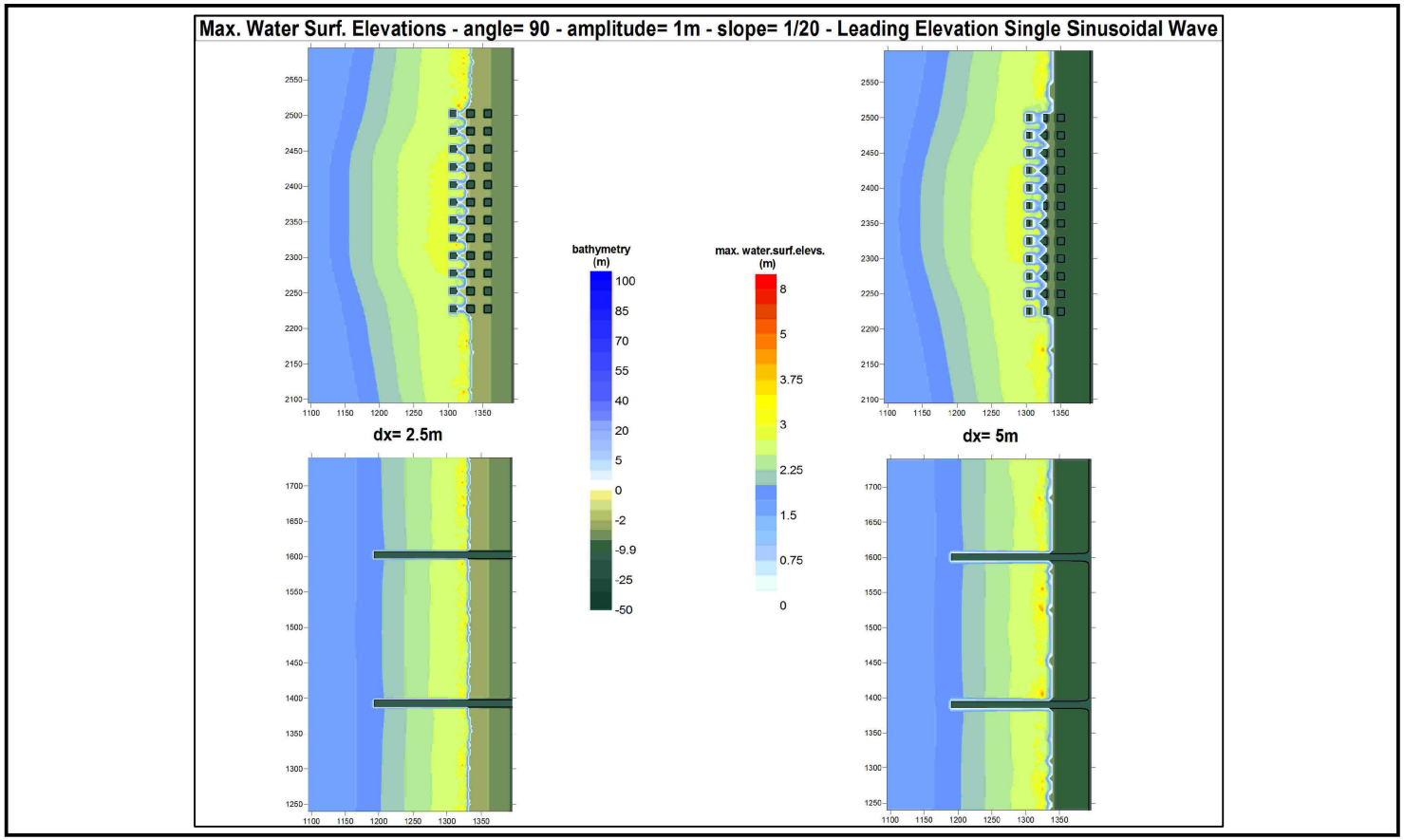

Figure 5.6: Comparison of Distribution of Maximum Positive Amplitudes for the Grid Sizes of 2.5*m* and 5*m*, with Perpendicular Approach of the Wave (angle=90º), Period of 3*min*. and Bottom Slope of *1/20* for LEW (Incoming Wave Amplitude= +1.0*m* at the toe)

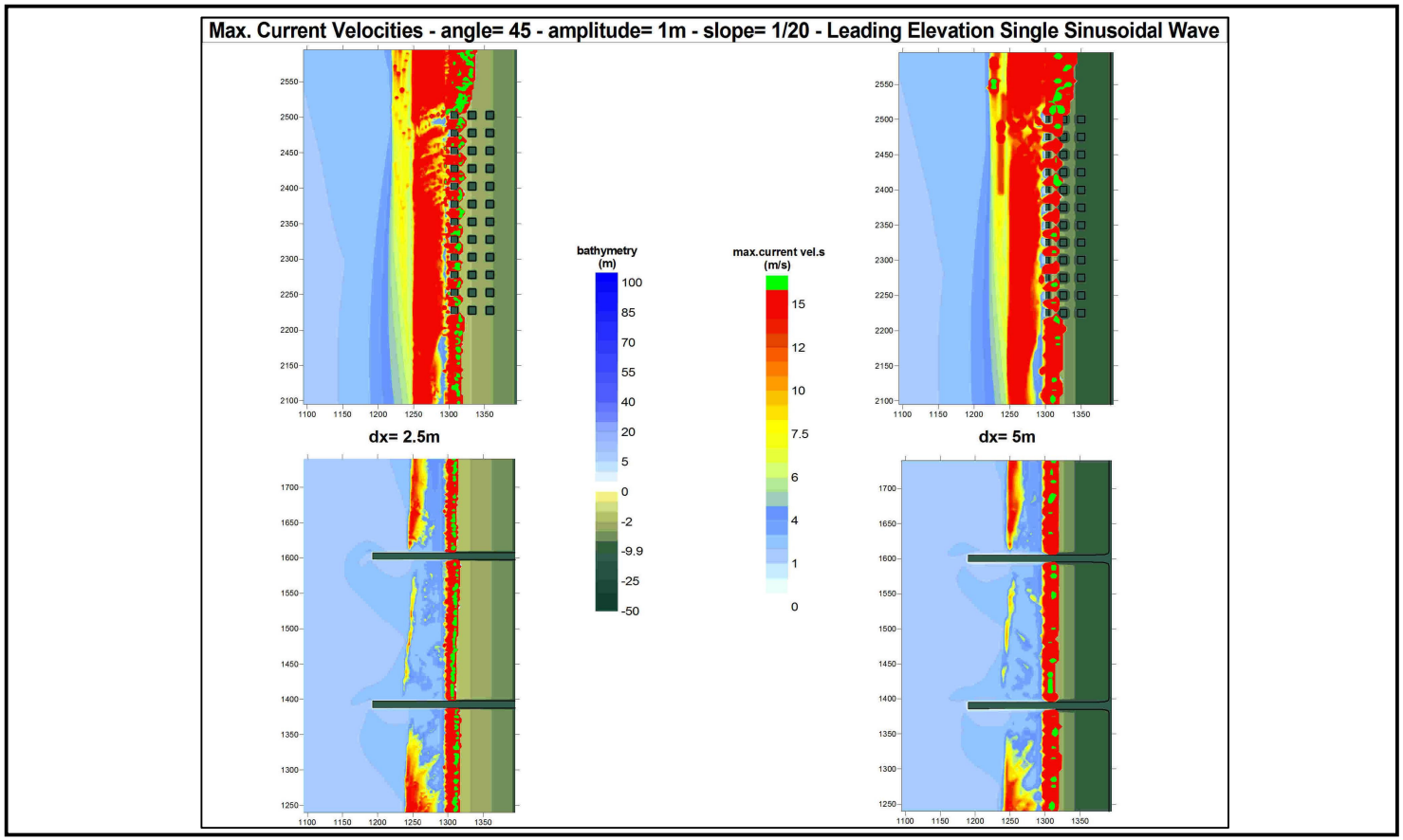

Figure 5.7: Comparison of Distribution of Maximum Current Velocities for the Grid Sizes of 2.5*m* and 5*m*, with Oblique Approach of the Wave (angle=45º), Period of 3*min*. and Bottom Slope of *1/20* for LEW (Incoming Wave Amplitude= +1.0*m* at the toe)

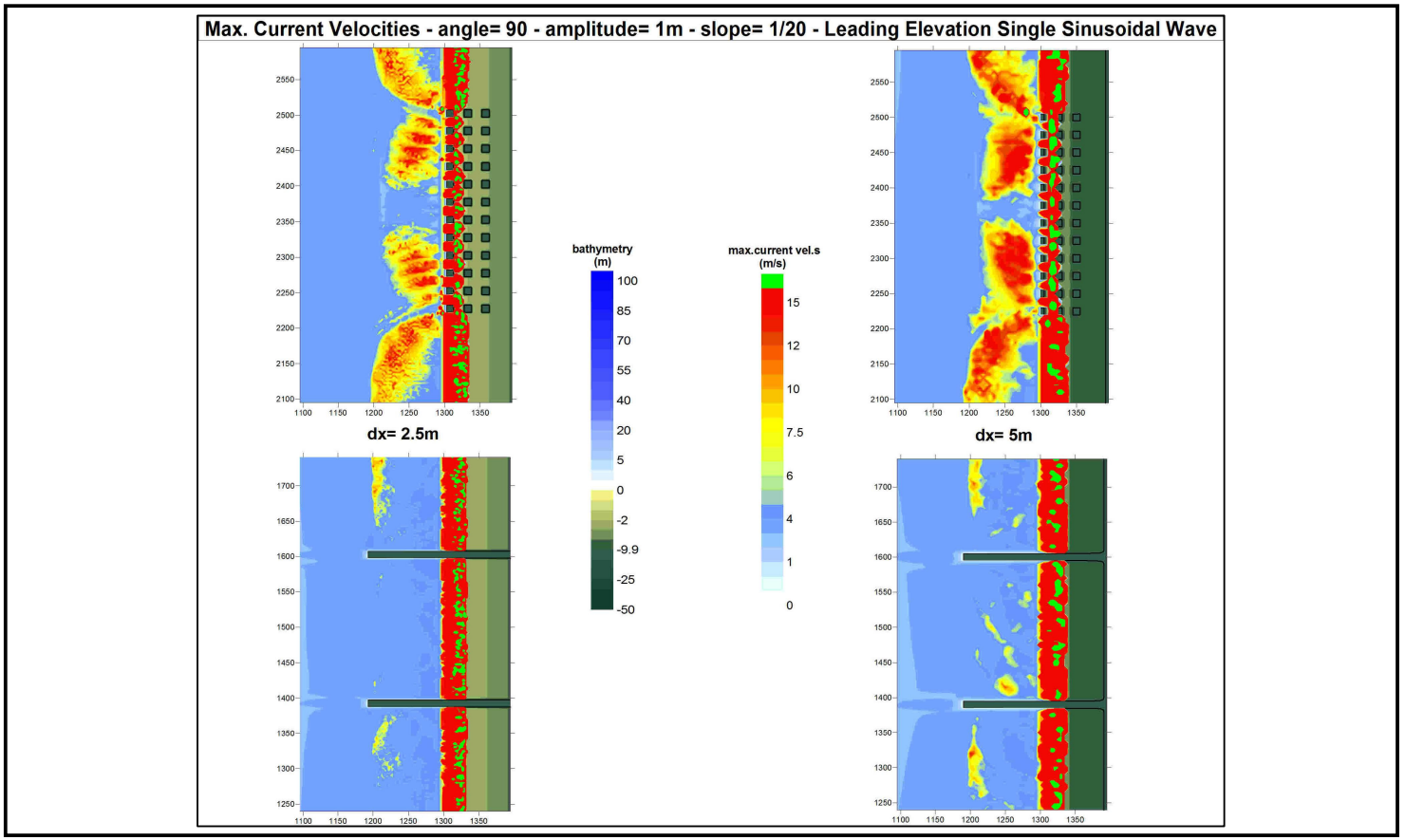

Figure 5.8: Comparison of Distribution of Maximum Current Velocities for the Grid Sizes of 2.5*m* and 5*m*, with Perpendicular Approach of the Wave (angle=90º), Period of 3*min*. and Bottom Slope of *1/20* for LEW (Incoming Wave Amplitude= +1.0*m* at the toe)

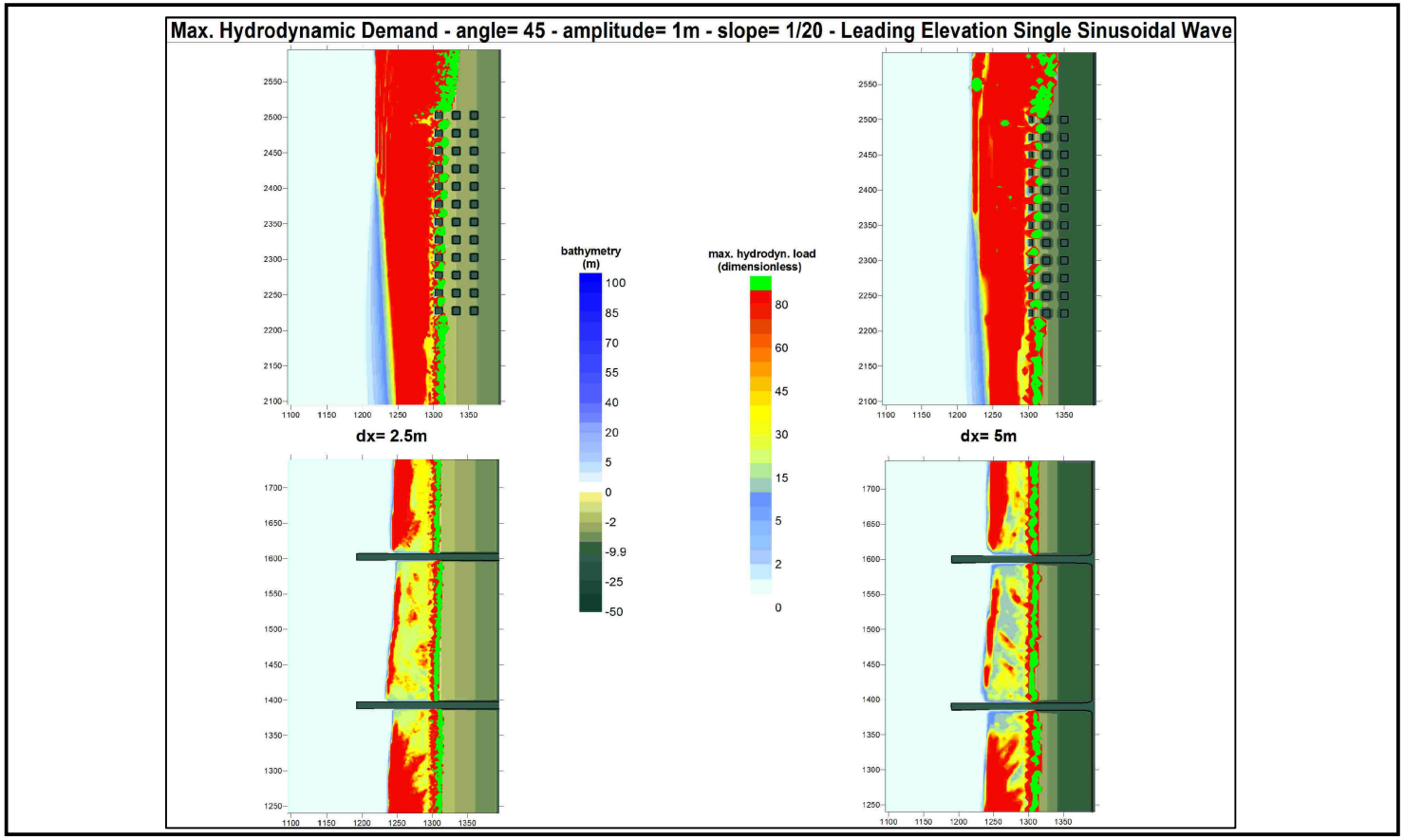

Figure 5.9: Comparison of Distribution of Maximum Hydrodynamic Demands for the Grid Sizes of 2.5*m* and 5*m*, with Oblique Approach of the Wave (angle=45º), Period of 3*min*. and Bottom Slope of *1/20* for LEW (Incoming Wave Amplitude= +1.0*m* at the toe)

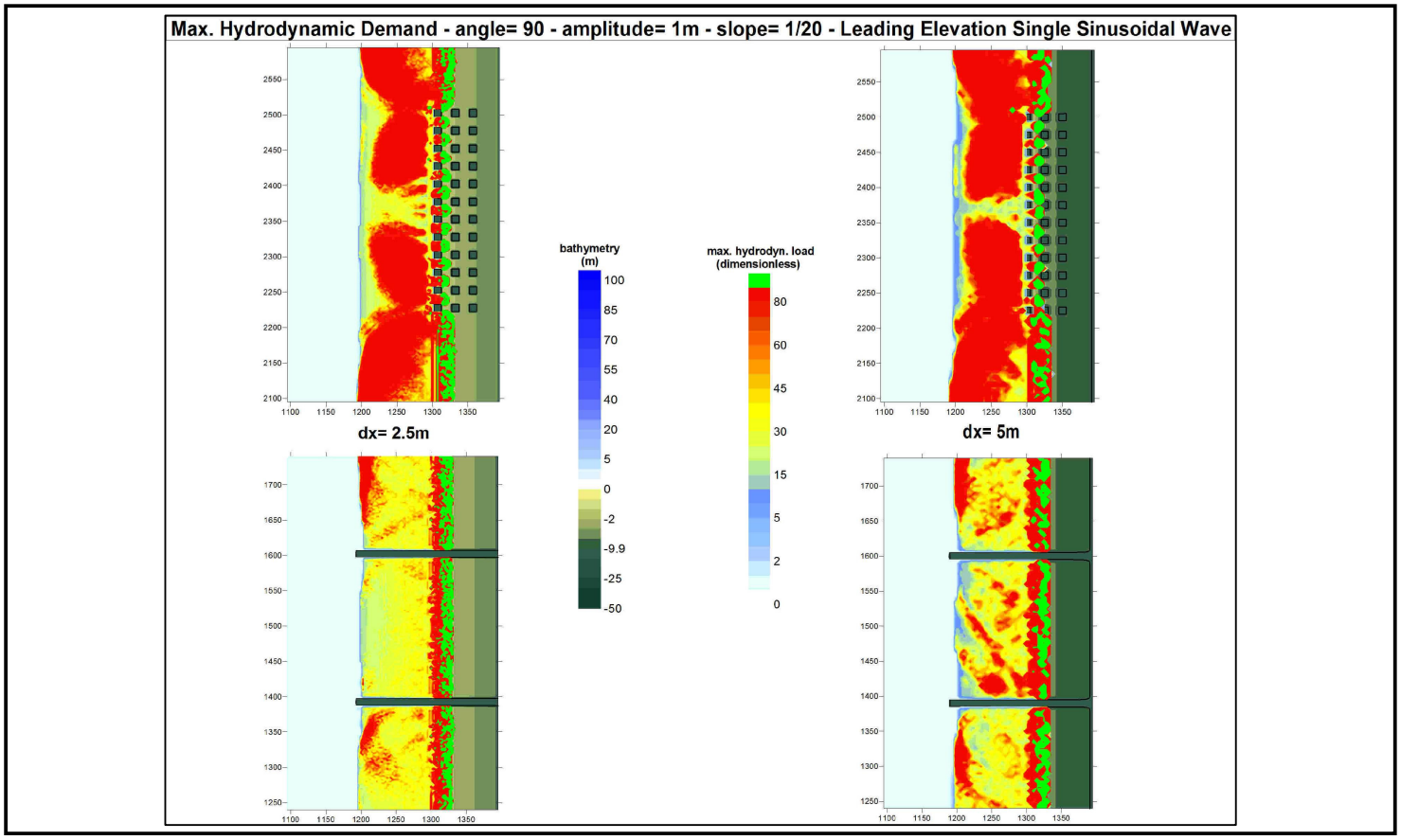

Figure 5.10: Comparison of Distribution of Maximum Hydrodynamic Demands for the Grid Sizes of 2.5*m* and 5*m*, with Perpendicular Approach of the Wave (angle=90º), Period of 3*min*. and Bottom Slope of *1/20* for LEW (Incoming Wave Amplitude= +1.0*m* at the toe)

5.7 Conclusions

In this study, two different kinds of single sinusoidal waves (LEW and LDW) have been used with different incoming wave amplitudes on two different bottom slopes (1/10 and 1/20). The numerical model TUNAMI-N2 was used in simulations with the grid size of 5*m*. The distributions of three important hydrodynamic parameters, as maximum positive amplitudes, maximum current velocities and hydrodynamic demand, were plotted and investigated in inundation zone by applying numerous simulations. The distributions of these three parameters were presented using the extracted parts of the whole bathymetry including the region of shore-parallel and shore-perpendicular structures, respectively. The grid size effect was also investigated by making simulations with the grid size of 2.5*m*. It is necessary to express that the following remarks are limited with these parameters and wave conditions.

As for the conclusions, the concluding remarks are summarized from the simulations and analysis of this study:

1. Higher-amplitude waves cause higher values of hydrodynamic parameters generally during tsunami inundation in shallower region and also inland.

2. Longer-period incoming waves cause higher maximum coastal amplitude and current. But in contrary, higher maximum hydrodynamic demands occur with shorter wave period.

3. Waves propagated slower on the shallower depth and through longer distances on milder slopes. However, stronger currents occurred on milder slopes. It was obtained that, for the maximum coastal amplitudes, the slope effect also depends on the shape of incoming wave.

As a result, milder slope caused higher maximum coastal amplitudes for LDW, and lower amplitudes for LEW cases.

4. It was noticed that there are significant differences between the coastal behaviors of two selected wave shapes. This difference is the result of the variations in forward-backward motion, in reflection pattern and in momentum distribution on the slope and in inundation zone. It was concluded that these differences are the main reason for the complexity in the determination of slope effect on hydrodynamic parameters.

5. The effects of wave direction on the hydrodynamic parameters were more complex since transformation phenomenon occurs in addition to shoaling and reflection phenomena, when waves are approaching to the shoreline obliquely. As generally expected for the oblique approach of the wave, higher values of hydrodynamic parameters were obtained at the wave side of shore-perpendicular and at the lee side of shore-parallel structures. However, some irregular distributions were found as the result of additional long wave transformation phenomenon. This complexity is important and specific study is necessary to understand long wave behavior in coastal regions for oblique approach for each case.

6. The results of simulations with the grid sizes of 2.5m and 5m provide that the distributions of all hydrodynamic parameters are similar for both grid sizes. It is observed that peak values of hydrodynamic parameters are also located in the same zones. Small difference can be acceptable since the distributions of hydrodynamic parameters are evaluated quantitatively throughout this study.

CHAPTER 6

SUGGESTIONS FOR FURTHER STUDIES

In this study, the distributions of three important hydrodynamic parameters, as maximum positive amplitudes, maximum current velocities and maximum hydrodynamic demands, were investigated in inundation zone on bottom slopes of 1/10 and 1/20, with the wave shapes of LEW and LDW, for the wave periods of 1 minute and 3 minutes. A single sinusoidal wave was propagated in inundation zone to identify the effects of hydrodynamic parameters on shore-parallel and shore-perpendicular structures.

It is suggested that further studies should be performed by using different bottom slopes, wave shapes, wave periods and directions with different number of waves to be able to generalize the numerical results. Various orientation and amount of coastal and land structures can also be used in simulations to have results for many different cases.

Beside the selected parameters, the distribution of other hydrodynamic parameters occurred during tsunami inundation can be investigated. For instance, the distribution of instantaneous flow depths, runup values and the direction of maximum currents in inundation zone can be determined.

Forward and backward maximum hydrodynamic demands can be determined in inundation zone. This study can give the opportunity to define the erosion/deposition pattern of coastal and land structures, and also vulnerability index that represents the resistance of structures depending highly on structure material. In further studies, after estimating the vulnerability index and drag coefficient, the risk level during tsunami inundation

can be determined as equal to the multiplication of hydrodynamic demand, vulnerability index and drag coefficient.

Simulations can be performed for solitary type of waves to investigate the distribution of hydrodynamic parameters for this type of wave, and to make comparisons and discussions with previous numerical and also analytical results.

This study indicates that there is proportionality with experimental and numerical results of wave front velocity. However, only one experiment is not sufficient for comparison. Therefore, it is necessary to make experiments to determine wave front velocity and current velocity for further comparisons. These experiments will also enable us to determine/ verify hydrodynamic demands by using both current velocities and wave front velocities and discuss the distribution of this ratio to see which velocity is more effective at which location of the inundation zone.

Experimental study is necessary for verification and for performing more reliable comparisons and discussions.

REFERENCES

Borrero J.C., Yalçıner, A.C., Kanoğlu, U., Titov, V.,McCathy, D., Synolakis, C.E., (2003). *Producing tsunami inundation maps in California*, *Submarine Landslides and Tsunamis*, Kluwer Academic Publishers, Dordrecht, 315-329.

Choi, B.H., Hong, S.J., Hwang, D., Hidayat, R., Kaistrenko, V., Korolev, Yu., Kurkin, A., Pelinovsky, E., Polukhin, N., Prasetya, G., Razzhigaeva, N., Subandono, D., Yalçıner, A.C., Yoon, S.B., and Zaitsev, A., (2005). *Catastrophic Tsunami in the Indian Ocean (December 26, 2004): Data of Two Field Surveys and Numerical Simulation*, Sumatra Tsunami on 26th December, 2004, Proceedings of the Special Asia Tsunami Session at APAC 2005, editors: Choi, B.H., Imamura, F., ISBN: 89-5708-082-1 98530, 159-187.

Demirbaş, E., (2002). *Comparison of Analytical and Numerical Approaches for Long Wave Run-up*, M.Sc. Thesis, Middle East Technical University.

Erdinç, R.E., (2001). *Tsunami Propagation Related to Offshore Subsidences*, M.Sc. Thesis, Middle East Technical University.

Kanoğlu, U., (2004). *Nonlinear Evolution and Runup-Rundown of Long Waves over a Sloping Beach*, J. Fluid Mech., **513**, 363-372.

Kanoğlu, U., and Synolakis, C.E., (1998). *Long Wave Runup on Piecewise Linear Topographies*, J. Fluid Mech., **374**, 1-28.

Kurkin A.A., Kozelkov A.c., Zaitsev A.I., Zahibo N., and Yalçıner A.C., (2003). *Tsunami risk for the Caribbean Sea Coast*, Izvestiya, Russian Academy of Engineering Sciences, vol. 4, 126 – 149 (in Russian).

Liu, P.L.-F., Cho, Y.-S., Briggs, M.J., Kanoğlu, U., and Synolakis, C.E. (1995). *Run-up of Solitary Waves on a Circular Island*, J. Fluid Mech. **320**, 259-285.

Ramsden J.D., Raichlen, F., (1990). *Forces on Vertical Wall Caused by Incident Bores*, J. Waterway Port, Coastal and Ocean Engineering, **116**(5), 592-613.

Shuto, N., Goto C., Imamura, F., (1990). *Numerical Simulation as a Means of Warning for Near-field Tsunamis*, Coastal Engineering in Japan, **33**(2), 173-193.

Sumer, B.M., Ansal, A., Cetin, K.O., Damgaard, J., Gunbak, A.R., Ottesen Hansen, N-E., Sawicki, A., Synolakis, C.E., Yalciner, A.C., Yuksel, Y., Zen, K., (2007). *Earthquake-Induced Liquefaction around Marine Structures*, J. of Waterway Port, Coastal and Ocean Engineering, ASCE, doi: 10.1061/ (ASCE)0733-950X(2007)133:1(55)

Synolakis, C.E., (2003). *Tsunami and Seiche*, in *Earthquake Engineering Handbook*, W.F. Chen and C. Scawthorn (eds), CRC Press, New York, 9-1 to 9-99.

Synolakis, C., Yalçıner, A.C., Borrero, J, Watts, P., (2000). *Modeling and Tsunami Inundation Maps for Los Angeles Coasts, California, USA*, University of Southern (USC) California), FEMA Research Report.

Synolakis, C.E. (1987). *Run-up of Solitary Waves*, J. Fluid Mech., **185**, 523-545.

Synolakis, C.E. (1986). *The Run-up of Long Waves*, Ph. D. Thesis, California Institute of Technology, Pasadena, California, 91125. 228 pp.

The Overseas Coastal Area Development Institute of Japan (OCDI), (2002). *Technical Standards and Commentaries for Port and Harbor Facilities in Japan,* editors for translation version: Goda, Y., Tabata, T., Yamamoto, S., printed by Daikousha Printing Co., Ltd.

Titov, V.V. and Synolakis, C.E., (1998). *Numerical modeling of tidal wave run-up*, Journal of Waterway, Port, Coastal and Ocean Engineering, **124** (4), 157-171.

Yalçıner, A.C., Karakuş, H., Özer, C., Özyurt, G., (2005). *Short Courses on Understanding the Generation, Propagation, Near and Far-Field Impacts of TSUNAMIS and Planning Strategies to Prepare for Future Events, Course Notes in Kuala Lumpur*, METU Civil Eng. Dept. Ocean Eng. Res. Center

Yalçıner, A.C., Perinçek, D., Ersoy, S., Prasetya,G., Rahman, H., McAdoo, B., (2005). *Report on January 21-31, 2005 North Sumatra Survey on December 26, 2004 Indian Ocean Tsunami*, by ITST of UNESCO IOC. Publ. in http://ioc.unesco.org/iosurveys/Indonesia/yalciner/yalciner.htm

Yalçıner, A.C., Pelinovsky, E., (2005). *A Short Cut Numerical Method for Determination of Resonance Periods of Free Oscillations in Irregular Shaped Basins*, Submitted to Ocean Engineering Journal.

Yalçıner, A., Pelinovsky, E., Talipova, T., Kurkin, A., Kozelkov, A. and Zaitsev, A., (2004). *Tsunamis in the Black Sea: Comparison of the Historical, Instrumental, and Numerical Data*, J. Geophys. Res., AGU, V 109, C12023, doi:10.1029/2003JC002113

Yalçıner, A.C., Pelinovsky, E., Synolakis C., Okal, E., (2003). *NATO SCIENCE SERIES, Submarine Landslides and Tsunamis*, Publisher: Kluwer Academic Publishers, Netherlands, (Editors; Yalçıner, A.C., Pelinovsky, E., Synolakis, C., Okal, E.), 329 Pages, ISBN: 1-4020-1348-5 (HB), ISBN: 1-4020-1349-3 (PB)

Yalçıner, A.C., Alpar,B., Altinok,Y., Ozbay,I., Imamura,F., (2002). *Tsunamis in the Sea of Marmara: Historical Documents for the Past, Models for Future*, Marine Geology, 2002, 190, pp:445-463

Yalçıner, A.C., Synolakis, C.E.,Alpar, B., Borrero, J., Altinok, Y., Imamura, F., Tinti, S., Ersoy, Ş., Kuran, U., Pamukcu, S., Kanoğlu, U., (2001). *Field Surveys and Modeling 1999 Izmit Tsunami*, International Tsunami Symposium ITS 2001, Paper 4-6, Seattle, Washington, 557-563

Yeh, H., (2006). *Tsunami Forces in the Runup Zone*, NSF Caribbean Tsunami Workshop, World Scientific, Editors: Mercado-Irizarry, A., Liu, P., 275-287

Yeh, H., Liu, P-L.F., Synolakis, C.E., (1996). *Long Wave Runup Models*, World Scientific, London.

Zahibo, N., Pelinovsky, E.,Yalçıner, A.C., Kurkin, A., Kozelkov, A., Zaitsev, A., (2003). *Modeling the 1867 Virgin Island Tsunami*, Journal of Natural Hazards and Earth Systems.

Zaitsev, A.I., Kozelkov, A.C., Kurkin, A.A.,Pelinovsky, E.N., Talipova, T.G., Yalçıner, A.C. (in Russian order of alphabet), (2002). *Tsunami Modeling in Black Sea*, published in Izvestiya of Russian Academy of Engineering Sciences, Series: Applied Mathematics and Mechanics, 2002, Vol. 3, pp 27-45.

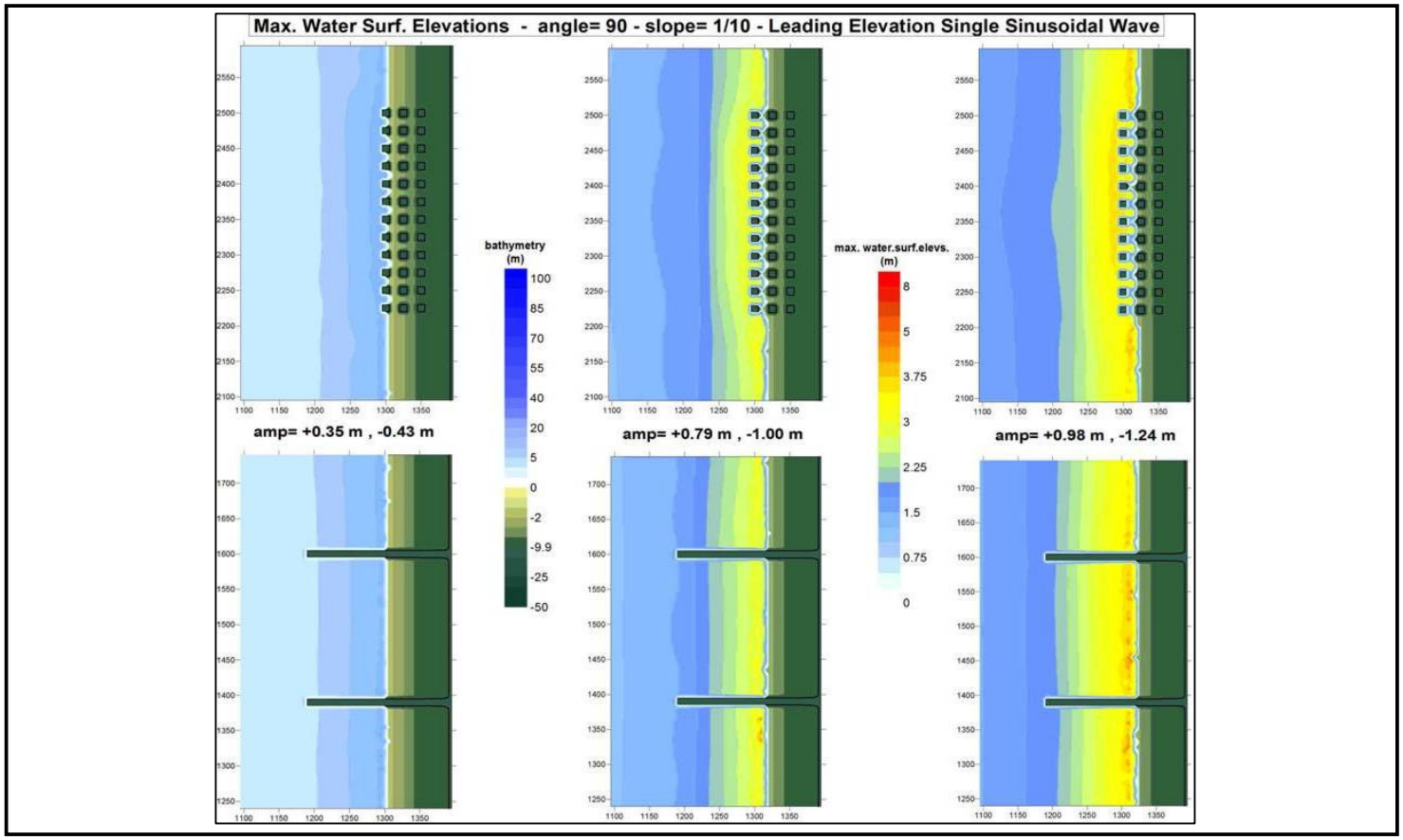

Figure A.1: Distribution of Maximum Positive Amplitudes for Perpendicular Approach of the Wave (angle=90º) with Period of 3 min. for LEW with the Bottom Slope of 1/10
(Incoming Wave Amplitudes= +0.33m, +0.74m, +0.92m at 235 m before the toe)

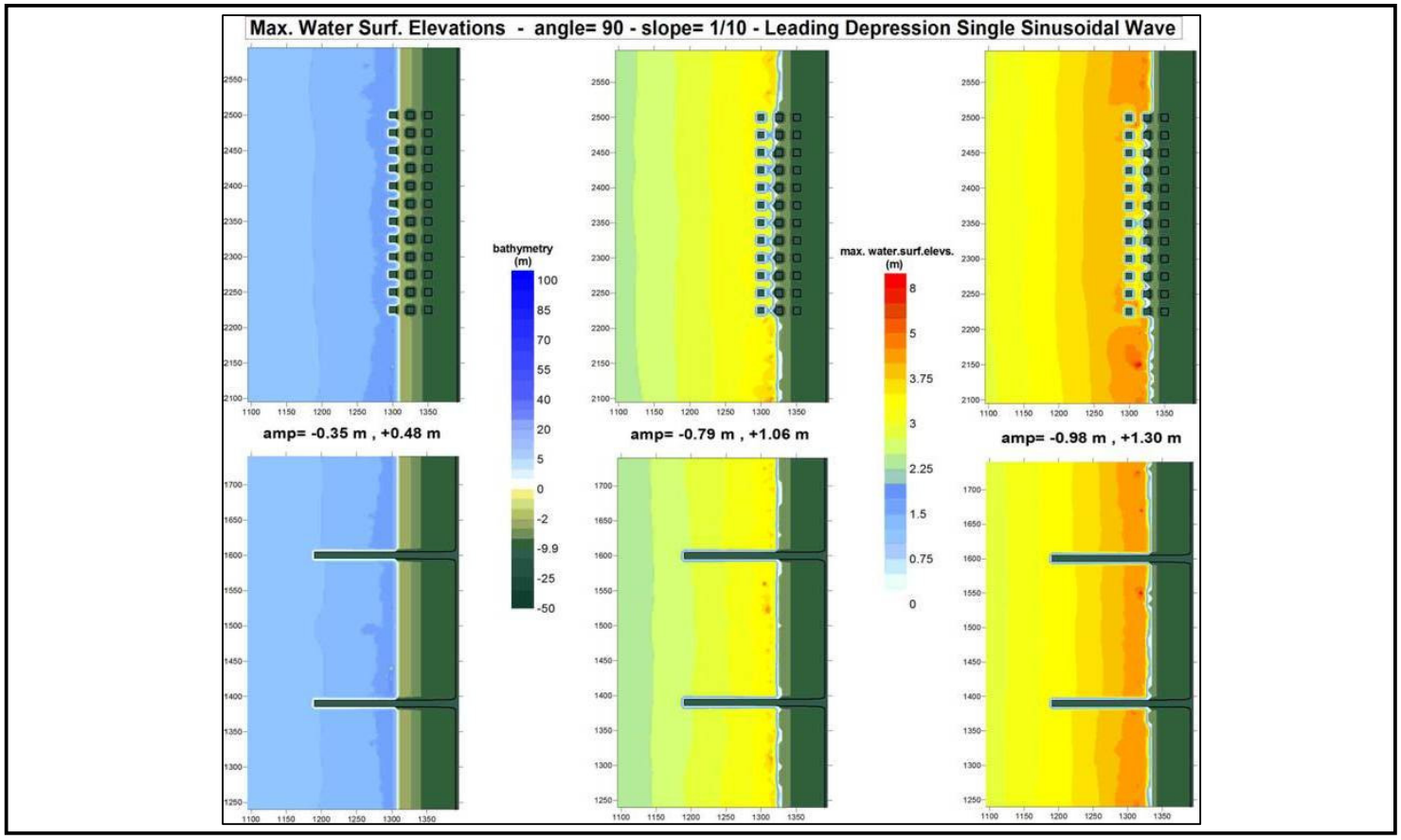

Figure A.2: Distribution of Maximum Positive Amplitudes for Perpendicular Approach of the Wave (angle=90º) with Period of 3 min. for LDW with the Bottom Slope of 1/10
(Incoming Wave Amplitudes= -0.33m, -0.74m, -0.92m at 235 m before the toe)

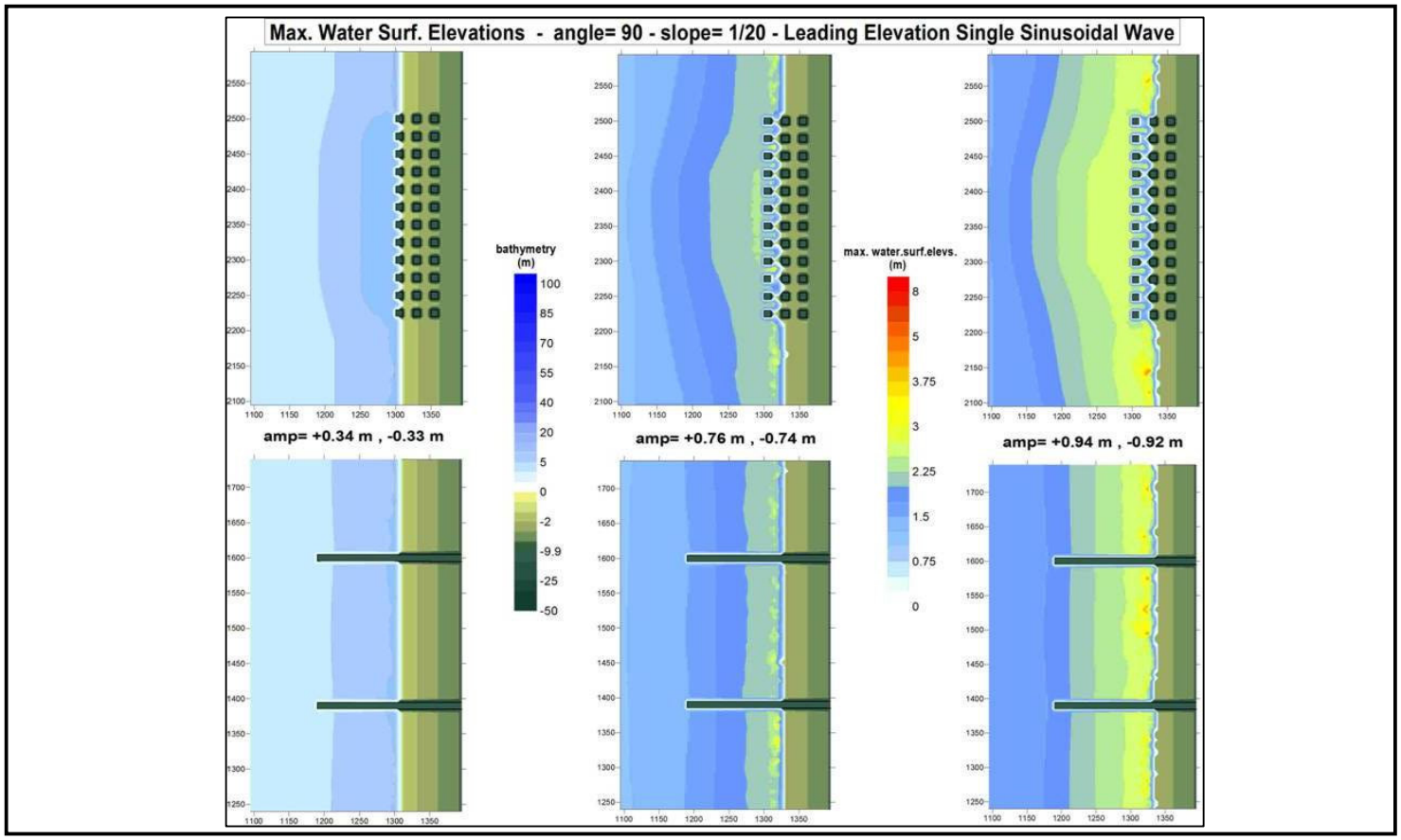

Figure A.3: Distribution of Maximum Positive Amplitudes for Perpendicular Approach of the Wave (angle=90º) with Period of 3 min. for LEW with the Bottom Slope of 1/20
(Incoming Wave Amplitudes= +0.33m, +0.74m, +0.92m at 235 m before the toe)

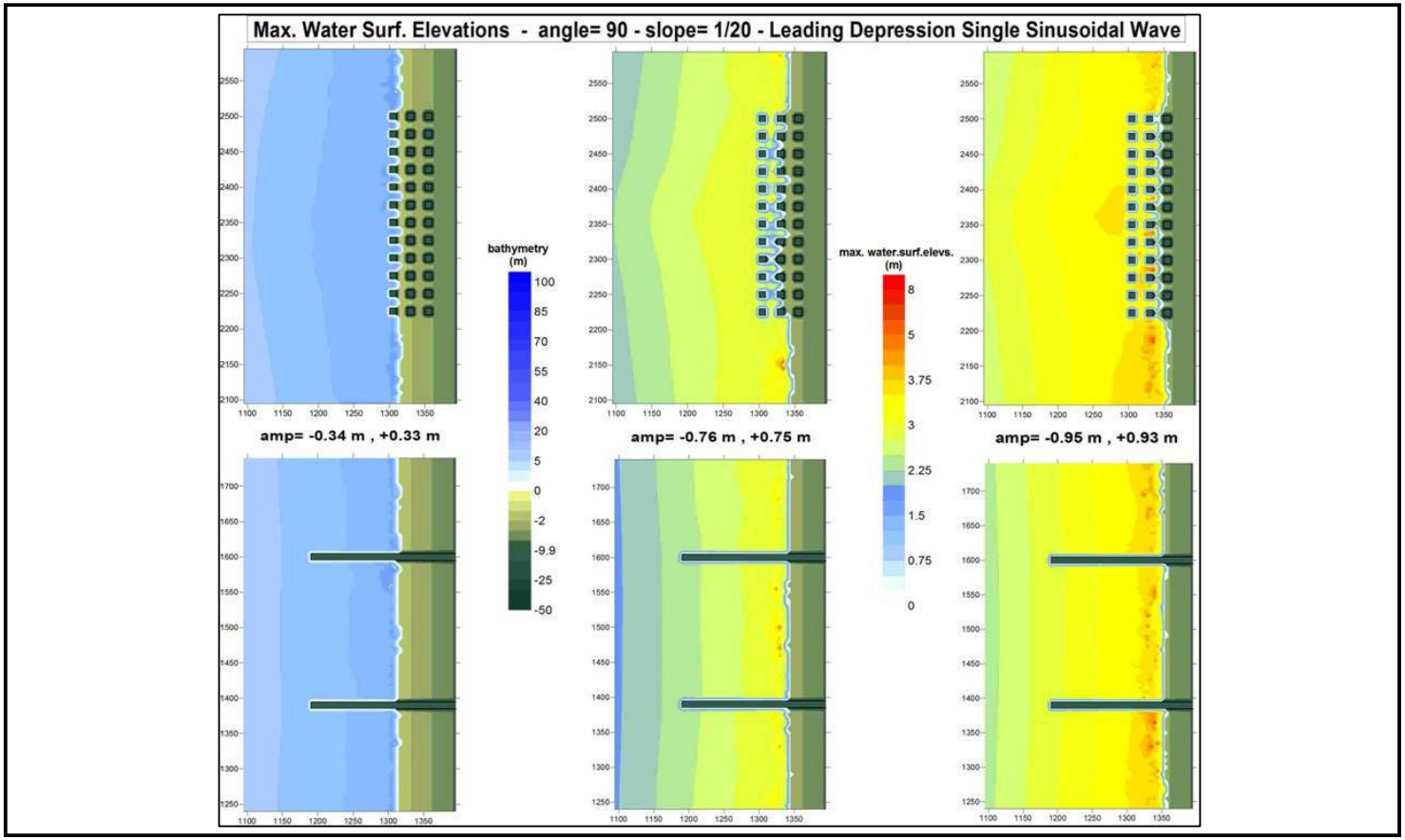

Figure A.4: Distribution of Maximum Positive Amplitudes for Perpendicular Approach of the Wave (angle=90º) with Period of 3 min. for LDW with the Bottom Slope of 1/20
(Incoming Wave Amplitudes= -0.33m, -0.74m, -0.92m at 235 m before the toe)

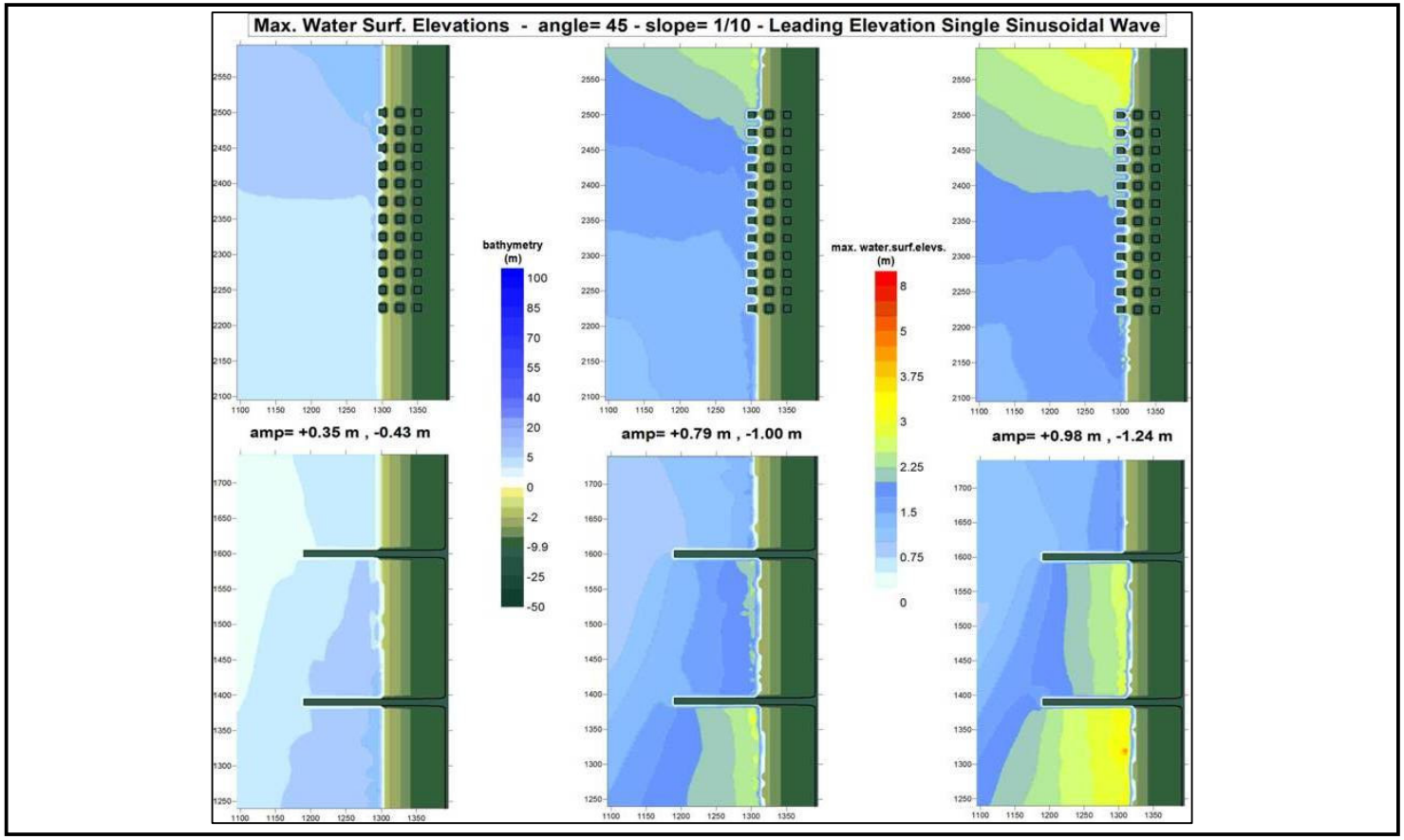

Figure A.5: Distribution of Maximum Positive Amplitudes for Oblique Approach of the Wave (angle=45º) with Period of 3 min. for LEW with the Bottom Slope of 1/10
(Incoming Wave Amplitudes= +0.33m, +0.74m, +0.92m at 235 m before the toe)

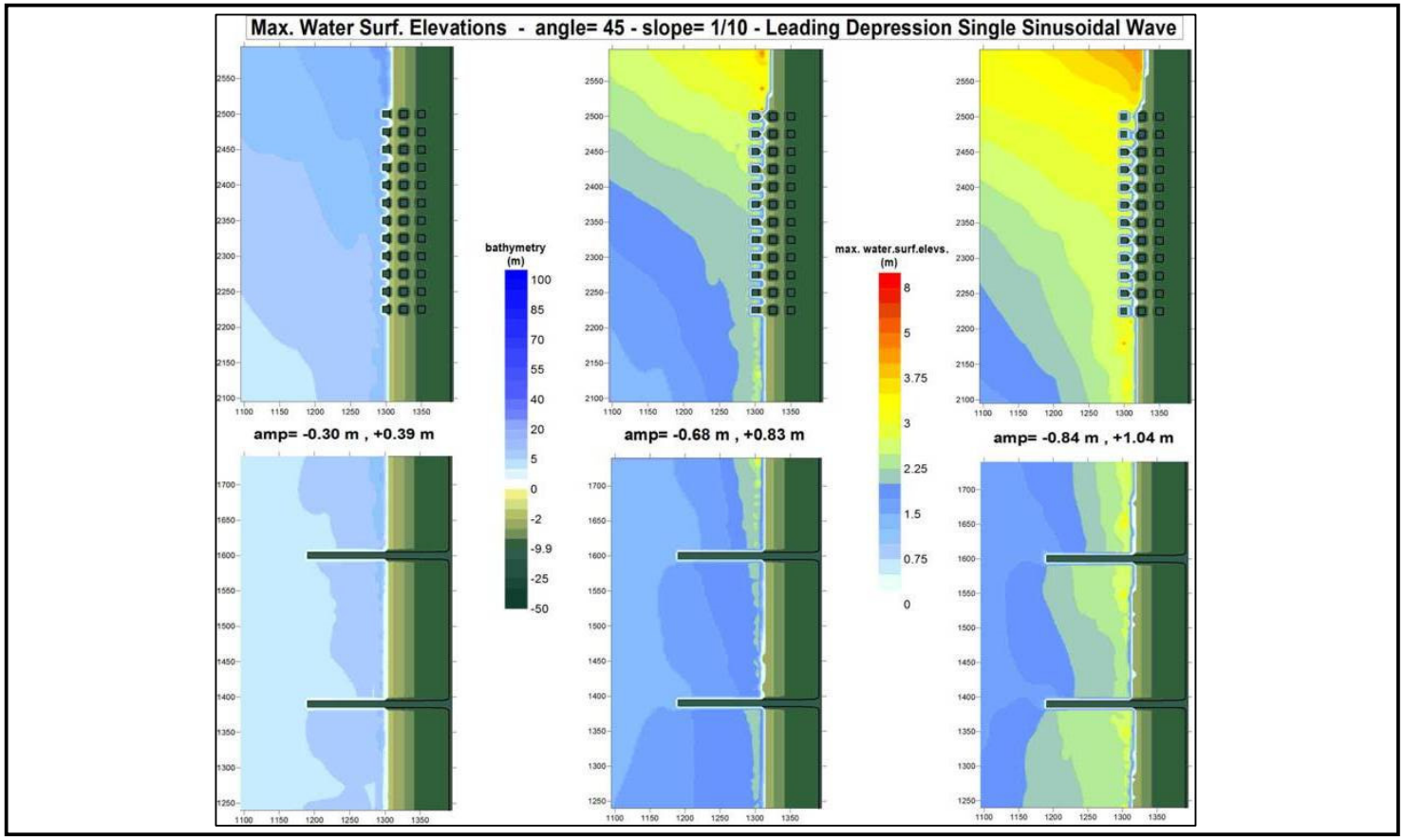

Figure A.6: Distribution of Maximum Positive Amplitudes for Oblique Approach of the Wave (angle=45º) with Period of 3 min. for LDW with the Bottom Slope of 1/10
(Incoming Wave Amplitudes= -0.33m, -0.74m, -0.92m at 235 m before the toe)

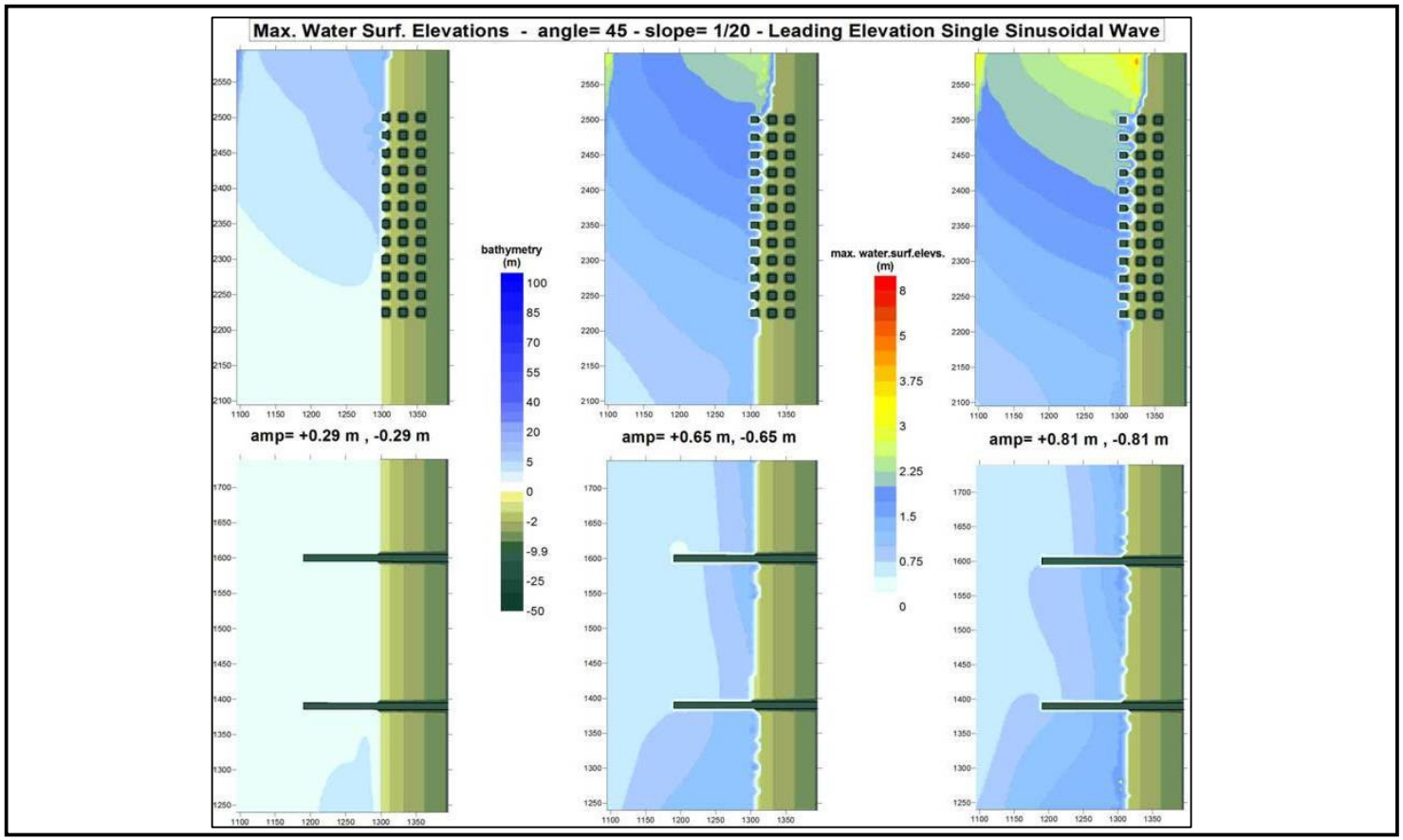

Figure A.7: Distribution of Maximum Positive Amplitudes for Oblique Approach of the Wave (angle=45º) with Period of 3 min. for LEW with the Bottom Slope of 1/20
(Incoming Wave Amplitudes= +0.33m, +0.74m, +0.92m at 235 m before the toe)

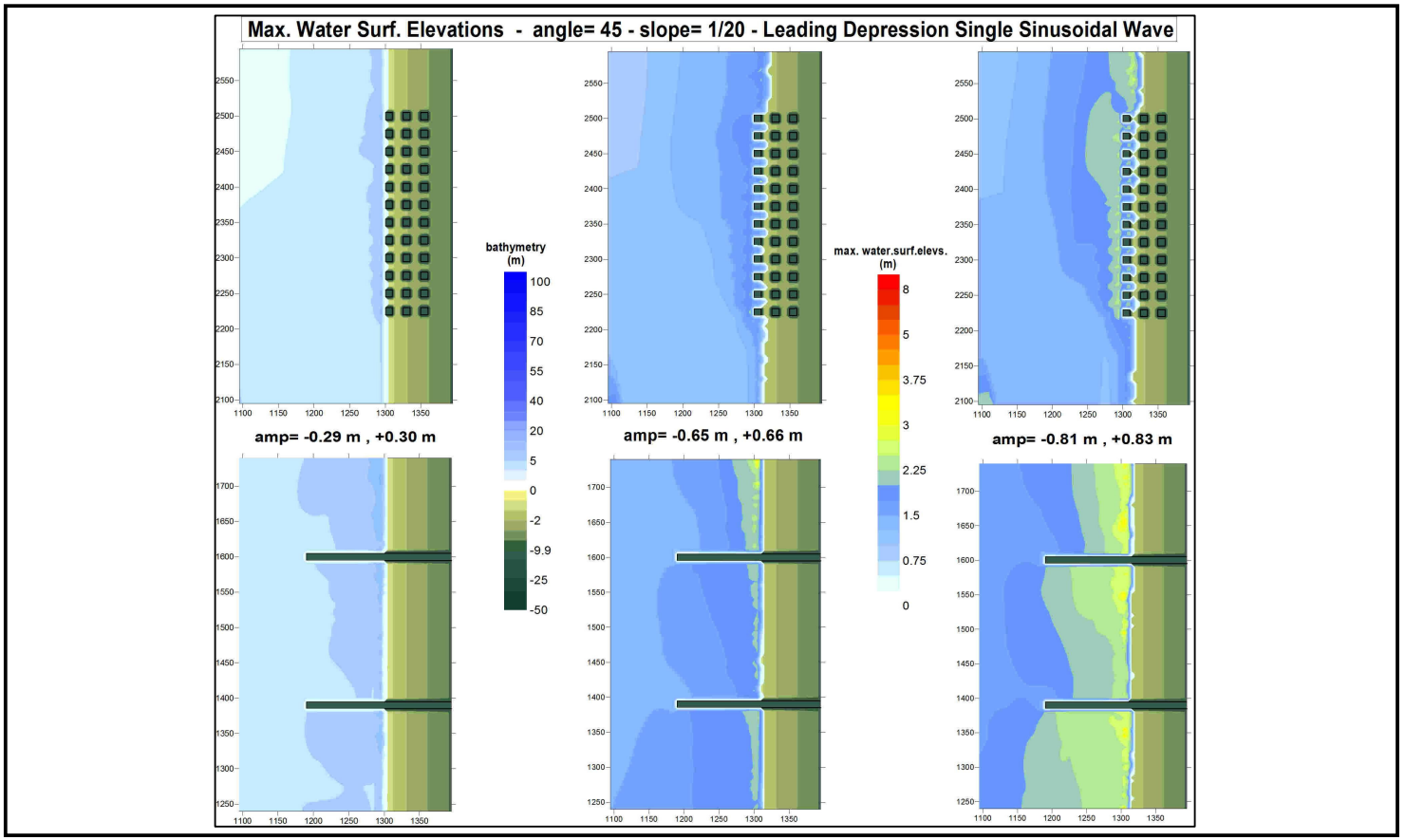

Figure A.8: Distribution of Maximum Positive Amplitudes for Oblique Approach of the Wave (angle=45º) with Period of 3 min. for LDW with the Bottom Slope of 1/20
(Incoming Wave Amplitudes= -0.33m, -0.74m, -0.92m at 235 m before the toe)

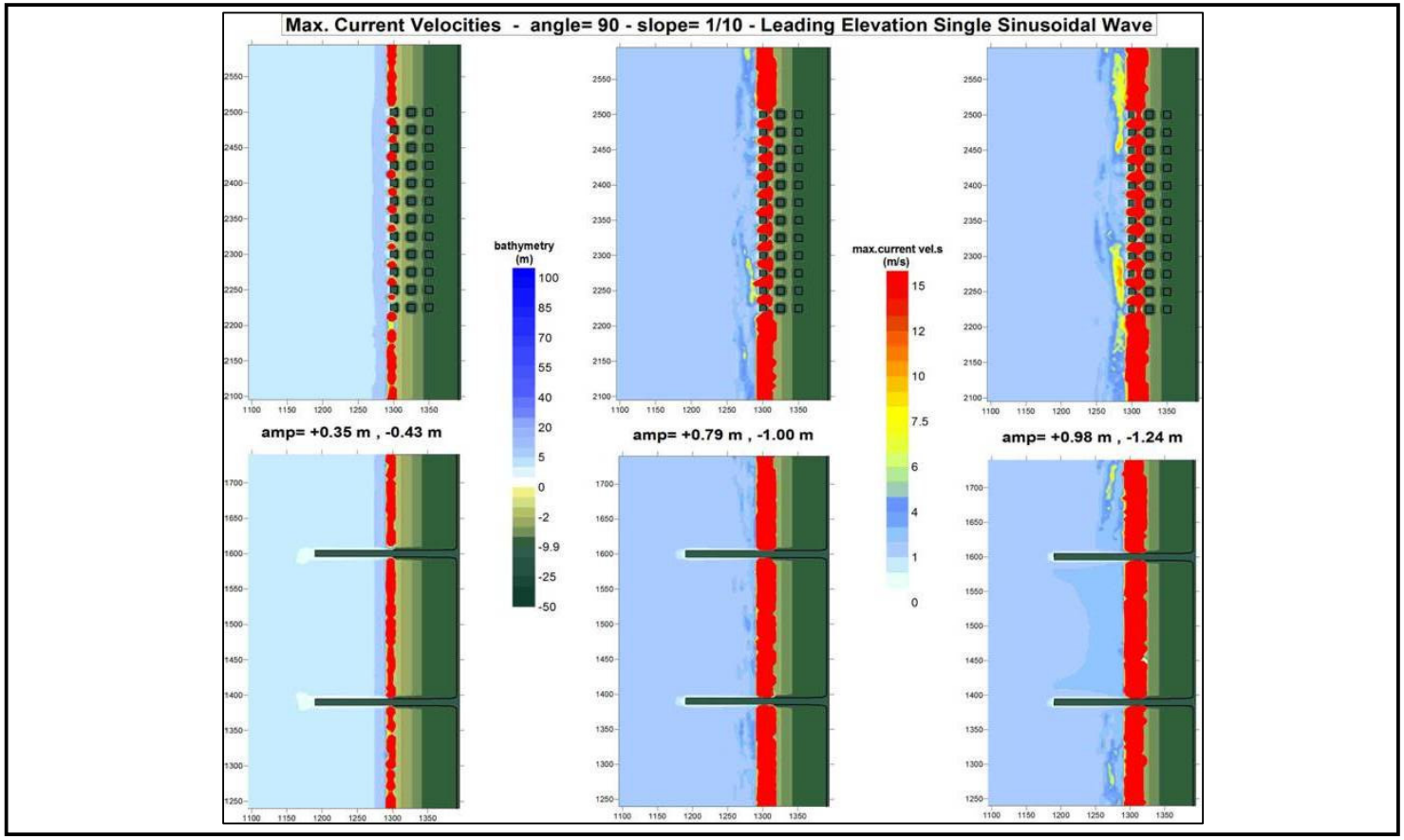

Figure A.9: Distribution of Maximum Current Velocities for Perpendicular Approach of the Wave (angle=90º) with Period of 3 min. for LEW with the Bottom Slope of 1/10
(Incoming Wave Amplitudes= +0.33m, +0.74m, +0.92m at 235 m before the toe)

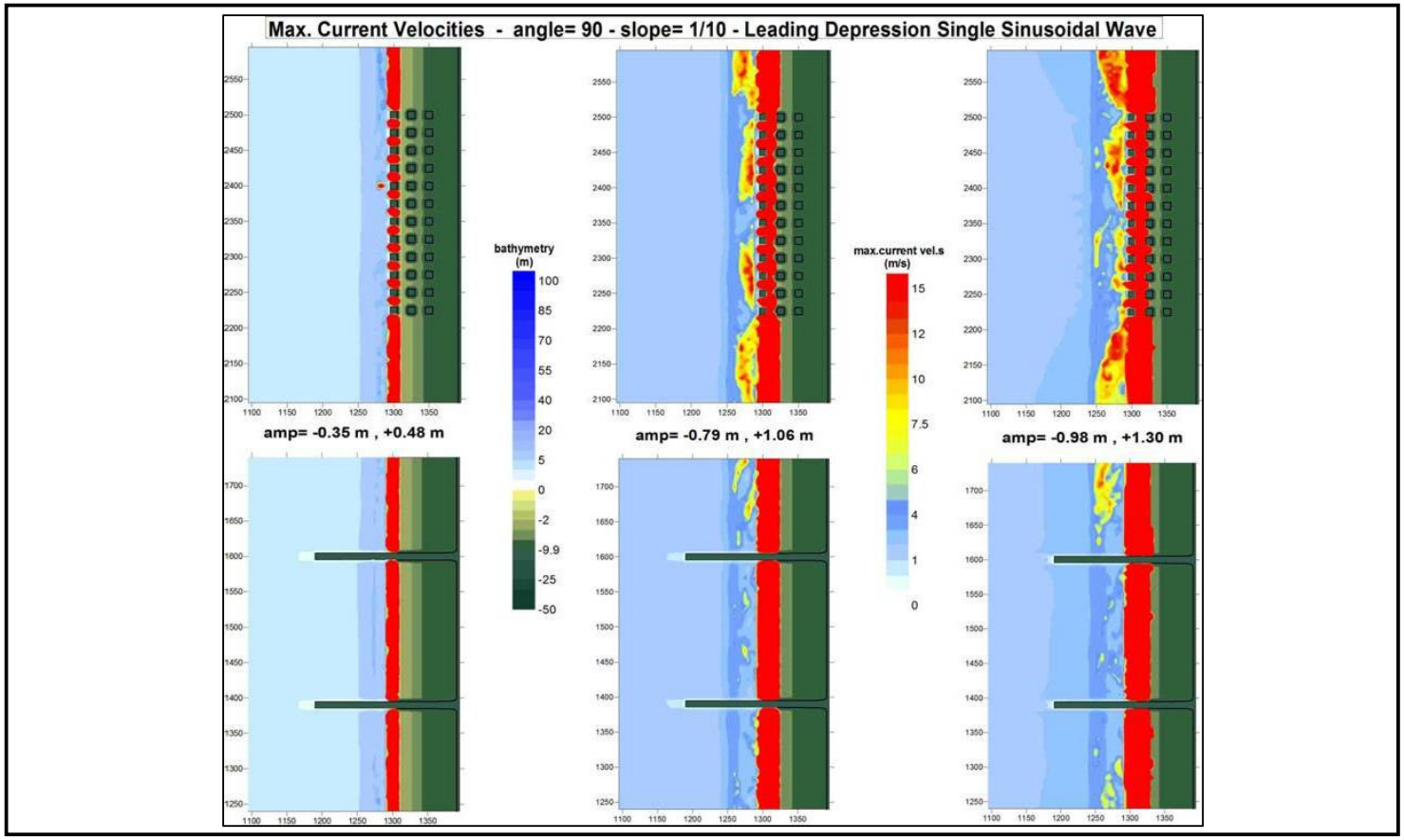

Figure A.10: Distribution of Maximum Current Velocities for Perpendicular Approach of the Wave (angle=90º) with Period of 3 min. for LDW with the Bottom Slope of 1/10
(Incoming Wave Amplitudes= -0.33m, -0.74m, -0.92m at 235 m before the toe)

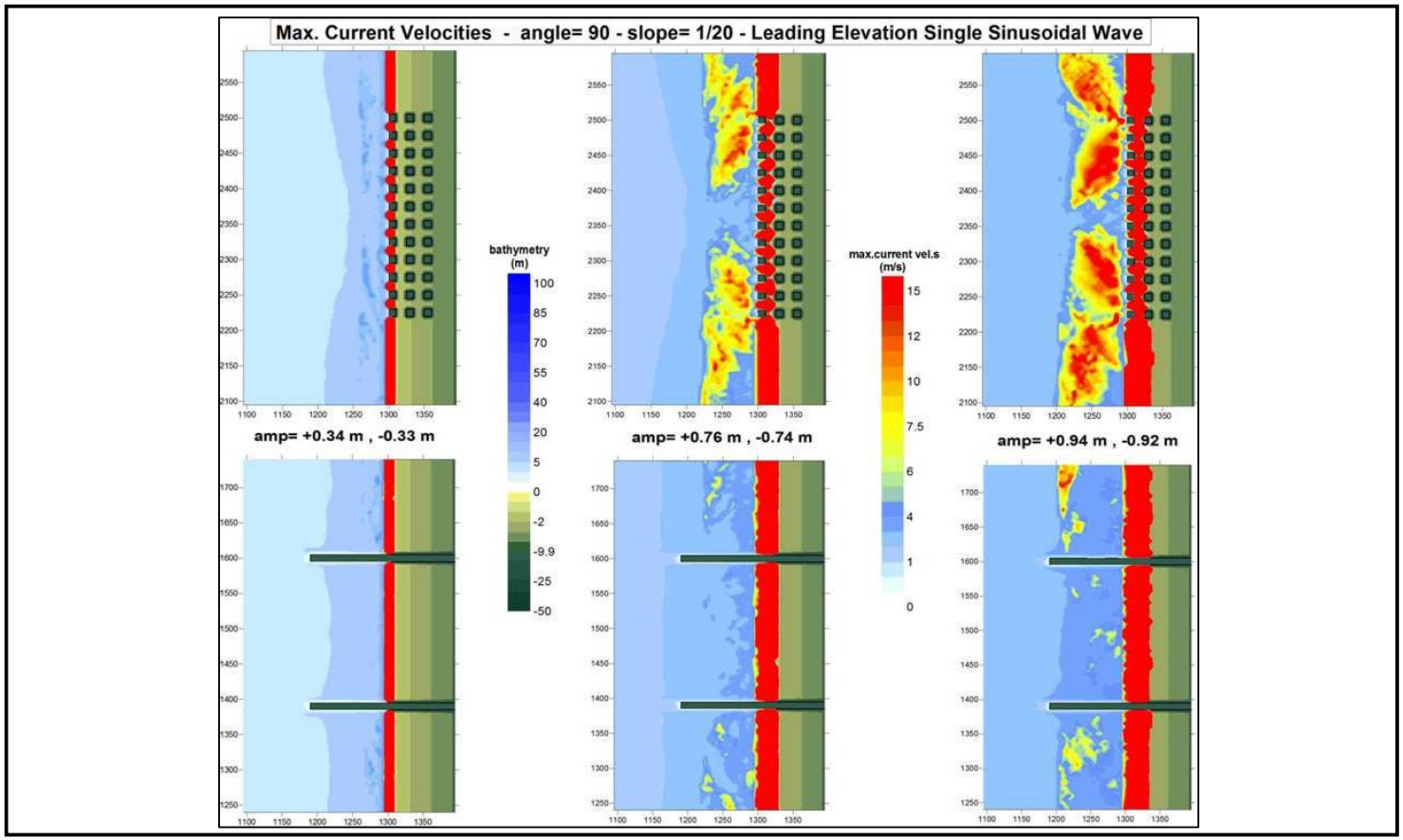

Figure A.11: Distribution of Maximum Current Velocities for Perpendicular Approach of the Wave (angle=90º) with Period of 3 min. for LEW with the Bottom Slope of 1/20
(Incoming Wave Amplitudes= +0.33m, +0.74m,+0.92m at 235 m before the toe)

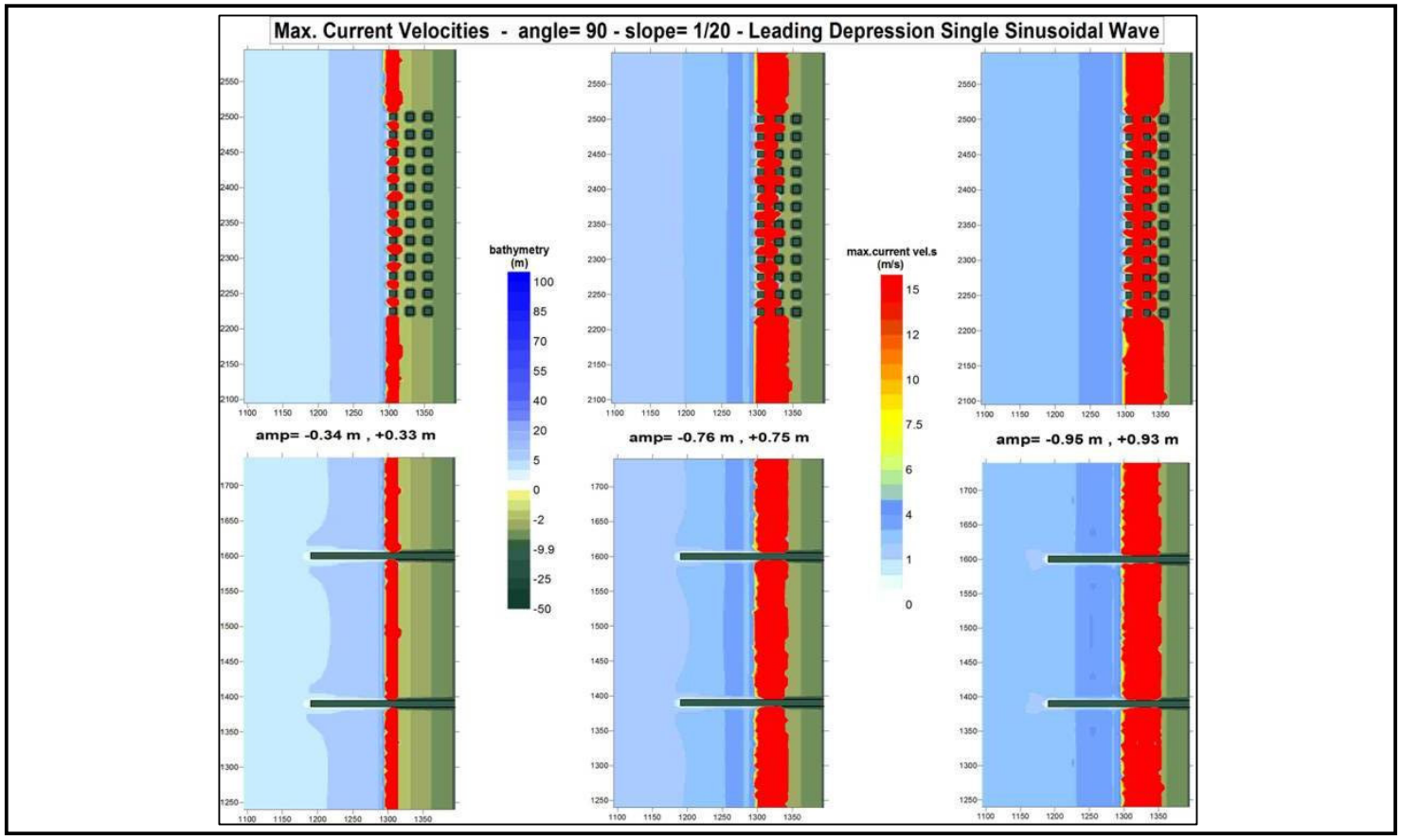

Figure A.12: Distribution of Maximum Current Velocities for Perpendicular Approach of the Wave (angle=90º) with Period of 3 min. for LDW with the Bottom Slope of 1/20
(Incoming Wave Amplitudes= -0.33m, -0.74m, -0.92m at 235 m before the toe)

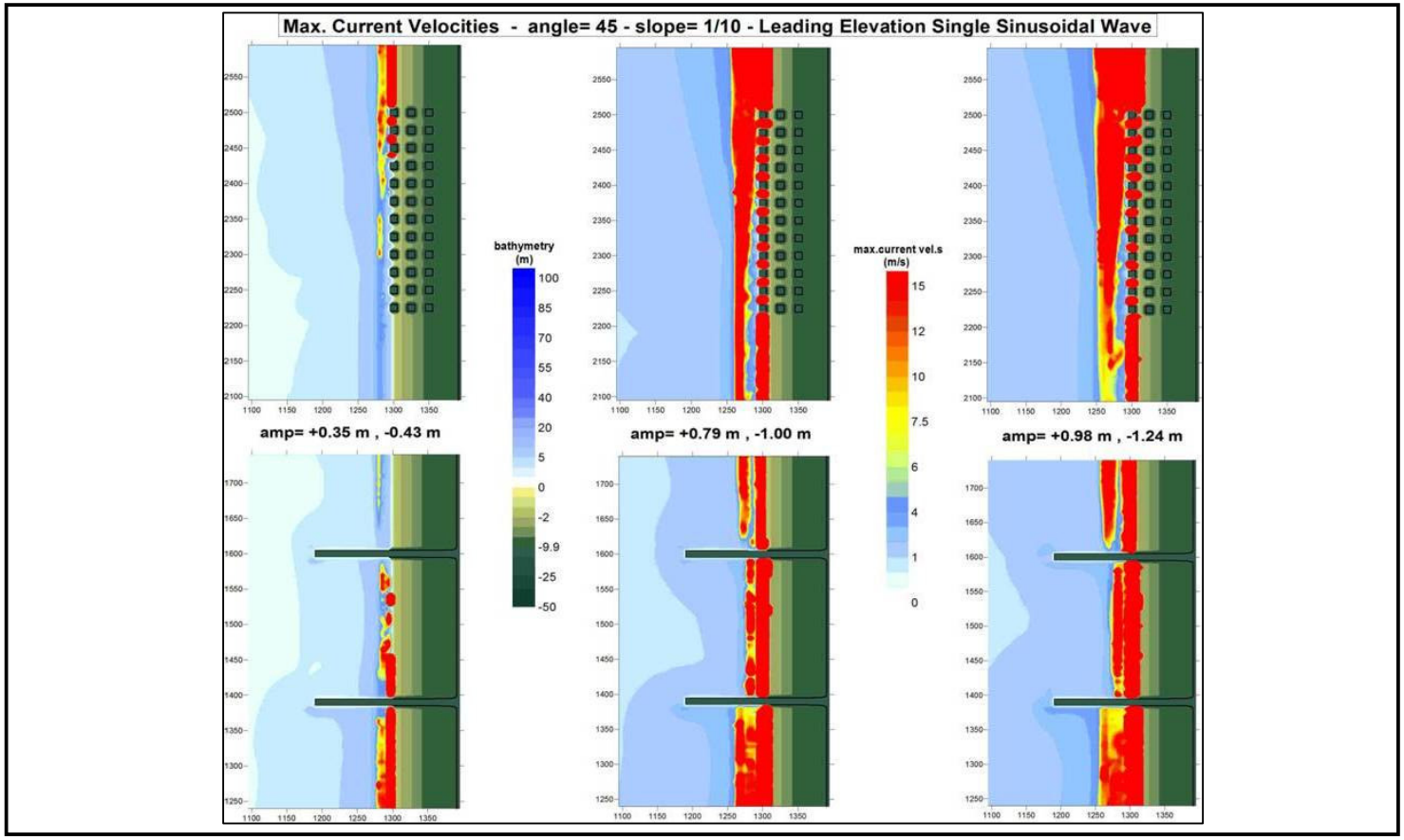

Figure A.13: Distribution of Maximum Current Velocities for Oblique Approach of the Wave (angle=45º) with Period of 3 min. for LEW with the Bottom Slope of 1/10
(Incoming Wave Amplitudes= +0.33m, +0.74m, +0.92m at 235 m before the toe)

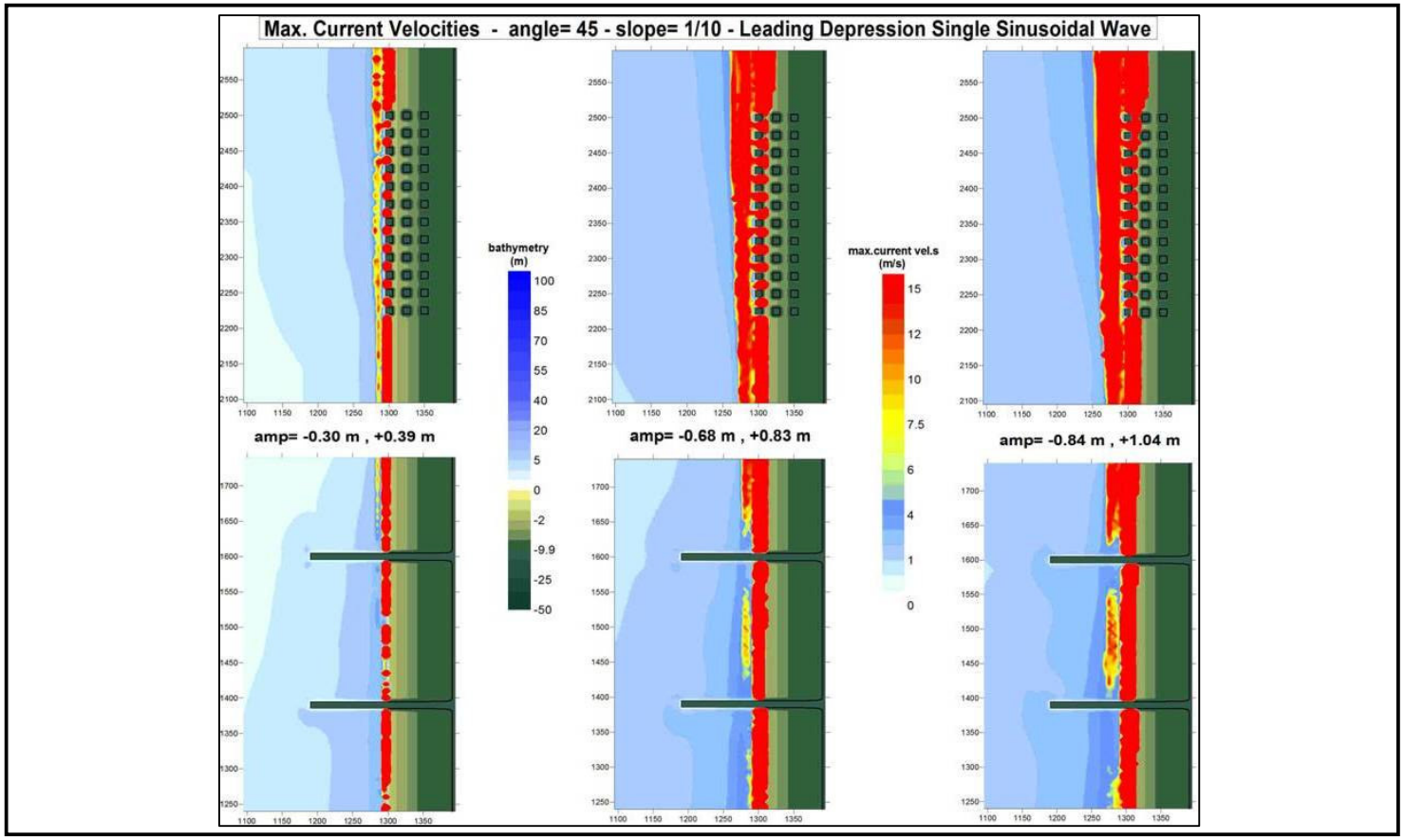

Figure A.14: Distribution of Maximum Current Velocities for Oblique Approach of the Wave (angle=45º) with Period of 3 min. for LDW with the Bottom Slope of 1/10
(Incoming Wave Amplitudes= -0.33m, -0.74m, -0.92m at 235 m before the toe)

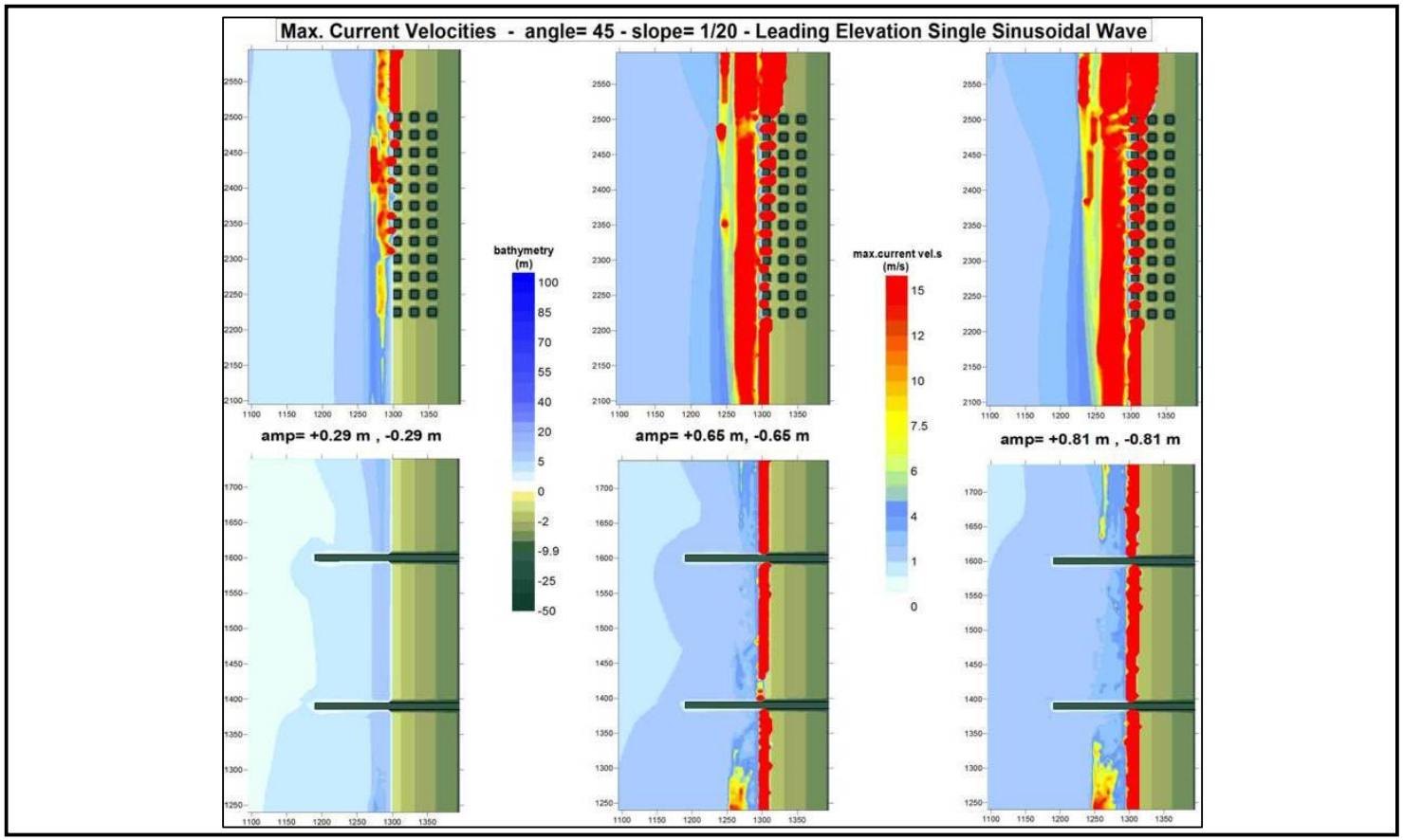

Figure A.15: Distribution of Maximum Current Velocities for Oblique Approach of the Wave (angle=45º) with Period of 3 min. for LEW with the Bottom Slope of 1/20
(Incoming Wave Amplitudes= +0.33m, +0.74m,+0.92m at 235 m before the toe)

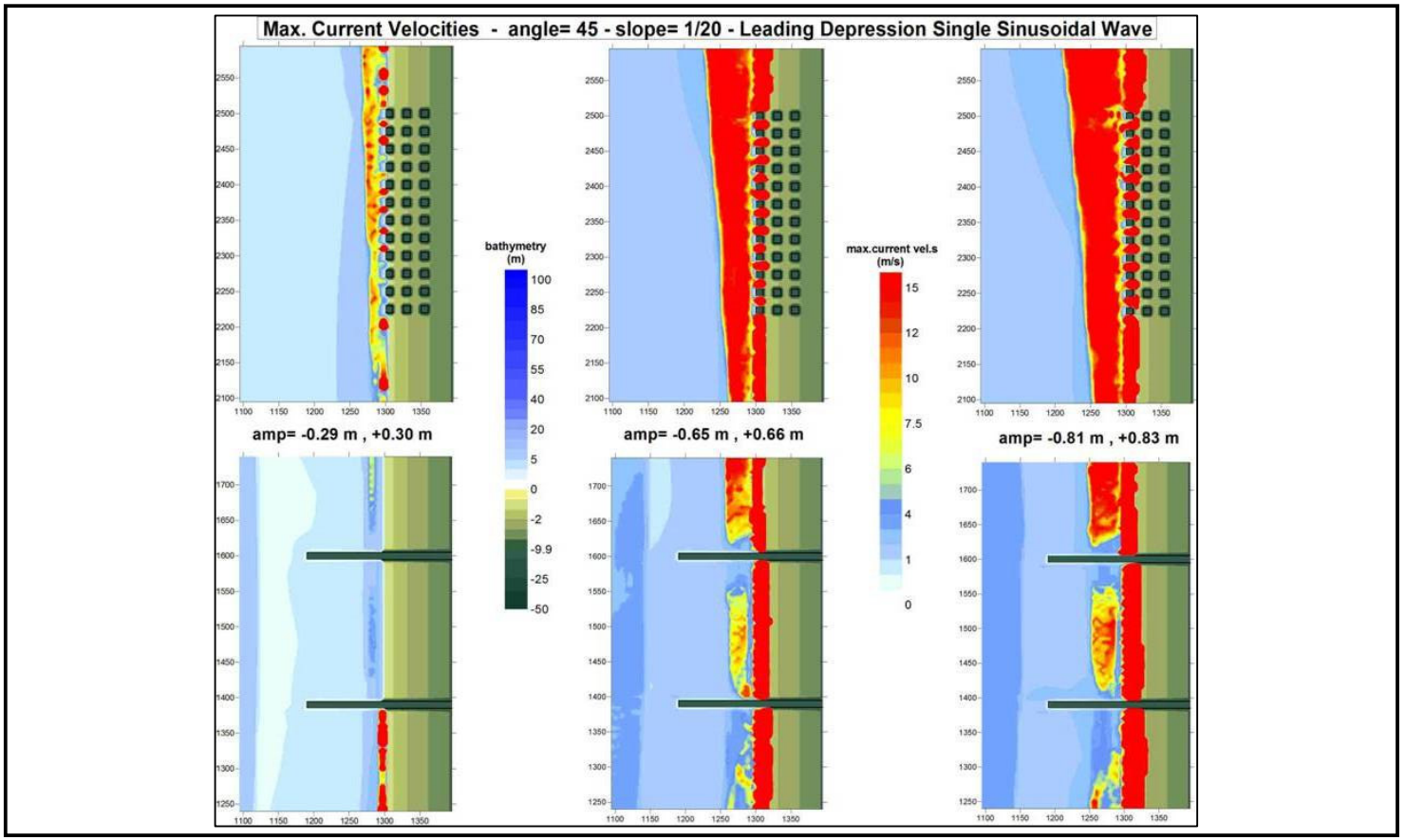

Figure A.16: Distribution of Maximum Current Velocities for Oblique Approach of the Wave (angle=45º) with Period of 3 min. for LDW with the Bottom Slope of 1/20 (Incoming Wave Amplitudes= -0.33m, -0.74m, -0.92m at 235 m before the toe)

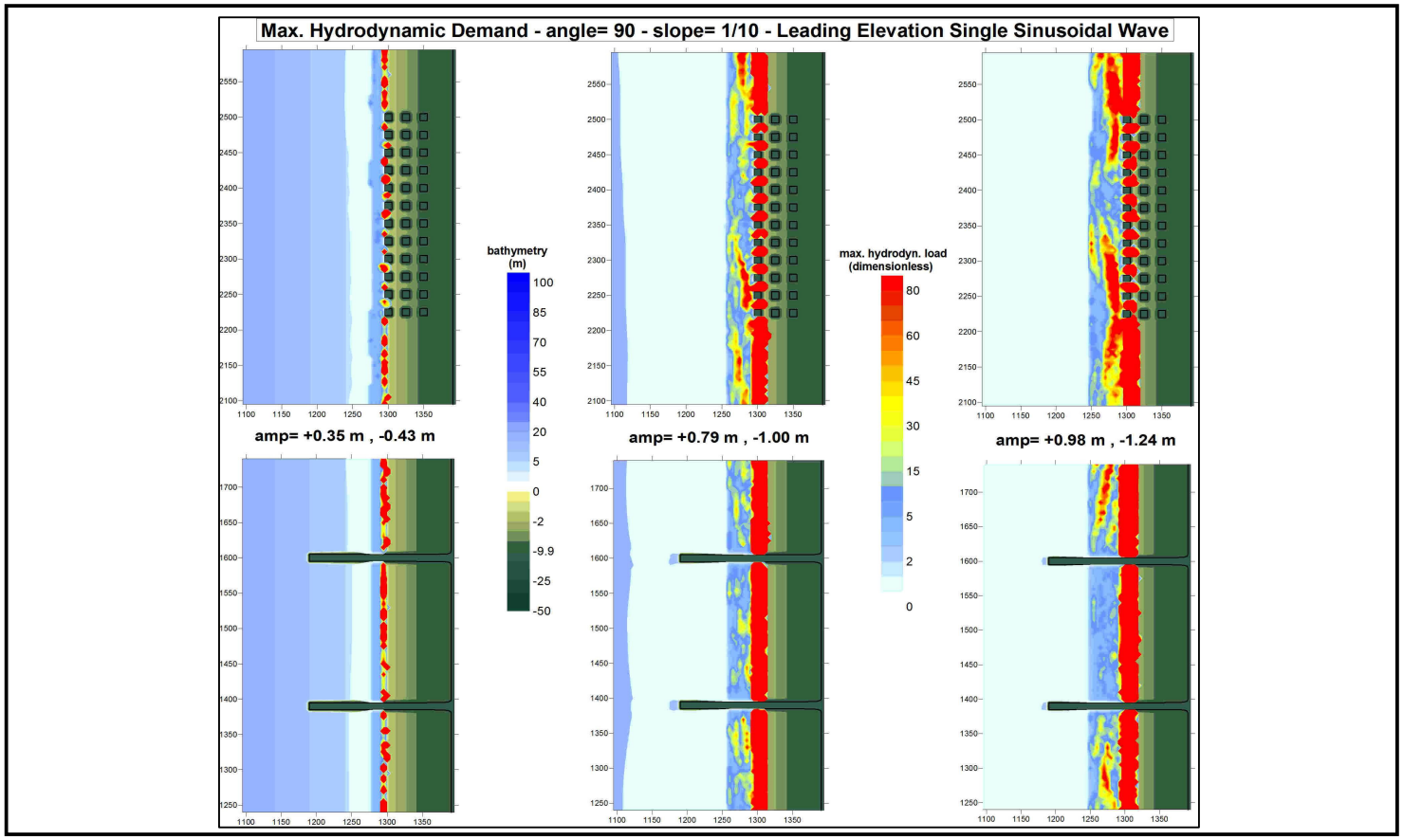

Figure A.17: Distribution of Maximum Hydrodynamic Demands for Perpendicular Approach of the Wave (angle=90º) with Period of 3 min. for LEW with the Bottom Slope of 1/10
(Incoming Wave Amplitudes= +0.33m, +0.74m, +0.92m at 235 m before the toe)

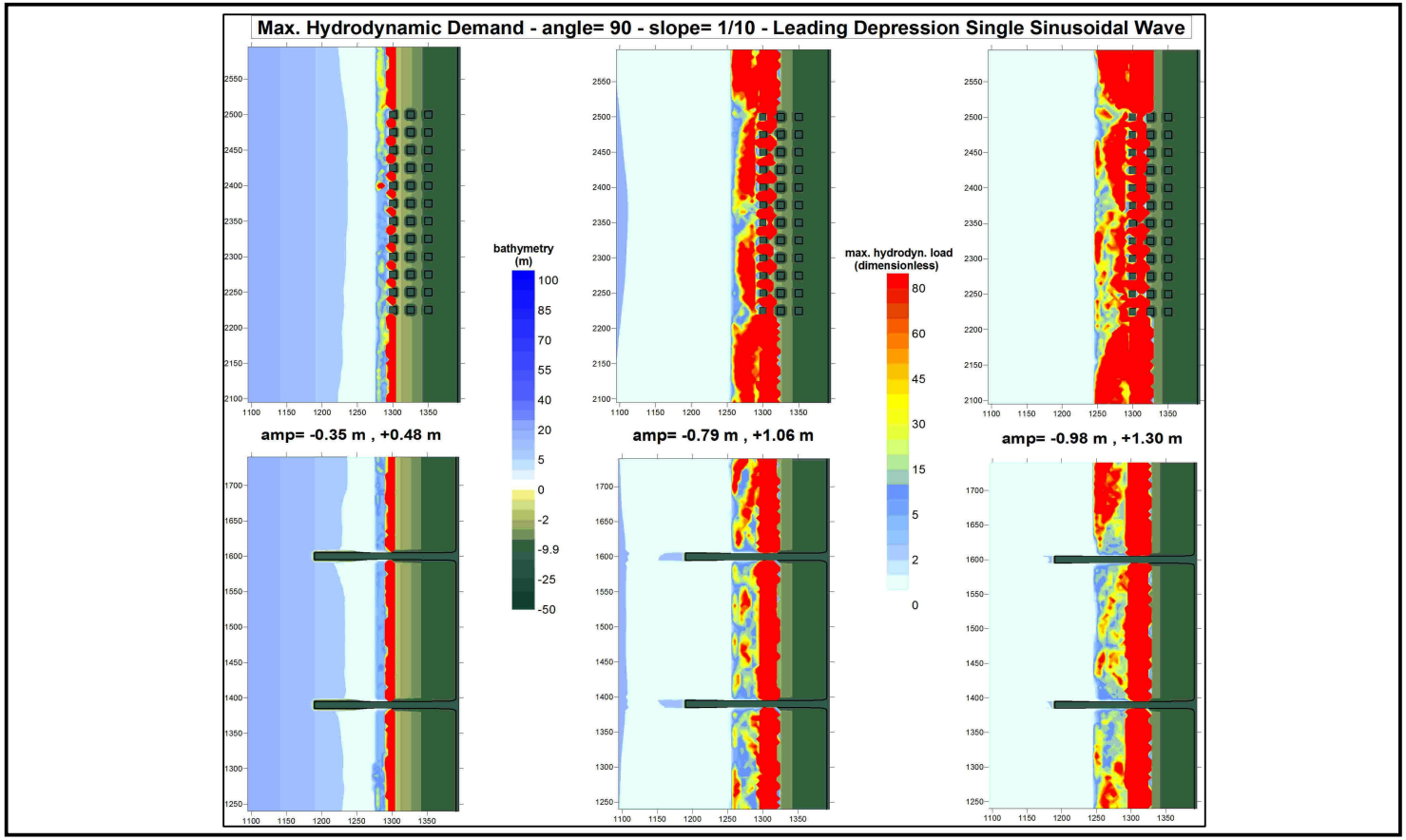

Figure A.18: Distribution of Maximum Hydrodynamic Demands for Perpendicular Approach of the Wave (angle=90º) with Period of 3 min. for LDW with the Bottom Slope of 1/10
(Incoming Wave Amplitudes= -0.33m, -0.74m, -0.92m at 235 m before the toe)

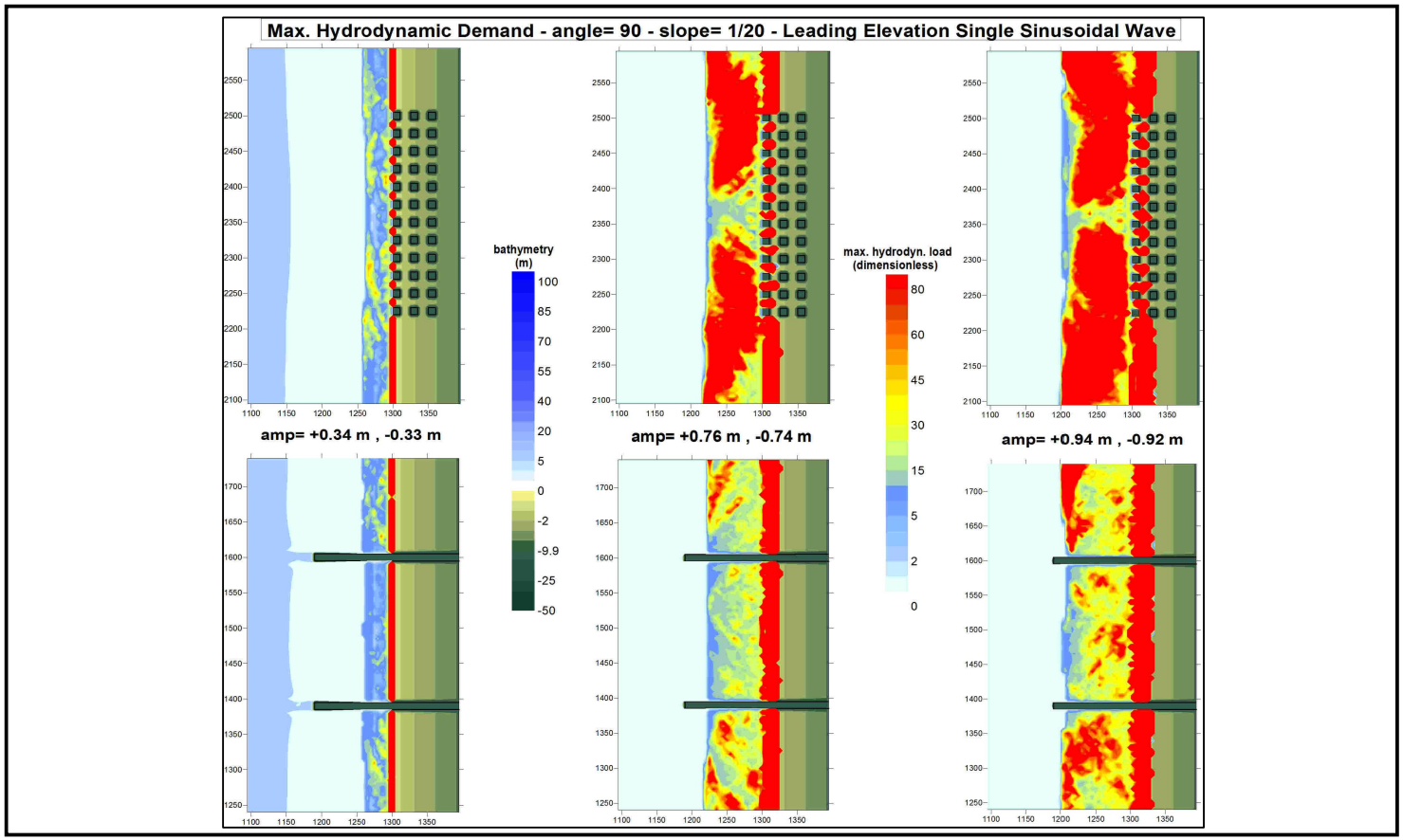

Figure A.19: Distribution of Maximum Hydrodynamic Demands for Perpendicular Approach of the Wave (angle=90º) with Period of 3 min. for LEW with the Bottom Slope of 1/20
(Incoming Wave Amplitudes= +0.33m, +0.74m,+0.92m at 235 m before the toe)

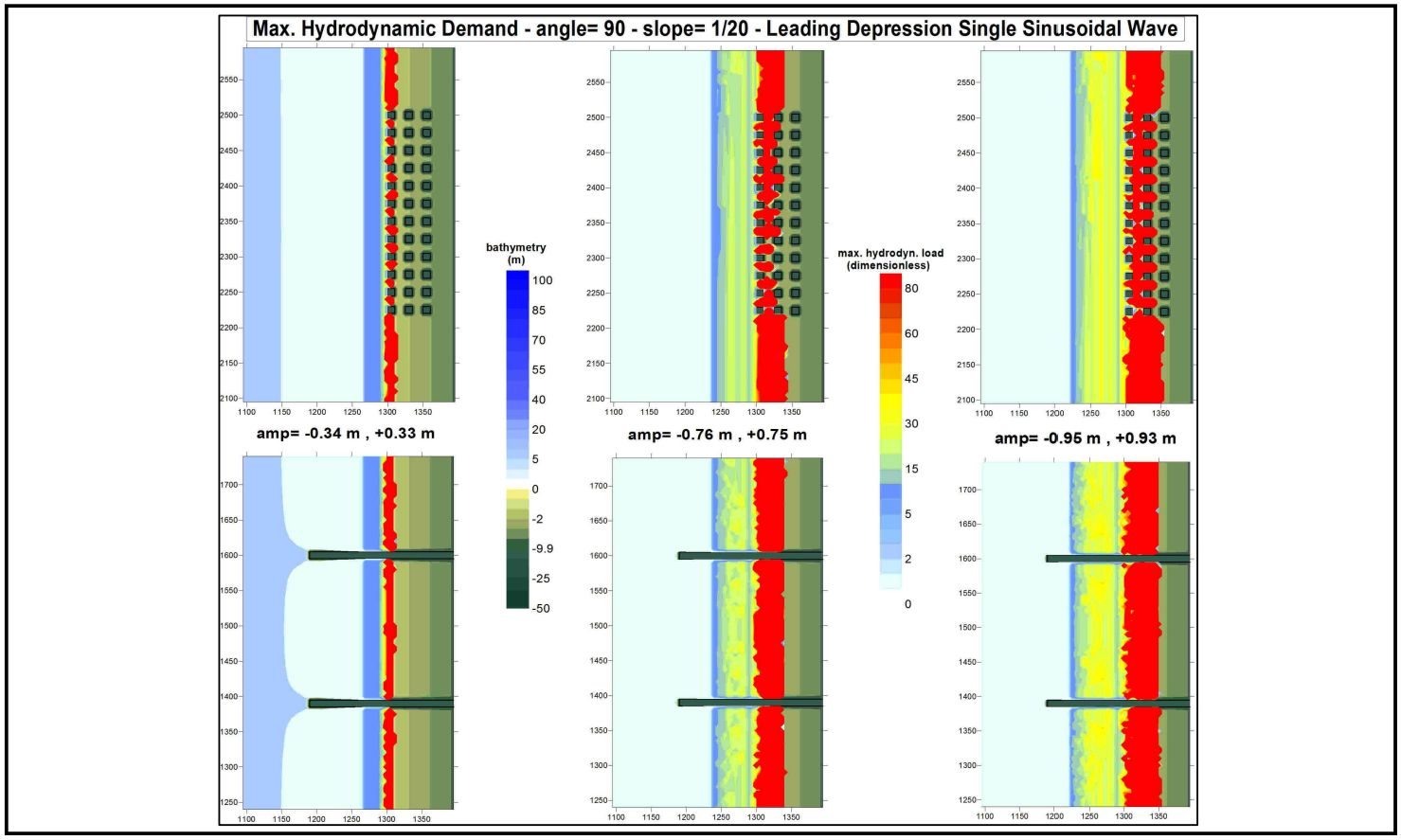

Figure A.20: Distribution of Maximum Hydrodynamic Demands for Perpendicular Approach of the Wave (angle=90º) with Period of 3 min. for LDW with the Bottom Slope of 1/20
(Incoming Wave Amplitudes= -0.33m, -0.74m, -0.92m at 235 m before the toe)

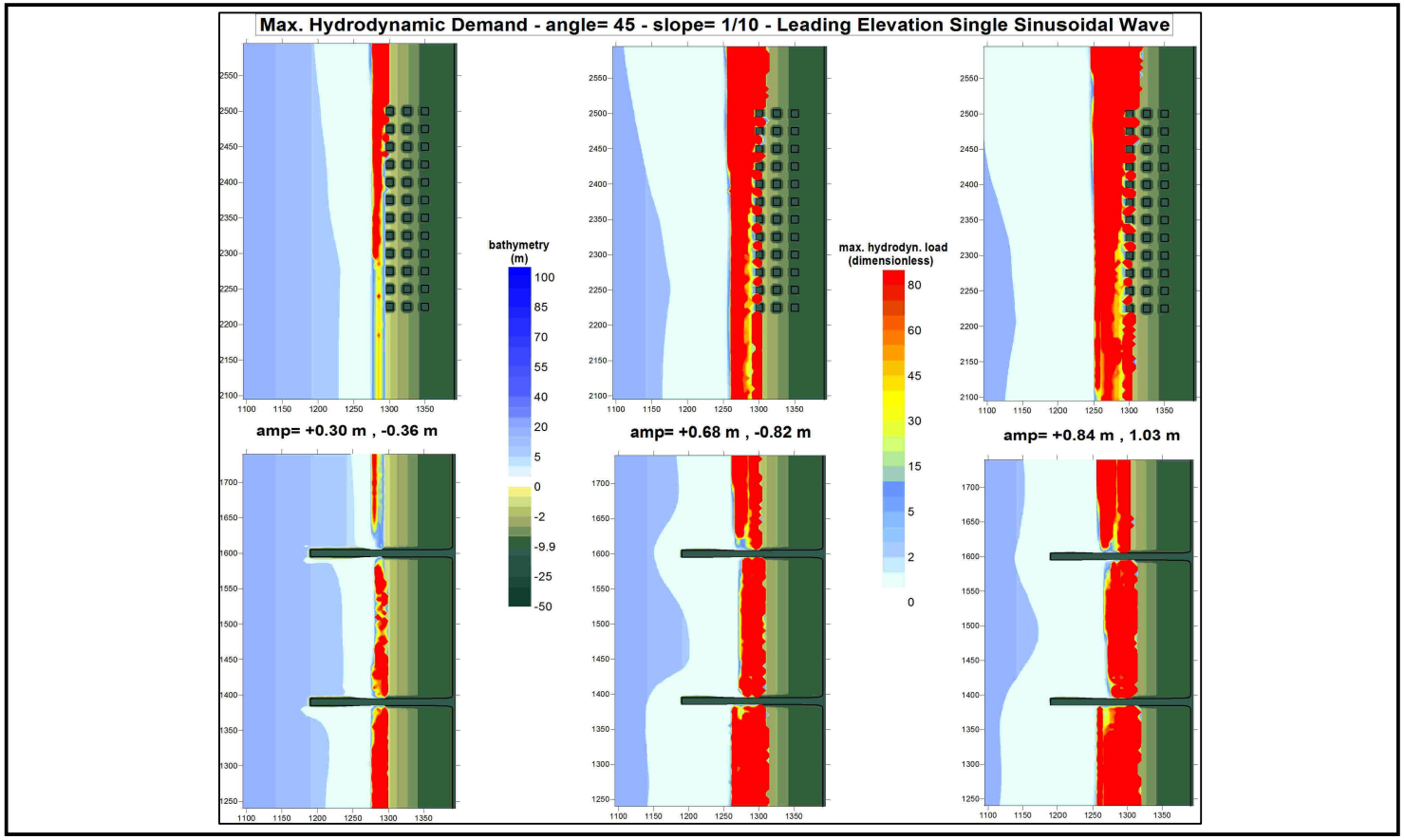

Figure A.21: Distribution of Maximum Hydrodynamic Demands for Oblique Approach of the Wave (angle=45º) with Period of 3 min. for LEW with the Bottom Slope of 1/10
(Incoming Wave Amplitudes= +0.33m, +0.74m, +0.92m at 235 m before the toe)

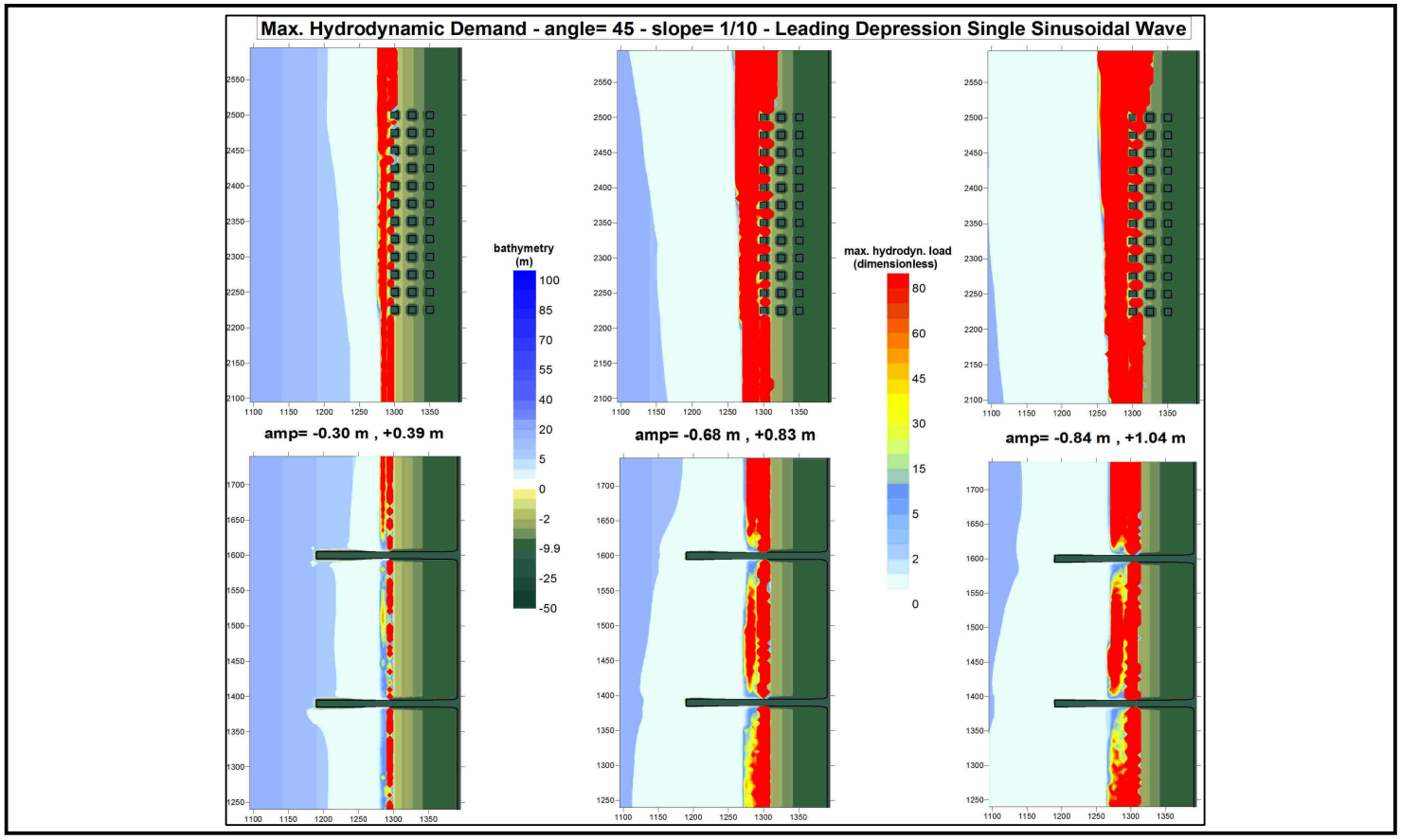

Figure A.22: Distribution of Maximum Hydrodynamic Demands for Oblique Approach of the Wave (angle=45º) with Period of 3 min. for LDW with the Bottom Slope of 1/10 (Incoming Wave Amplitudes= -0.33m, -0.74m, -0.92m at 235 m before the toe)

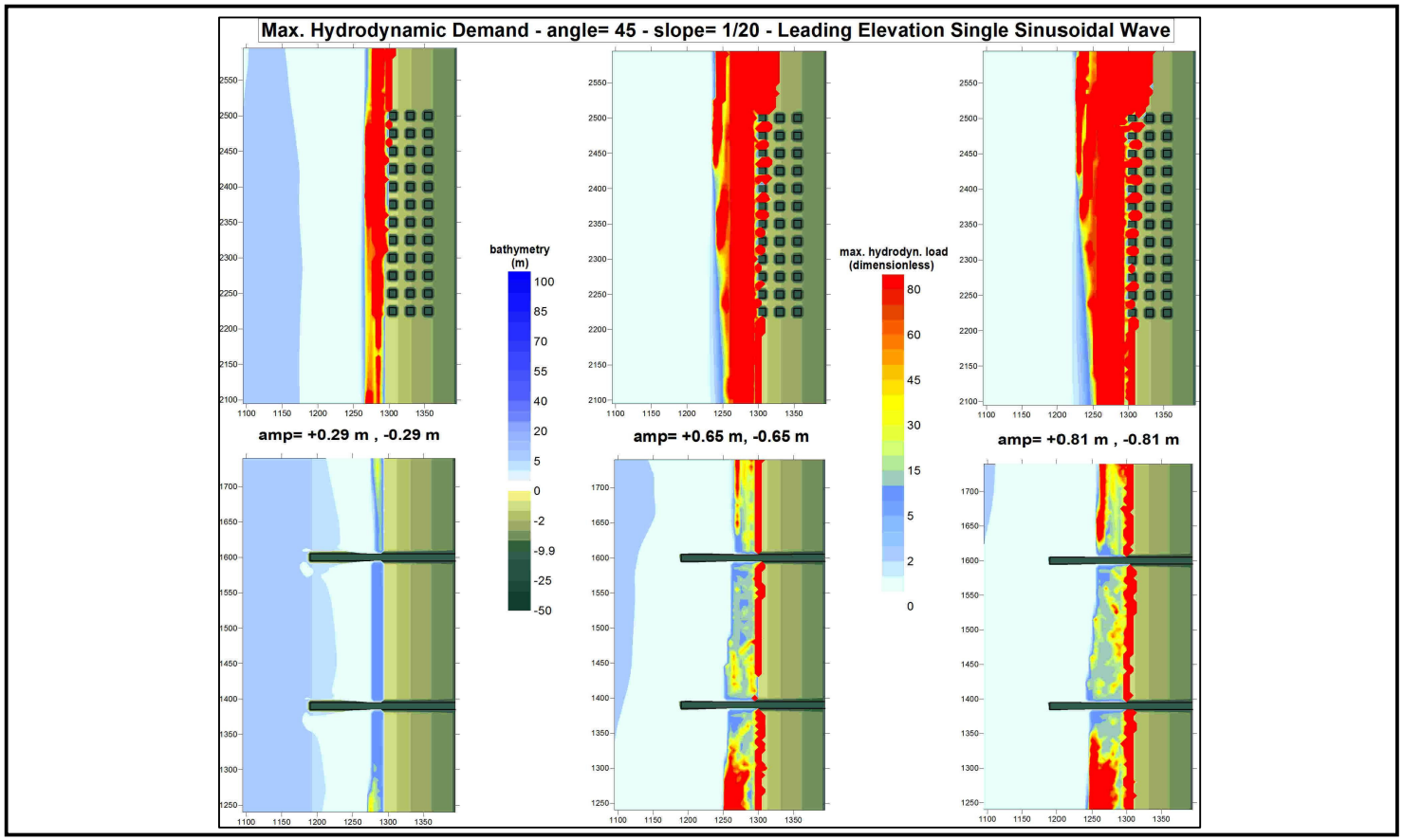

Figure A.23: Distribution of Maximum Hydrodynamic Demands for Oblique Approach of the Wave (angle=45º) with Period of 3 min. for LEW with the Bottom Slope of 1/20
(Incoming Wave Amplitudes= +0.33m, +0.74m,+0.92m at 235 m before the toe)

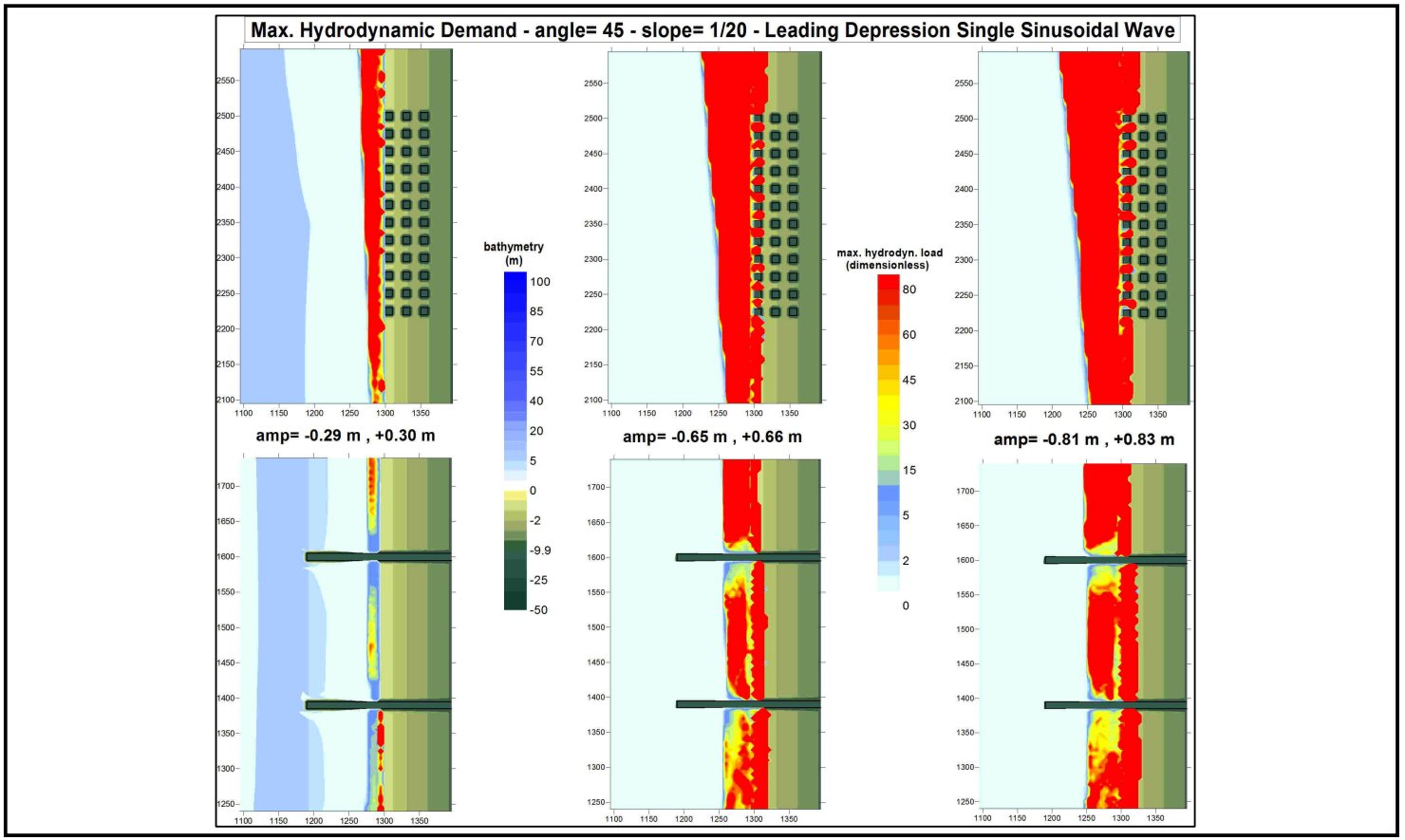

Figure A.24: Distribution of Maximum Hydrodynamic Demands for Oblique Approach of the Wave (angle=45º) with Period of 3 min. for LDW with the Bottom Slope of 1/20
(Incoming Wave Amplitudes= -0.33m, -0.74m, -0.92m at 235 m before the toe)